치의과학박사 학위논문

The study on the effect of nicotinamide in bone metabolism

니코틴아마이드의 뼈 대사 조절 효과에 관한 연구

2023년 2월

서울대학교 대학원

치의과학과 분자유전학 전공

윤 희 인

The study on the effect of nicotinamide in bone metabolism

니코틴아마이드의 뼈 대사 조절 효과에 관한 연구

지도교수 류 현 모

이 논문을 치의과학박사 학위논문으로 제출함
2022년 12월

서울대학교 대학원
치의과학과 분자유전학 전공
윤 희 인

윤희인의 치의과학박사 학위논문을 인준함
2023년 1월

위 원 장 백 정 화 (인)

부위원장 류 현 모 (인)

위 원 최 제 용 (인)

위 원 김 현 정 (인)

위 원 조 영 단 (인)

Abstract

The study on the effect of nicotinamide in bone metabolism

Heein Yoon

Department of Molecular Genetics

The Graduate School

Seoul National University

(Directed by Prof. Hyun-Mo Ryoo, D.D.S., Ph.D.)

Nicotinamide (NAM), a water-soluble amide form of vitamin B3, has been used to treat various disorders for many years with safety profile. NAM is generated during sir2-like proteins (sirtuins) reaction, which is nicotinamide adenine dinucleotide (NAD^+)-dependent class III histone deacetylases. Many studies have revealed that sirtuins are responsible for normal skeletal development and bone homeostasis. However, the effect of NAM in bone homeostasis is not clear. In this study, we investigated whether and howNAM can regulate bone homeostasis.

The mitochondrial respiration to supply the energy required for differentiation is very important during osteogenic differentiation. The action of antioxidant enzymes is critical to

maintain the naturally occurring reactive oxygen species (ROS), a natural by-product of cellular respiration, at an appropriate level. In part1, we showed that NAM enhanced osteoblast differentiation by inducing antioxidant enzymes. NAM improved mitochondrial respiration which is necessary to supply energy for osteoblast differentiation. NAM also induced the expression of antioxidant enzymes by activating mitochondrial SIRT3 and subsequential activation of FOXO3a. These results suggest that NAM promoted osteoblast differentiation by enhancing mitochondrial respiration and antioxidant enzymes.

Patients with cleidocranial dysplasia (CCD) caused by RUNX2 haploinsufficiency exhibit premature closure of cranial sutures, hypoplastic clavicles, and dental anomalies. The chief complaint of CCD patients is the delayed or unerupted permanent teeth. However, the only therapeutic intervention has been a combination of surgical and orthodontic treatment. In part 2, we examined whether NAM improve delayed tooth eruption in *Runx2*$^{+/-}$ mice, a well-established CCD animal model. *Runx2*$^{+/-}$ mice showed delayed tooth eruption and the delay was significantly rescued by NAM administration. Primary osteoblasts from *Runx2*$^{+/-}$ mice showed decreased expression of colony stimulating factor 1 (CSF1) which is critical factor to induce osteoclast differentiation. NAM induced osteoclast differentiation by increasing expression of both RUNX2 and CSF1. RUNX2 directly regulated the expression of Csf1 through binding to the promoter region. The improved expression and activity of RUNX2 by nicotinamide was due to the inhibition of Sirt2. These results suggest that the delayed tooth eruption in CCD

mice was due to the decreased level of Csf1 in *Runx2*−defificient osteoblasts and NAM can be a candidate therapeutic drug promoting RUNX2 level.

In this study, we revealed that NAM induces mitochondrial respiration and the expression of antioxidant enzymes in osteoblasts to maintain bone homeostasis, confirming that the possibility of alleviating musculoskeletal disorders related to oxidative stress. In addition, we also showed the mechanism of delayed tooth eruption in CCD patients and explored the possibility as a candidate therapeutic drug to treat dental abnormalities by direct administration of NAM to *Runx2*$^{+/-}$ mice.

Keyword: nicotinamide, osteoblast, osteoclast, antioxidant enzyme, Runx2, cleidocranial dysplasia

Student Number: 2016−22038

Table of Contents

List of Figures

Part 1. Nicotinamide enhances osteoblast differentiation through the activation of mitochondrial antioxidant defense system

Part 2. Nicotinamide improves delayed tooth eruption in *Runx2*$^{+/-}$ mice

List of Table

I. Literature review

1. Histone deacetylases (HDACs)

DNA is condensed with histone proteins in the form of chromatin. 146 to 147 base pairs (bp) of core DNA surrounds a histone octamer composed of four core histone proteins, H2A, H2B, H3 and H4, as a nucleosome unit (Kornberg 1974, Olins and Olins 1974).

Posttranslational modifications (PTMs) of histone tails can regulate chromatin structure. Histone modifications, such as acetylation, phosphorylation, methylation, and ubiquitylation, can affect inter-nucleosomal interactions accompanying chromosome structure change (Bannister and Kouzarides 2011).

Protein acetylation is catalyzed by histone acetyltransferases (HATs) on lysine residues of histone proteins and non-histone proteins (Lee and Workman 2007). Histone deacetylases (HDACs) have the opposite effect of HATs, inhibiting lysine acetylation (Seto and Yoshida 2014). The presence of less condensed euchromatin or highly condensed heterochromatin is regulated by several histone modifications. In particular the positively charged lysine residues, deacetylated by the action of HDACs, regulate the chromatin structure through tightly packing their architecture in concert with negatively charged phosphate backbone of DNA (Drazic, Myklebust et al. 2016). The compact structure of chromatin diminishes gene expression

by making it difficult to access the transcript machinery, thereby inhibiting gene expression (Park and Kim 2020).

The histone deacetylase family is divided into two families depending on the presence of conserved deacetylase domain and the type of cofactors. Class I (HDAC1−3, and 8), class IIa (HDAC4, 5, 7, and 9), class IIb (HDAC6, and 10) and class IV (HDAC11) are Zn2+−dependent HDACs. Class III HDACs, requiring NAD+ as a co−factor, are consists of 7 sirtuins (SIRT1−7) in mammals (Park and Kim 2020). Class I HDACs possess the completely conserved deacetylase domain and ubiquitously expressed. They are dominantly expressed in the nucleus with strong histone deacetylase activity. Recently, nonhistone proteins are also known as substrates of class I HDACs. HDAC1 and 2 are part of a complex that includes the mitotic deacetylase complex, transcriptional regulatory protein Sin3A, and the nucleosome remodeling and deacetylase complex (NuRD). HDAC3 and SMRT/NCoR form a complex (Ayer 1999, Wen, Perissi et al. 2000). HDAC8 functions independently without forming a complex (Hu, Chen et al. 2000). Class II HDACs have a conserved C−terminal deacetylase domain and can be subdivided into class IIa and IIb. Class IIa have low enzymatic activity and an adapter domain at the N−terminus that serves as a binding site for transcription factors (Mihaylova and Shaw 2013). Class IIb HDACs show an extra tail domain at C−terminus. HDAC 11 only belongs to Class IV HDAC.

However, Class IIb and Class IV HDACs have not been studied well.

It is well known that HDACs play a significant role in regulating bone formation. In humans, bone expresses HDAC1, HDAC3, HDAC5, HDAC6, and HDAC7 at high levels, while articular cartilage expressed HDAC2, HDAC5, HDAC6, and HDAC7 (Bradley, Carpio et al. 2015). Furthermore, many studies have revealed that *Hdac* knockout mice showed impaired bone pheonotype (McGee-Lawrence and Westendorf 2011).

2. Sirtuins

The yeast silent information regulator 2 (Sir2) are highly conserved in many organisms and known to homologous to sirtuins in human (Blander and Guarente 2004). Class III HDACs are composed of seven sir2-like proteins (SIRT1-7). Unlike other classes of HDACs, class III HDACs exhibit NAD^+-dependent enzymatic activity. Sirtuins show various kinds of enzymatic activity depending on their types (Carafa, Rotili et al. 2016). In addition to deacetylation activity (SIRT1-3, and 5-7), some have ADP-ribosylation (SIRT4 and 6), demalonylation and desuccinylation activity (SIRT5). Sirtuins are located in the nucleus (SIRT1-3 and SIRT6-7), cytoplasm (SIRT1 and 2), and mitochondria (SIRT3-5).

SIRT1 was discovered first among other SIRT families and has been studied well. It has been reported that

SIRT1 has a close relation with calorie restriction (CR) and aging. CR induce the expression of SIRT1 and increased cell survival (Cohen, Miller et al. 2004). Furthermore, SIRT1 transgenic mice showed reduced disease syndromes, diabetes, neurodegenerative diseases, liver steatosis, bone loss and inflammation. SIRT1 is also involved in neurodegenerative disorders (Qin, Yang et al. 2006, Donmez, Arun et al. 2012, Jeong, Moon et al. 2013), such as Alzheimer's disease (AD), Parkinson's disease (PD), and Huntington's disease (HD), and tumorigenesis. Recent studies showed that the role of SIRT1 in cancer is controversial. It has been reported that the upregulated SIRT1 is correlated with numerous types of cancer malignancy (Derr, van Hoesel et al. 2014). But it has also been reported that SIRT1 acts as tumor suppressor in vivo (Wang, Sengupta et al. 2008, Derr, van Hoesel et al. 2014). SIRT1 increases bone formation by promoting transcription factors such as Runx2 and Sp7 in osteoblasts (Zainabadi, Liu et al. 2017), and promotes bone resorption by regulating NFkB (Edwards, Perrien et al. 2013) and FOXO (Kim, Han et al. 2015) in osteoclasts. Therefore, SIRT1 has been suggested as an important target to treat bone disorders including osteoporosis.

SIRT2 is known to be involved in age-related neurodegeneration of neurological disease (Fourcade, Outeiro et al. 2018) and metabolism of adipogenesis by inhibiting adipocyte differentiation (Wang and Tong 2009). It

has been reported that SIRT2 is related to tumorigenesis. SIRT2 deacetylated RUNX3 and p300 acetyltransferase and reduced their stability in bladder tumor (Kim, Lee et al. 2011). However, the role of SIRT2 in osteoblasts and osteoclasts has not been clearly elucidated yet.

The three mitochondrial SIRTs (SIRT3, 4, and 5) have different enzymatic activities (Morigi, Perico et al. 2018). SIRT3 has deacetylase activity, whereas SIRT4 has ADP-ribosyltransferase activity. SIRT5 shows NAD-dependent demalonylase and desuccinylase activity in addition to deacetylase activity. Among the three mitochondrial SIRTs (SIRT3, 4, and 5), SIRT3 has been showed the protective role against oxidative stress in various tissues (Dikalova, Pandey et al. 2020, Ma, Sun et al. 2020). SIRT3 is known to induce SOD2, one of antioxidant enzymes, to control the intracellular Reactive Oxygen Species (ROS) level, and promote osteogenic differentiation (Gao, Feng et al. 2018).

SIRT4 functions as ADP-ribosyltransferase and regulates metabolic processes in mitochondria (Ahuja, Schwer et al. 2007), not NAD^+-dependent deacetylase. SIRT4 is known to play the different role to SIRT3 in terms of mitochondrial function and oxidative stress. SIRT4 deficiency upregulates fatty acid β-oxidation and oxidative phosphorylation (Nasrin, Wu et al. 2010). In addition, SIRT4 inhibited the SIRT3-mediated SOD2 activation in cardiac hypertrophy model (Luo, Tang et al. 2017). In contrast to

SIRT3, SIRT4 activation raises ROS levels.

SIRT5 is involved in deacetylation, demalonylation, and desuccinylation of various proteins (Du, Zhou et al. 2011). In mitochondria, SIRT5 has been reported to regulate oxidative stress-related enzymes, such as SOD1 (Lin, Xu et al. 2013), IDH2 and G6PD (Zhou, Wang et al. 2016) to eliminate ROS via desuccinylation.

SIRT6 is localized in nucleus as a chromatin-associated protein and SIRT6 regulates cellular homeostasis, DNA repair, genomic stability, and cellular senescence (Chang, Ferrer et al. 2019). SIRT6 upregulates NRF2-induced antioxidants by interaction with NRF2 (Pan, Guan et al. 2016). Also, it has been reported that SIRT6 induces the expression of SOD2 and catalase through AMPK-FOXO3a pathway (Wang, Wang et al. 2016).

SIRT7 is located in nucleoli and increase mitochondrial function and regulate energy metabolism via mitochondrial unfolded protein response [UPR(mt)]with NRF1 in aged hematopoietic stem cells (Mohrin, Shin et al. 2015). The role of sirtuins in bone was summarized by focusing on the phenotype in knockout mice (Table 1).

Table 1. The summary of sirtuins knockout mice phenotype regarding bone

Sirtuin	Type of mutant	Phenotypes	References
SIRT1	Whole body	Defects in craniofacial suture closure and delayed mineralization of the skull, vertebrae and digits (E17.5−18)	(Lemieux, Yang et al. 2005)
	Whole body	Decreased bone volume (1−month−old and 4−month−old). No difference in heterozygous knockout mice in bone mass	(Zainabadi, Liu et al. 2017)
	Prx1−cre (mesenchymal stem cells)	Decreased bone mass in aged mice (2.2 years old) not in young mice (2−month−old).	(Simic, Zainabadi et al. 2013)
	Osx−cre (osteoblast progenitors)	bone loss in cortical bone and females (12−week−old)	(Iyer, Han et al. 2014)
	2.3kb Col1a1−cre (osteoblast)	Decreased bone volume in female mice (16−week−old)	(Edwards, Perrien et al. 2013)
SIRT3	Whole body	Decreased bone mass in KO mice due to the decreased osteoblast function	(Gao, Feng et al. 2018)
		Decreased bone mass in KO mice due to the enhanced osteoclast differentiation (8−week−old)	(Huh, Shin et al. 2016)
		Deletion of SIRT3 attenuated age−associated bone loss comparing 6−month−old and 16−month−old mice	(Ling, Krager et al. 2021)
SIRT6	Ocn−cre (osteoblast/ osteocyte)	Decreased bone mass (8, 16, and 48−week−old)	(Kim, Piao et al. 2020)

	Whole body	low bone mass with decreased bone formation and bone resorption	(Sugatani, Agapova et al. 2015)
SIRT7	2.3kb Col1a1−cre	bone loss due to decreased bone formation	(Fukuda, Yoshizawa et al. 2018)
	Whole body	severe osteopenia (14−15 weeks old)	

3. The NAD biosynthesis pathway

The NAD+ can be generated through de novo and salvage pathways (She, Sheng et al. 2022). During de novo pathway, a dietary amino acid L-tryptophan is converted into quinolic acid and nicotinic acid mononucleotide (NaMN) in consecutive order. Then, nicotinic acid adenine dinucleotide (NaAD) is formed followed by amidtation by NAD synthase (NADS) and consequently generates NAD+ (Srivastava 2016). Meanwhile, NAD+ can be recycled via the salvage pathway using NAD+ precursors, namely NAM, NA, NMN and NR. NAM and NR are converted into NMN by the action of nicotinamide phosphoribosyltransferase (NAMPT) and nicotinamide riboside kinase (NRK), respectively. The NMN is converted into NAD+ via nicotinamide mononucleotide adenyltransferase (NMNAT).

4. Nicotinamide as a SIRT activator or inhibitor

Sirtuins are class III histone deacetylases and firstly discovered in yeast as the yeast sirtuin silent information regulator 2 (Sir2) (Imai, Armstrong et al. 2000). The deacetylation reaction of sirtuins releases NAM from NAD^+ and the NAM can react with the O-alkyl-amidate intermediate in a process known as nicotinamide exchange, functions as a non-competitive inhibitor (Avalos, Bever et al. 2005). As NAM exhibit feedback inhibition in sirtuin activity, it has been used as an inhibitor of sirtuins. However, when NAM treated to cells, the NAM rapidly transformed to NAD^+

with decreased NAM concentration (Hwang and Song 2017). In addition, the low dose of NAM (μM) functions as NAD^+ supplier, but high dose of NAM (mM) regulated not only cell survival, differentiation, DNA repair but also deacetylation by inhibiting the activity of sirtuins (Meng, Ren et al. 2018). NAM showed different effects on sirtuins depending on the subcellular localization or the type of cells (Ma, Maruwge et al. 2014). It is also known that increased NAD^+ level through the supplementation of precursors, such as NAM, NA and NR, induce the activation of sirtuins (e.g., SIRT1, SIRT3) accompanying activation of transcriptional regulators (e.g., PGC1-α, FOXO) and increased mitochondrial biogenesis and function (Cantó and Auwerx 2012, Cantó, Houtkooper et al. 2012, Srivastava 2016). Due to these numerous conflicting studies, more researches are required to fully understand the action of NAM on sirtuins.

5. Reactive oxygen species and bone homeostasis

The transfer of electrons from substrate oxidation and ATP synthesis occurs at the mitochondrial electron transport chain (ETC) (Feher 2017). More than 90% of intracellular ROS are produced by mitochondrial ETC and most of the non-mitochondrial ROS are produced by NADPH oxidases (Noxs) (Balaban, Nemoto et al. 2005). During the electron transfer, electron leak and proton leak occur and ROS can be generated as a natural by-product of normal cellular activity (Auten and Davis 2009). It has been

known that the normal physiological level of ROS is necessary to maintain cell homeostasis and transduce cellular signaling, including differentiation, autophagy, metabolic adaptation, and immunity (Sena and Chandel 2012).

However, the oxidative stress caused by excessive accumulation of ROS can result in numerous chronic diseases, such as cardiovascular disease, neurological diseases, cancer, inflammation, diabetes, obesity, and many elderly diseases (Lin and Beal 2006, Khansari, Shakiba et al. 2009, Uddin, Al Mamun et al. 2020). In terms of macromolecules, excessive ROS accumulation changes the structure of lipids, protein, nucleic acids, and DNA, which alters their functions and cellular signaling (Begum, Howlader et al. 2021).

In addition, the normal physiological level of ROS regulates osteogenic differentiation and matrix mineralization as well as survival in mesenchymal stem cells (MSCs) (Li, Gao et al. 2017). It has been reported that ROS induce osteogenic differentiation in osteogenic precursor cells (Arakaki, Yamashita et al. 2013). Also, the physiological levels of intracellular ROS or the low concentrations of H_2O_2 promoted osteogenic differentiation through Erk1/2 signaling pathway (Khalid, Yamazaki et al. 2020). However, higher dose of H_2O_2 induces stress-activated protein kinases JNK and P38 (MAPKs) pathway leading to cell death. Furthermore, oxidative stress shifts

the fate of the senescent cells from osteogenic to adipogenic lineages and inhibited osteogenic differentiation of MSCs and MC3T3-E1 preosteoblast cells (Mody, Parhami et al. 2001, Lee, Lim et al. 2006, Zheng, Sui et al. 2020). The increased ROS and excessive oxidative stress are associated with bone aging, postmenopausal osteoporosis and osteoarthritis, characterized by impaired bone function and degenerative bone tissue (Li, Li et al. 2021). Therefore, it is crucial to manage oxidative stress in order to preserve bone homeostasis.

6. Antioxidants against oxidative stress

To maintain a regulated ROS level without oxidative stress, there are several defensive mechanisms and antioxidants. Through enzymatic or nonenzymatic reactions, the ROS can change one another. Among endogenous antioxidants, the enzymatic antioxidants include superoxide dismutase (SOD), catalase (CAT), glutathione peroxidase (GPx) (Begum, Howlader et al. 2021).

Hydrogen peroxide can be generated from superoxide anion radical by the action of superoxide dismutase (SOD) (Okado-Matsumoto and Fridovich 2001). In mammals, three isoforms of SODs (SOD1-3) are found. SOD1 is copper/zinc-dependent isoform is located in the cytoplasm (Crapo, Oury et al. 1992) and mitochondrial intermembrane space (Okado-Matsumoto and Fridovich 2001). SOD3 is also copper/zinc-dependent enzyme and

located in the extracellular space (Fukai, Folz et al. 2002). SOD2 is manganese SOD and presents in the mitochondrial matrix. The generated hydrogen peroxide is transformed into water by the actions of CAT and GPx (Wassmann, Wassmann et al. 2004). Meanwhile, there are the non-enzymatic antioxidants, like glutathione (GSH), vitamin A, C and E, flavonoids, carotenoids, which reduce free radicals by contributing electrons (Janciauskiene 2020).

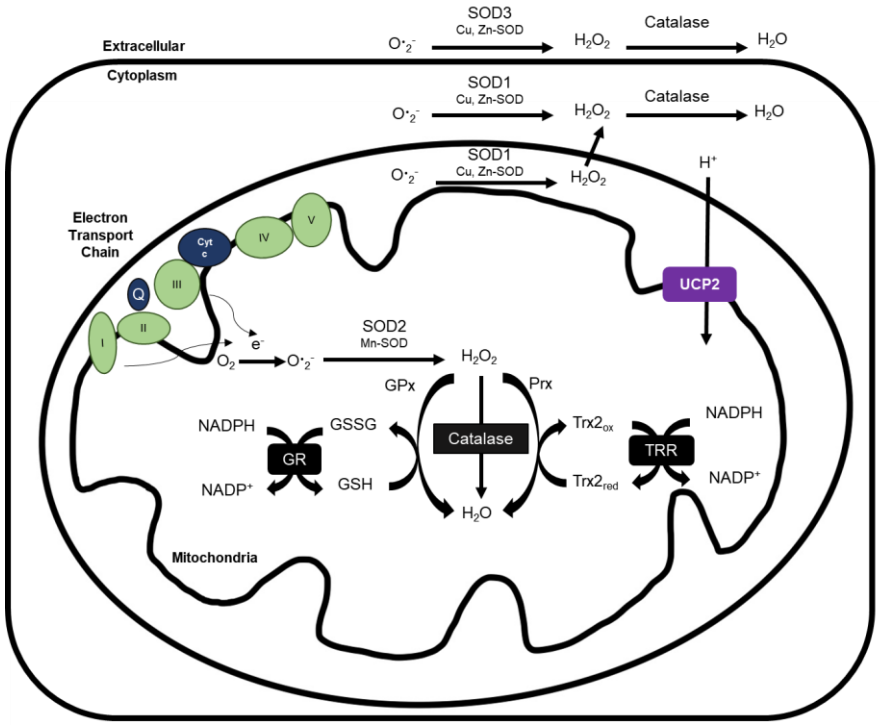

Mitochondrial oxidative stress and antioxidant system

Superoxide can be produced by complex I and III of the electron transport chain. SOD2 converts O_2^- into H_2O_2 in the mitochondrial matrix. SOD1 and SOD3 function in cytoplasm and extracellular space, respectively. Catalase converts H_2O_2 into H_2O. In addition, peroxiredoxins (Prx) and glutathione peroxidases (Gpx) can detoxify mitochondrial H_2O_2. Glutathione reductase (GR) uses the reducing equivalents of NADPH to produce reduced glutathione after Gpxs oxidize glutathione (GSH) into GSSG. Thioredoxin (Trx) is oxidized by Prxs, and Thioredoxin Reductase (TRR), which is activated by NADPH, regenerates the reduced Trx. Uncoupling protein 2 (UCP2) activations induce proton leak leading to membrane depolarization and the decrease in ROS production.

7. Mitochondria and bone health

The osteogenic differentiation of MSCs and osteoprogenitors are regulated by mitochondrial metabolism, referring to glycolysis and oxidative phosphorylation (OXPHOS). As MSCs/preosteoblasts differentiate into mature osteoblasts, the energy supply from glycolysis gradually shifts to OXPHOS (Li, Gao et al. 2017). This transition occurs in order to efficiently supply the abundant energy necessary for osteogenic differentiation. Therefore, the mitochondrial oxygen consumption rate (OCR) and ATP production increased during osteogenic differentiation (Gao, Feng et al. 2018). The inhibition of electron transport chain caused the impaired osteoblast differentiation (Chen, Shih et al. 2008, Gao, Feng et al. 2018, Shares, Busch et al. 2018). It has been reported that the increased active mitochondria promoted osteogenic differentiation in C3H10T1/2 BMSC-like cells by supplying acetyl-CoA for the acetylation of β-catenin to increase Wnt/β-catenin signaling pathway (Shares, Busch et al. 2018). The upregulated OXPHOS during osteoblast differentiation can lead to the increased production of ROS. However, there is an antioxidant defense system preventing the accumulation of ROS, such as catalase and SOD2 (Chen, Shih et al. 2008, Gao, Feng et al. 2018). The SOD2 deficient mice showed decreased osteogenic differentiation and osteoporosis with increased oxidative stress (Treiber, Maity et al. 2011, Gao, Feng et al. 2018). Furthermore, decreased OXPHOS and increased

oxidative stress were observed in senile osteoporosis mouse model (Senescence Accelerated Mouse Strain P6, SAMP6) (Lv, Yang et al. 2018). These results suggest that the mitochondrial metabolism and oxidative stress are significant to maintain bone homeostasis and prevent bone pathologies.

8. RUNX2

RUNX2 (Runt-related transcription factor2, Cbfa1, AML3), a master transcription factor of osteogenesis, is an indispensable for bone and cartilage formation (Komori, Yagi et al. 1997). Runx2 is involved in the RUNX family of transcription factor. The *Runx2* gene spans approximately 220kbp and located on human chromosome 6 and mouse chromosome 17. RUNX2 recognizes 5' -PuACCPuCA-3' or its complementary sequence 5' -TGPyGGTPy-3' (Melnikova, Crute et al. 1993). RUNX2 protein exist in two major types of isoforms (Geoffroy, Corral et al. 1998). The MASNS isoform, transcribed from P1 promoter (the distal promoter product, Runx2-type II), is involved in the later stages of differentiation. The MRIPV isoform, transcribe from P2 promoter (the proximal promoter product, Runx2-typeI), is involved in under-differentiated sutural mesenchymal cells, pre-osteoblasts in osteogenic fronts and osteocalcin-positive osteoblasts lining parietal bones (Choi, Lee et al. 2002).

Runx2 determines the lineage of mesenchymal stem

cells to differentiate into osteoblast in concert with Sp7/Osterix and canonical Wnt signaling (Komori 2010). Runx2 is required from the early stage of osteoblast differentiation to decide the fate of mesenchymal stem cells, while Sp7 and Wnt signaling are necessary for the determination of the osteoblast lineage and preventing the mesenchymal cells from the differentiation into chondrocyte. On the contrary, at a late stage, Runx2 inhibits osteoblast maturation. Runx2 transgenic mice under the control of the 2.3 kb col1a1 promoter show osteopenic symptoms with decreased fully differentiated osteoblasts and increased less mature osteoblasts (Liu, Toyosawa et al. 2001). Furthermore, in the long-term culture of MC3T3-E1 cells with osteogenic medium, the expression of Runx2 peaked on the 4th day of differentiation and gradually decreased thereafter (Cho, Yoon et al. 2009). According to these findings, the timely expression of Runx2 is important in the osteoblast differentiation.

Runx2 is regulated by a variety of osteogenic signaling pathway including FGF (Park, Kim et al. 2010), BMP (Jun, Yoon et al. 2010), TGF-β (Lee, Kim et al. 2000) and WNT (Gaur, Lengner et al. 2005). As a central regulator of osteogenic differentiation, Runx2 controls the expression of bone marker genes such as alkaline phosphatase, type I collagen, bone sialoprotein and osteopontin in bone and cartilage (Otto, Lübbert et al. 2003). Therefore, it is necessary to understand the role of Runx2

and the mechanism of osteogenic differentiation regulated by Runx2.

9. Cleidocranial dysplasia

The mutations of *Runx2* causes cleidocranial dysplasia (CCD;OMIM#119600), an autosomal dominant skeletal disease (Mundlos, Otto et al. 1997). CCD appears with a prevalence of 1 per million regardless of gender or race (Hordyjewska, Jaruga et al. 2017). The typical clinical manifestations of CCD patients are short stature, delayed closure of fontanelles and sutures, hypoplastic clavicles, and other skeletal anomalies. Specifically, the craniofacial features of CCD patients are an inverted pear-shaped calvaria, a broad flattened nasal bridge and hypoplastic maxillary bone causing midface retrusion and mandible prognathism (Farrow, Nicot et al. 2018). Additionally, CCD patients suffer from a variety of dental problems, such as Class III malocclusion, prolonged retention of primary teeth, delayed eruption of permanent teeth and hyperdontia.

A multidisciplinary approach is required for dental management in CCD. For the high quality of life and satisfying social life of CCD patients, dental treatment considering normal functions and cosmetic aspects should be performed. Several kinds of orthodontic-surgical regimens are executed, including the Toronto-Melbourne, Belfast-Hamburg, and Jerusalem approaches (Park, Vargervik et al. 2013). The Toronto-Melbourne approach is based on timed,

serial extraction of primary teeth to support the spontaneous eruption of permanent teeth, but the Belfast–Hamburg approach requires a single surgical procedure to extract all retained primary and supernumerary teeth with expose of all unerupted teeth (Roberts, Stephen et al. 2013). The Jerusalem approach is based on 2 surgical interventions according to the state of the root development of the permanent teeth. To restore craniofacial and dental function, the planning of dental management is necessary considering the needs, the age and social and economic conditions of patients.

10. Runx2 and dental development

Runx2 is a master transcription factor for osteoblast differentiation, but it is also essential for tooth development and eruption. The expression of Runx2 in the dental papilla and dental sac, give rise to odontoblasts and osteoblasts respectively, implies their involvement in the differentiation of odontoblasts and osteoblasts in the periodontium (Camilleri and McDonald 2006). *Runx2*$^{-/-}$ mice showed an arrest of tooth development at the cap stage with misshapen tooth organs. The expression of mesenchymal Runx2, regulated by dental epithelium, affects the growth and differentiation of dental epithelium. Runx2 is necessary to control morphogenesis and differentiation of the epithelial enamel organ in the process of epithelial–mesenchymal interactions (D'Souza, Aberg et al. 1999).

The precise interaction between osteoblast and osteoclast is essential to pave the eruption pathway. Csf1 (Colony-stimulating factor-1) knockout mice, known as osteopetrotic *op/op* mice, show arrested tooth eruption. In addition, Rankl (Receptor activator of nuclear factor kappa-B ligand) knockout mice also fail to tooth eruption (Kong, Yoshida et al. 1999). Opg (Osteoprotegerin) expression pattern, a soluble decoy receptor binding to RANKL, is correlated with osteoclast formation in murine dental follicle cells (Wise, Lumpkin et al. 2000). Spatiotemporal expression patterns of CSF1, RANKL and OPG determine site-specific osteoclastogenesis during eruption process (Heinrich, Bsoul et al. 2005).

In CCD patients, primary teeth erupt on time, but permanent teeth show delayed eruption. Human dental follicle cells isolated from CCD patients show decreased RANKL/OPG ratio and osteoclast formation in the co-culture system with peripheral blood mononuclear cells (PBMCs) (Wang, Sun et al. 2016). Furthermore, heterozygous Runx2 knockout mice also show delayed tooth eruption at postnatal day 8 and 10 with decreased tartrate resistant acid phosphate (TRAP)-positive osteoclasts on the bone surface of erupting tooth (Yoda, Suda et al. 2004). *Runx2*$^{-/-}$ mice show decreased osteoclast differentiation due to the deficiency of Rankl (Enomoto, Shiojiri et al. 2003). These results suggest that impaired alveolar bone resorption causes delayed tooth eruption in CCD patients.

II. Purpose of study

In order to maintain bone homeostasis, osteoblasts and osteoclasts must function in a balanced manner. It is well known that an imbalance between the two causes several bone disorders. As a result, it is critical to control the activity of osteoblasts and osteoclasts to preserve bone homeostasis.

NAM, a water-soluble vitamin B3, is well known for its safety profile and has been used for a long time to treat various diseases. As a one of the NAD+ precursors, NAM modulates the action of sirtuins, a class III HDAC.

In this study, we sought to determine whether NAM regulate osteoblast differentiation and, if so, what the mechanism is. Additionally, the interaction between osteoblasts and osteoclasts is crucial to resorb the alveolar bone around the erupting tooth. We investigated the causes of the delayed tooth eruption in *Runx2*$^{+/-}$ mice and explored if NAM could restore them.

The purpose of this study is to evaluate the potential of NAM as a candidate drug to regulate osteoblast differentiation, which is crucial for sustaining bone homeostasis. Moreover, this study was performed to elucidate the mechanism of delayed tooth eruption symptoms in CCD and determine whether NAM treat this by regulating cross-talk between osteoblasts and osteoclasts.

III. Part1

Nicotinamide enhances osteoblast differentiation through the activation of mitochondrial antioxidant defense system

Abstract

The normal physiological level of oxidative stress is important for maintaining bone homeostasis. The imbalance between reactive oxygen species (ROS) production and antioxidant defense can cause various bone diseases such as osteoporosis. Nicotinamide (NAM), an NAD^+ precursor, is the amide form of vitamin B3 and has been used to treat various diseases. The purpose of this study was to see whether NAM could support the maintenance of bone homeostasis via regulating osteoblasts. Here, we demonstrate that NAM significantly enhanced osteoblast differentiation and mitochondrial metabolism during osteogenic differentiation. We also observed that NAM increased the expression of proliferator-activated receptor γ coactivator α (Pgc1-α), the key regulator of mitochondrial biogenesis, and antioxidant enzymes, including SOD1, SOD2, UCP2, and TRX2. NAM-induced upregulation of antioxidant enzymes was due to increased FOXO3a transcriptional activity and nuclear translocation via SIRT3 activation. NAM also prevented not only the impairment of osteoblast differentiation caused by chronic exposure to H_2O_2 accompanying mitochondrial dysfunction but also the apoptotic and necrotic cell death caused by acute exposure of H_2O_2. In summary, NAM increased mitochondrial biogenesis as well as antioxidant enzyme expression via SIRT3-FOXO3a activation, promoting osteoblast differentiation. Our study suggests NAM as a potential preventive and therapeutic drug for bone health and bone diseases.

Introduction

Reactive oxygen species (ROS) are highly reactive molecules that are mainly generated from the mitochondrial electron transport chain (ETC) (Alfadda and Sallam 2012). ROS are inevitably produced during normal metabolic processes as a natural byproduct and also play various roles in normal physiological processes, activating signaling pathways to initiate biological processes as "secondary messengers" in normal condition (Auten and Davis 2009). The imbalance between ROS production and the antioxidant defense system induces oxidative stress (Wilson 2014, Kim, Kim et al. 2022).

Maintaining the balance of ROS is also important in bone homeostasis and pathology (Balaban, Nemoto et al. 2005). SOD2, an antioxidant enzyme, play a critical role in osteoblast differentiation by regulating mitochondrial ROS at an appropriate level to avoid their accumulation (Gao, Feng et al. 2018). ROS-induced oxidative stress is also related to bone pathologies, such as bone aging (Callaway and Jiang 2015), postmenopausal osteoporosis (Yang, Cao et al. 2022) and osteoarthritis (Lepetsos and Papavassiliou 2016). Therefore, targeting the dysfunctional mitochondria accompanying an imbalanced ROS level and regulating antioxidant enzymes are potential targets to enhance bone health.

Among the several subcellular organelles that generate ROS, mitochondria are the major source of intracellular ROS production, accounting for over 90% of them (Balaban, Nemoto et al. 2005). To maintain an appropriate level of ROS, various antioxidant enzymes are involved in scavenging mitochondrial ROS (He, He et al. 2017). The highly reactive radical superoxide molecules are catalyzed to a

less-radical ROS, hydrogen peroxide, by the activity of the superoxide dismutase (SOD) family (Richter, Konzack et al. 2015). Next, these H_2O_2 molecules are further catalyzed into H_2O by the intervention of antioxidant enzymes such as catalase, thioredoxin peroxidase, and glutathione peroxidase (Andreyev, Kushnareva et al. 2005).

Nicotinamide (NAM), the water-soluble form of vitamin B3, has been categorized as a food additive rather than a pharmaceutical (Rolfe 2014) and showed a favorable safety profile in a clinical trial (Chen, Martin et al. 2015). As one of the precursors of nicotinamide adenine dinucleotide (NAD^+), NAM can increase the level of NAD^+ just like nicotinic acid (NA), nicotinamide mononucleotide (NMN), and nicotinamide riboside (NR). NAD^+ is a vital cofactor/coenzyme in regulating cellular metabolism and energy homeostasis including glycolysis in the cytosol, and the tri-carboxylic acid (TCA) cycle, OXPHOS, and fatty acid and amino acid oxidation in the mitochondria (Srivastava 2016). An increase in NAD^+ level by the supplementation of its precursors, such as NAM, NA, and NR, was reported to induce the activation of sirtuins (e.g., SIRT1 and SIRT3) accompanying the activation of transcriptional regulators (e.g., PGC-1α and FOXO) (Srivastava 2016) and increased mitochondrial biogenesis and function (Cantó and Auwerx 2012, Cantó, Houtkooper et al. 2012). Modulating NAD+ levels using these precursors may have benefits to protect cells from oxidative stress via enhancing mitochondrial function.

In this study, we observed that NAM stimulates osteoblast differentiation, and RNA-sequencing (RNA-seq) was performed to fully understand the mechanism underlying NAM-induced osteogenic differentiation. We demonstrate that NAM significantly

enhanced osteoblast differentiation by alleviating mitochondrial oxidative stress, and prevented ROS-induced osteoblast dysfunction.

Materials and Methods

Cell culture and osteoblast differentiation

MC3T3-E1 cells were cultivated in growth medium composed of α-MEM with 10% fetal bovine serum containing 100 U/mL penicillin and 100 μg/mL streptomycin. The cells were differentiated in osteogenic medium that was supplemented with 10 mM β-glycerophosphate and 50 μg/mL ascorbic acid in growth medium 65.

Reagents

30% hydrogen peroxide solution (H1009) add nicotinamide (N0636) were purchased from Sigma-Aldrich (St. Louis, MO, USA).

Alkaline phosphatase staining and alizarin red S staining

Alkaline phosphatase (ALP) staining and alizarin red S (ARS) staining were performed as described previously 3. Briefly, an ALP staining kit (COSMO BIO, Tokyo, Japan) was used and we performed the staining in accordance with the manufacturer's protocol. For the ARS staining, mineralized cells were fixed with 4% paraformaldehyde and stained with 0.5% alizarin red S staining solution, pH 4.2, for 10 min at room temperature.

Reverse Transcription and Quantitative Real-Time Polymerase Chain Reaction

Total RNA extraction from cells, reverse transcription and quantitative real-time polymerase chain reaction were performed

as described previously 66. Total RNA isolation was performed using RNeasy Mini Kit (Qiagen, Mannheim, Germany). Total RNA was reverse-transcribed into cDNA via the PrimeScriptTM RT Master Mix (Takara Bio, Shiga, Japan) The Takara SYBR Premix Ex Taq (Takara Bio) was used for qPCR in an Applied Biosystems 7500 RT-PCR system or a StepOnePlusTM Real-Time PCR System. The primes are listed in Supplemental Table 1.

Subcellular fractionation

NE-PERTM nuclear and cytoplasmic extraction reagents (Life Technologies, CA, USA) were used for nuclear-cytoplasmic fractionation, in accordance with the manufacturer's protocol. The mitochondrial fraction was isolated with Mitochondria/Cytosol Fractionation kit (abcam, Cambridge, UK), in accordance with the manufacturer's protocol.

siRNA transfection

When MC3T3-E1 cells reached approximately 70%-80% confluence, they were transfected with 100 nM siRNA using Lipofectamine RNAiMax Reagent (Invitrogen, USA) in accordance with the manufacturer's instructions 3.

Immunoprecipitation

Cell lysates were pre-cleared by incuabtion with PierceTM Protein G Magnetic Beads (Thermo ScientificTM, USA) for 30 min on a rotator at 4°C. The supernatant was incubated overnight with anti-acetyl lysine antibody (Cell Signaling Technology, USA) on a

rotator at 4℃. The Protein G Magnetic Beads were added to the supernatant and incubated for 2 h at 4℃. These beads were then collected and washed five times with lysis buffer, followed by the addition of protein sample buffer. The samples were subsequently boiled for 10 min and used for immunoblotting 67.

Immunoblotting

Cellular proteins obtained using a PRO-PREP protein extraction solution (iNtRON, South Korea) were used for immunoblotting (IB). The proteins were resolved by sodium dodecyl sulfate polyacrylamide gel electrophoresis (SDS-PAGE) and transferred through a polyvinylidene fluoride (PVDF) membrane. Then, 5% nonfat skim milk in PBS containing 0.05% Tween-20 was used for blocking. The membrane was incubated with primary and secondary antibodies and developed via the enhanced chemiluminescence method (ClarityTM Western ECL substrate; Bio-Rad, CA, USA). FUSION FX (VILBER, France) was used for visualization. IB was conducted using antibodies detecting cytochrome c, α-TUBULIN (Santa Cruz, Biotechnology, Inc, USA), PGC1α, UCP2, TRX2 (Proteintech, USA), Total OXPHOS Rodent WB Antibody Cocktail (abcam, UK), SOD2, FOXO3a and Phospho-FOXO3a (Ser253) (Cell Signaling Technology, USA).

Oxygen consumption rate

MC3T3-E1 cells were plated in XF 96-well microplates (Agilent Technologies, USA). Oxygen consumption was measured with an XF96 Extracellular Flux Analyzer (Agilent Technologies,

USA) and Seahorse XF Cell Mito Stress Test Kit. The oxygen consumption rate was measured using 1.5 μM oligomycin, 0.5 μM FCCP, and 0.5 μM rotenone/antimycin A. The results were normalized by counting the number of nuclei through Hoechst 33342 staining (Sigma-Aldrich, USA).

Biochemical analysis

The activity of SOD2 was measured using a Superoxide Dismutase Activity Assay kit (abcam, UK), in accordance with the manufacturer's protocol. The cellular ATP level was determined by using an ATLP bioluminescence assay kit (Sigma-Aldrich, USA) in accordance with the manufacturer's instructions.

Intracellular ROS determination

Cellular ROS were visualized using CellROXTM Deep Red Reagent (Invitrogen, USA) and observed by confocal microscopy (Zeiss, Germany). MitoSOXTM Red Reagent was used to determine the mitochondrial ROS level. Briefly, MC3T3-E1 cells were seeded on coverslips and cultured with 5 μM NAM in osteogenic medium and the cultured cells were then stained with 5 μM CellROXTM or MitoSOXTM diluted in HBSS for 20 min at 37℃. Hoechst 33342 was used to visualize the nucleus. The coverslips were washed three times with HBSS and observed by confocal microscopy (LSM 800 Airyscan; Zeiss, Germany).

Luciferase reporter assay

The transcription-activating activity of FOXO3a was

evaluated with the FHRE-Luc reporter gene purchased from Addgene. Passive lysis buffer, Bright-Glo Luciferase Assay System, and GloMax-Multi Detection System (Promega, USA) were used to measure luciferase activity 68.

Immunofluorescence staining and confocal microscopy

Immunofluorescence analysis was performed as described previously 3. In brief, cells were plated and cultured on coverslips. The cells were fixed, permeabilized and stained with the designated primary and secondary antibodies. After 4′,6-diamidino-2-phenylindole (DAPI) staining (Sigma-Aldrich, USA), the coverslips were mounted on slide glasses for visualization using an LSM 800 confocal microscope (Zeiss, Germany) 69.

Quantification of γH2AX foci

Quantification of γ-H2AX foci was performed as previously described 3. Briefly, cells were treated with 10 μM NAM in osteogenic medium and stained with anti- γH2AX antibody (Cell Signaling Technology, USA). The nucleus was stained with DAPI and visualized via confocal microscopy. The number and intensity of γ-H2AX foci were analyzed by ImageJ software. Cells with 10 or more foci with an intensity of ≥10,000 were counted.

Flow cytometry

Apoptosis was evaluated using an FITC Annexin V/Dead Cell Apoptosis Kit (Invtirogen, USA), in accordance with the manufacturer's instructions. MC3T3-E1 cells were treated with

H_2O_2 and NAM, and then harvested and washed with ice-cold PBS. The cells were stained with FITC-labeled annexin V and PI at RT for 10min and analyzed by a fluorescence-activated cell sorter flow cytometer (FACSverse; BD, USA). At least 20,000 cells were used for each experiment were performed in triplicate.

RNA-sequencing analysis

MC3T3-E1 cells were treated with 10 μM NAM in the presence or absence of 100 μM H_2O_2 for 4 or 10 days. Total RNA isolation was performed using a RNeasy Mini Kit. Total RNA concentration was calculated using Quant-IT RiboGreen (#R11490; Invitrogen). To assess the integrity of the total RNA, samples were run on the TapeStation RNA screentape (#5067-5576; Agilent). High-quality RNAs with RNA Integrity Number (RIN) greater than 7.0 were used for RNA library construction.

A library was independently prepared with 1 μg of total RNA for each sample using an Illumina TruSeq Stranded mRNA Sample Prep Kit (#RS-122-2101; Illumina, Inc., San Diego, CA, USA). The first step in the workflow involves purifying the poly-A containing mRNA molecules using poly-T-attached magnetic beads. Following purification, the mRNA was fragmented into small pieces using divalent cations under an elevated temperature. The cleaved RNA fragments were copied into first strand cDNA using SuperScript II reverse transcriptase (#18064014; Invitrogen) and random primers. This was followed by second strand cDNA synthesis using DNA Polymerase I, RNase H and dUTP. These cDNA fragments then underwent an end repair process, the addition

of a single 'A' base, and then ligation of the adapters. The products were then purified and enriched by PCR to create the final cDNA library.

The libraries were quantified using KAPA Library Quantification kits for Illumina Sequencing platforms, in accordance with the qPCR Quantification Protocol Guide (#KK4854; KAPA BIOSYSTEMS) and qualified using the TapeStation D1000 ScreenTape (# 5067-5582; Agilent Technologies). Indexed libraries were then submitted to Illumina NovaSeq (Illumina, Inc., San Diego, CA, USA), and paired-end (2×100 bp) sequencing was performed by Macrogen, Inc. (Seoul, South Korea).

RNA-sequencing data processing

Paired-end RNA-seq data obtained from three biological replicates were analyzed under the conditions of Vehicle (Veh), 10 μM NAM, 100 μM H_2O_2, and 100 μM H_2O_2 in combination with 10 μM NAM for 4 or 10 days with osteogenic medium in MC3T3-E1 preosteoblasts. The average read depth was 1.2 107 read pairs/sample. Reads were aligned to the mouse genome (mm10) using bcbio-nextgen (v1.2.9), which includes Bowtie2 (v2.2.5) 70, Samtools (v1.13) 71, and Sambamba (v0.8.2) 72,73. The expression calling was performed using Salmon (v1.7.0) 74 and Kallisto (v0.46.2) 75.

Differentially expressed gene (DEG), Gene Ontology (GO) and correlation analysis

DESeq2 (v1.32.0) 76 was performed for DEGs analysis with

adjust p value<0.05 and fold change>1.2. EnrichGO and gofilter of cluster profiler (v4.0.5) 77 were used for GO analysis. Correlation analysis was performed to determine the relationship among DEGs, included in GO analysis. This analysis used baseMean, log2 fold change, and statistical parameter information calculated by performing DEG analysis, through corrplot (v0.92) 78.

Statistics

Each experiment was performed at least two or three times, and representative results are shown in the figures. The significance of differences was evaluated by Student's t test with Prism 9 software (GraphPad Software, USA). Data are presented as mean ± SD, and differences were considered significant at $P < 0.05$. P values are as follows: $*P < 0.05$; $**P < 0.01$; $***P < 0.001$; $****P < 0.0001$.

Results

NAM stimulated osteoblast differentiation and mitochondrial respiration in osteoblasts

To investigate whether NAM promotes osteoblast differentiation, MC3T3-E1 osteoblasts were treated with NAM in osteogenic medium. As shown in Figure 1.1A, ALP and ARS staining showed that ALP activity and mineralization were enhanced in an NAM dose-dependent manner, and 10 μM NAM had the greatest effect on osteoblast differentiation (Figures 1.1B, C). The expression levels of marker genes of osteoblast differentiation including *Runx2, Osx, Dlx5*, *Bsp, Mepe*, *Opn* and *Ocn*, were significantly increased by NAM treatment (Figure 1.2). In particular, late osteoblast differentiation markers, *Ocn*, *Opn*, and *Mepe*, were very highly stimulated by NAM treatment.

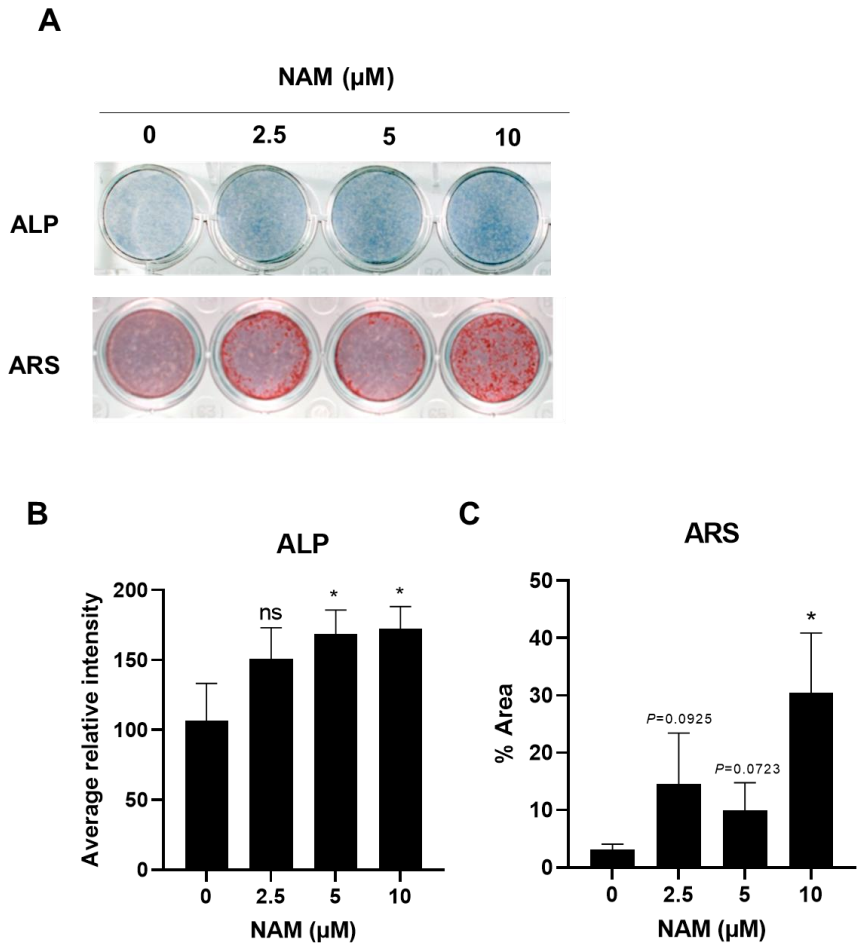

Figure 1.1. Nicotinamide (NAM) stimulated osteoblast differentiation.

(A) ALP and Alizarin Red S (ARS) staining were performed in MC3T3-E1 cells cultured in osteogenic media supplemented with the indicated concentrations for NAM for 5 and 12 days, respectively. (B-C) Quantification of each staining was performed by ImageJ. Data are expressed as mean ± SD. NAM, nicotinamide. *P<0.05. **P<0.01. ***P<0.001. ****P<0.0001. ns, not significant.

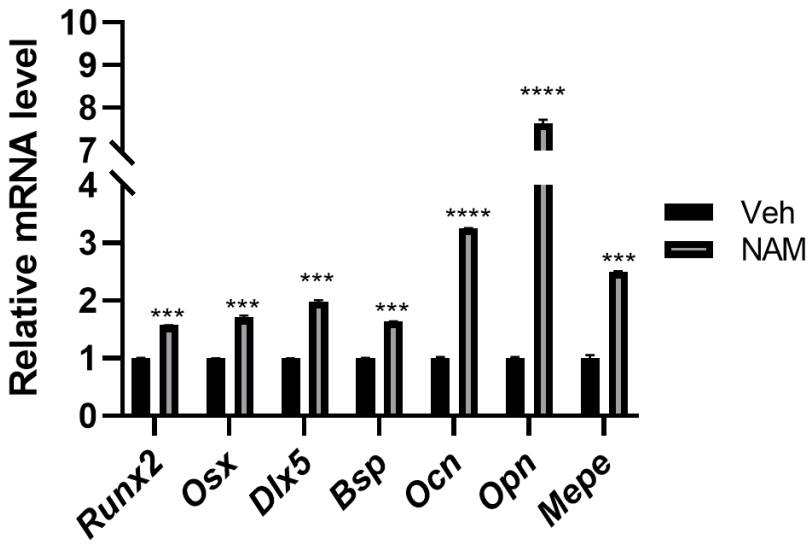

Figure 1.2. NAM increased the expression of osteogenic marker genes in MC3T3-E1 cells.

MC3T3-E1 cells cultured in osteogenic media supplemented with the indicated concentrations for 10 μM NAM for 12 days, respectively. The mRNA levels of osteoblast differentiation marker genes were determined by RT-qPCR. Data are expressed as mean ± SD. NAM, nicotinamide. *P<0.05. **P<0.01. ***P<0.001. ****P<0.0001. ns, not significant.

To understand the mechanism by which NAM-stimulated osteoblast differentiation, MC3T3-E1 cells were treated with or without NAM during osteogenic differentiation for 4 or 10 days, followed by RNA sequencing analysis (RNA-seq). In total, the number of differentially expressed genes (DEGs) was higher on day 10 (3,858 genes) than on day 4 (2,246 genes). MA plots showed differential gene expression and the genes congregated around log2 fold change 0.5 (approximately 1.4 times) on both days (Figures 1.3A-B). Consistent with the results shown in Figure 1.1 and Figure 1.2, Gene Ontology (GO) analysis on the DEGs upregulated by NAM treatment showed the enrichment of GO terms regarding osteoblast differentiation and regulation of ossification on both day 4 and day 10 (Figure 1.3C).

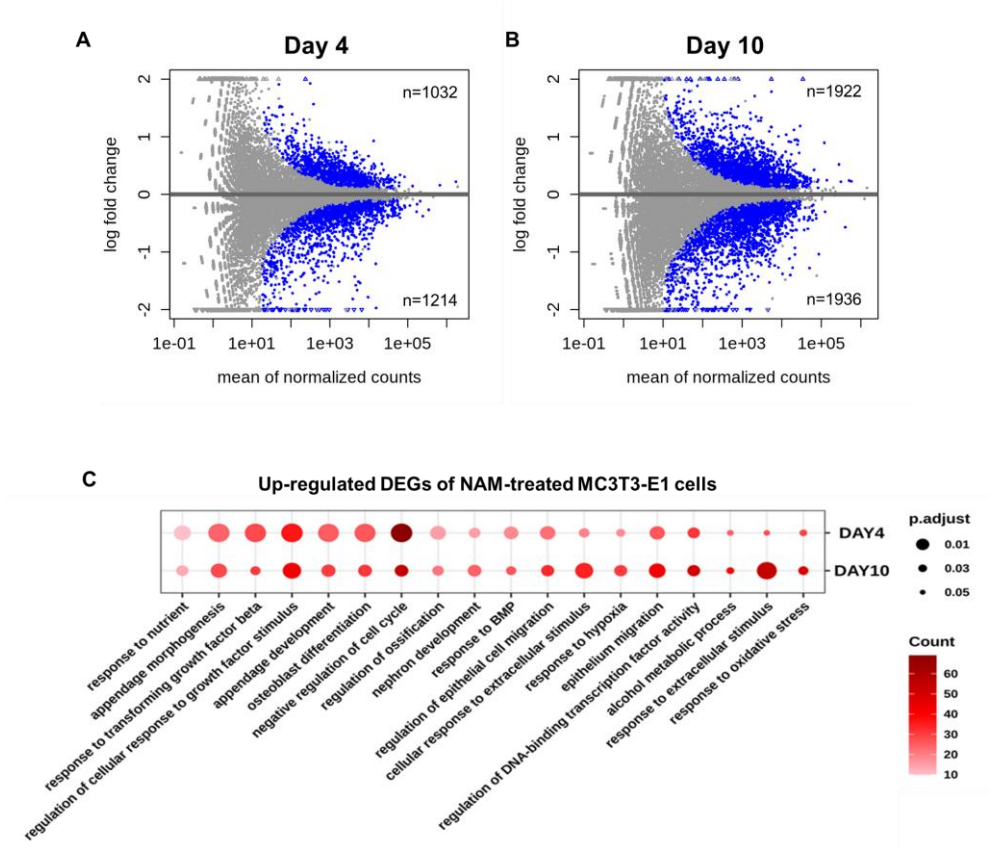

Figure 1.3. RNA-seq analysis on the DEGs regulated by NAM treatment for 4 or 10 days in MC3T3-E1 cells.

(A-B) The differential expression of genes by 10 μM NAM were visualized using MA plots on day 4 (A) and day 10 (B).

(C) GO analysis was performed using upregulated and downregulated DEGs by NAM on day 4 and 10. GO terms were selected and sorted based on enrichment score.

Given that gene expression correlation analysis can be used to identify functional correlations between genes (Oliver, Lukic et al. 2014, Miller and Bishop 2021), correlation analysis of DEGs upregulated by NAM was performed here to identify genes associated with NAM-induced osteoblast differentiation (Figures 1.4A and 1.6A). On day 4, osteoblast differentiation and response to oxygen level showed correlation in cluster 4 (Figure 1.5D). Furthermore, genes related to the cell cycle were highly enriched in all clusters (Figure 1.4B). On day 10, oxidative stress-related genes were included in all clusters (Figure 1.6B), and we found that osteoblast differentiation and response to oxidative stress were associated together in cluster 4 (Figure 1.7D). The genes affiliated with cluster 4 were shown using a heatmap (Figure 1G). These genes included *Ndufa6*, *Gpx8*, and *Foxo3a*, which are involved in regulating oxidative stress as well as *Sod2*, which encodes a mitochondrial antioxidant enzyme. These results suggested that the enhancement of osteoblast differentiation by NAM might be related to the regulation of oxidative stress.

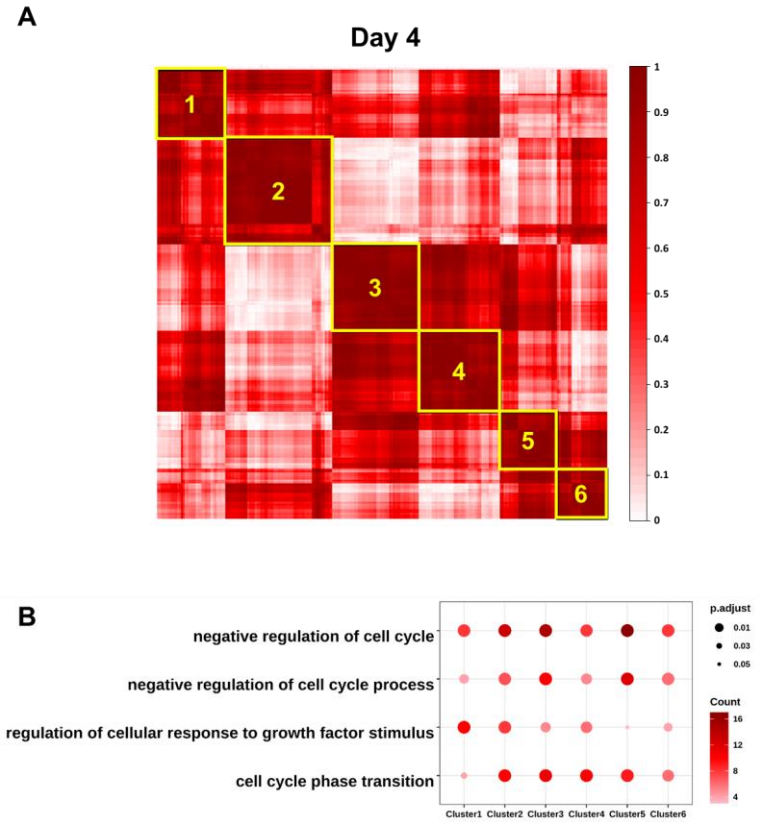

Figure 1.4. Correlation analysis of DEGs upregulated by NAM in MC3T3-E1 cells on day 4.

(A) Correlation analysis of upregulated genes by NAM on day 4. A normalized correlation matrix was performed to show correlation among genes.

(B) GO analysis was performed with genes included in each cluster. GO terms commonly included in all clusters are indicated.

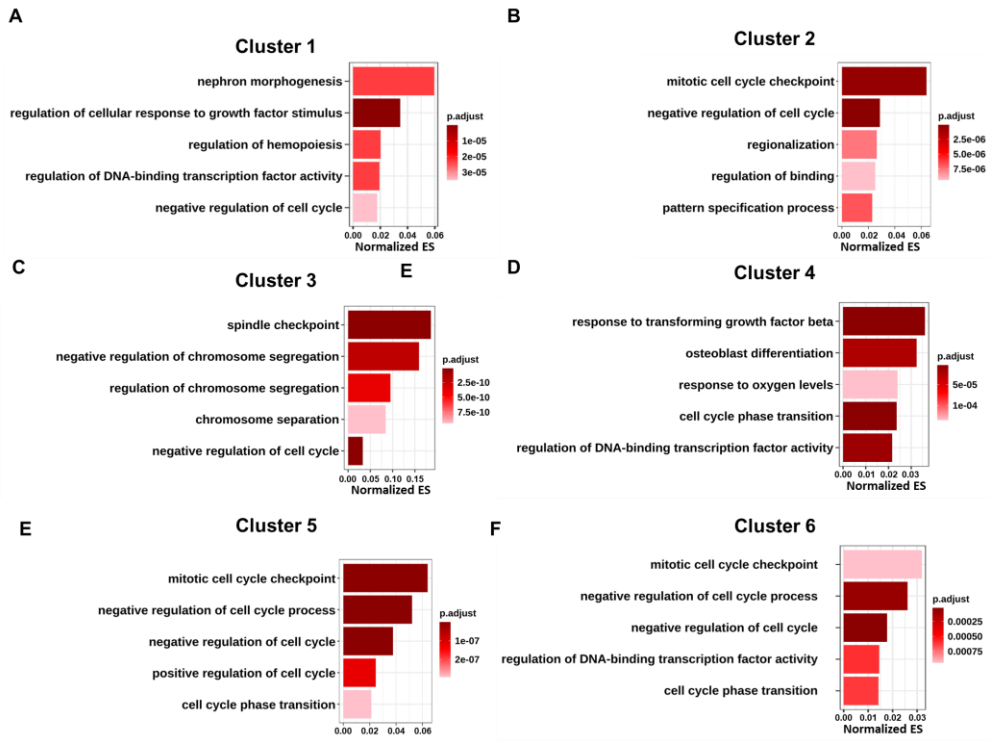

Figure 1.5. GO analysis of genes clustered by correlation analysis on day 4. Related to figure 1.4.

(A–F) GO analysis of genes enriched in each cluster are displayed.

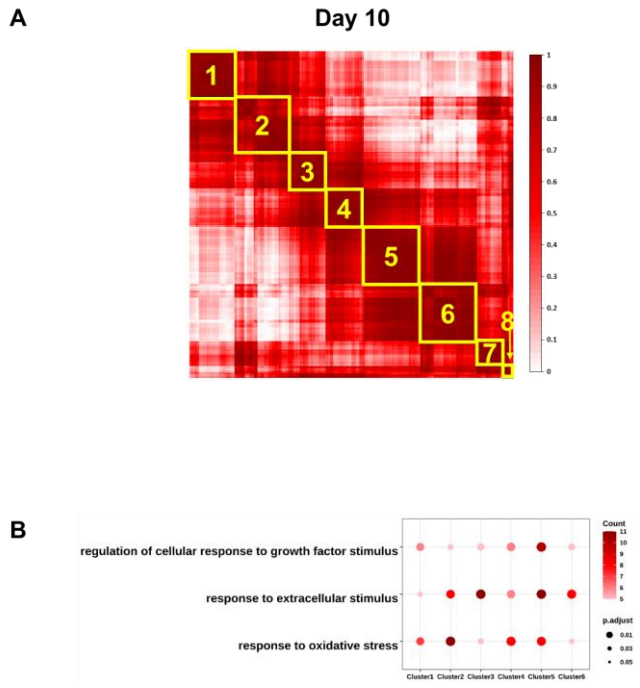

Figure 1.6. Correlation analysis of DEGs upregulated by NAM in MC3T3-E1 cells on day 10.

(A) Correlation analysis of upregulated genes by NAM on day 10. A normalized correlation matrix was performed to show correlation among genes.

(B) GO analysis was performed with genes included in each cluster. GO terms commonly included in all clusters are indicated.

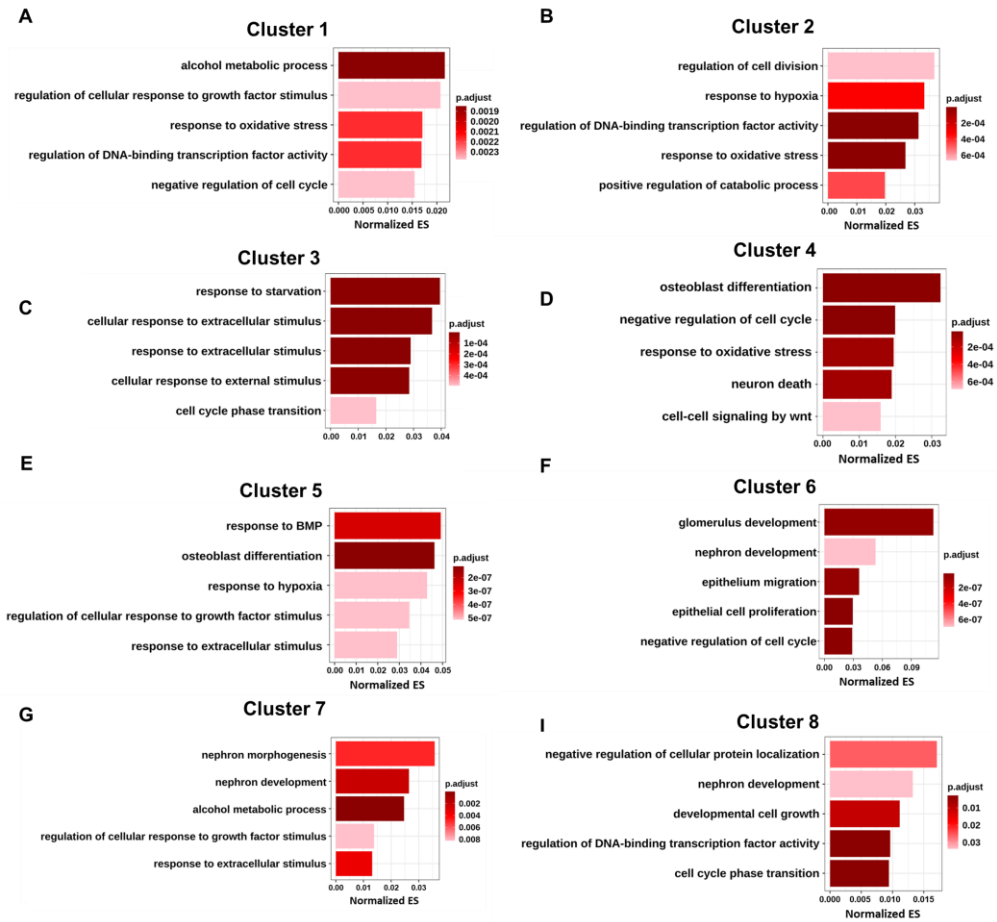

Figure 1.7. GO analysis of genes clustered by correlation analysis on day 10. Related to figure 1.6.

(A–F) GO analysis of genes enriched in each cluster are displayed.

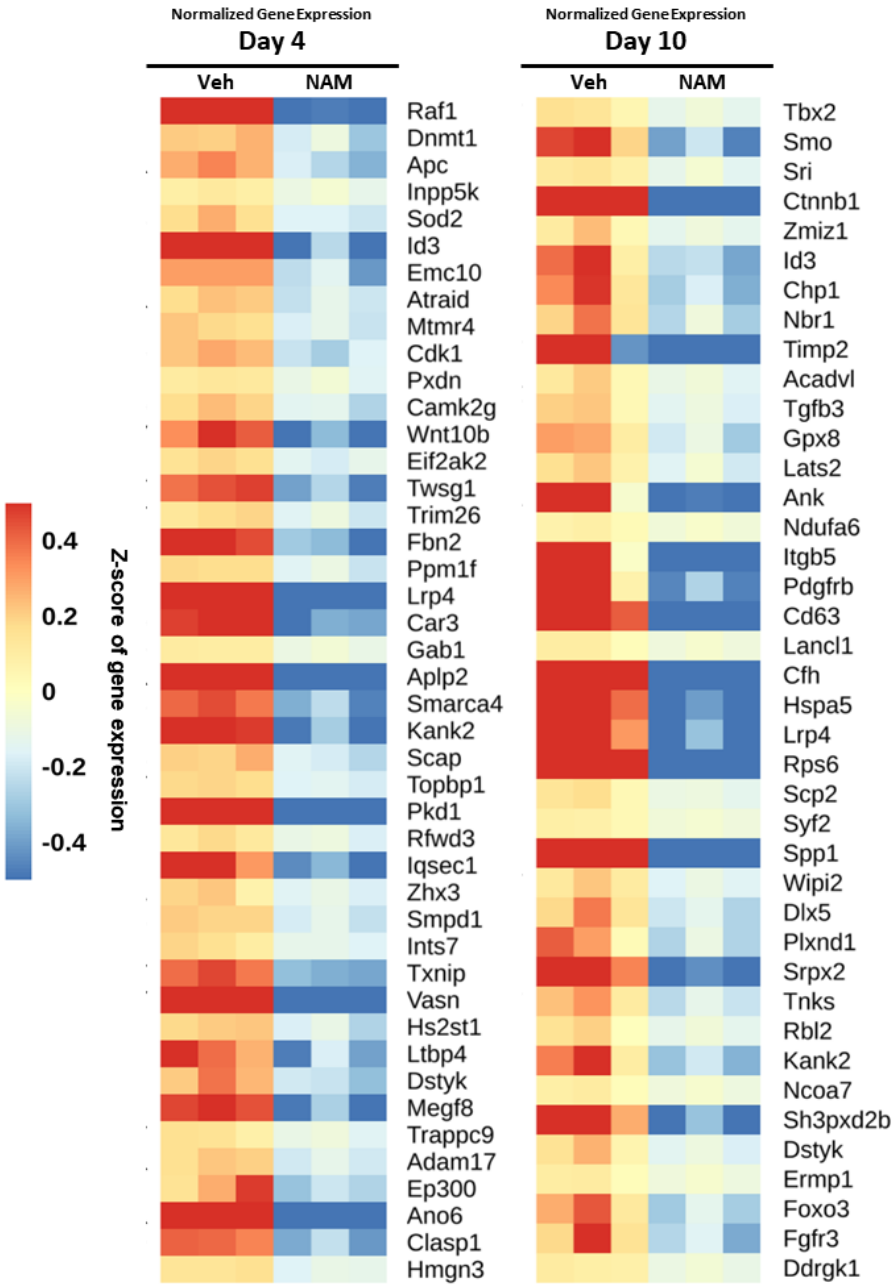

Figure 1.8. Heat map of the genes affiliated with cluster 4 on day 4 and day 10.

Heatmap of the genes included in Figure 1.5D and 1.7D are shown, respectively. Z-score normalization was performed based on statistics calculated by DEseq2. NAM, nicotinamide.

NAM relieves mitochondrial ROS by enhancing mitochondrial antioxidant enzymes

To determine the effect of NAM on the cellular oxidative stress level, MC3T3-E1 cells were stained with a fluorogenic probe, CellROX™, which measures the ROS level in the cytosol, and MitoSOX™, which measures superoxide production in mitochondria. We observed that NAM treatment significantly reduced the accumulation of ROS in the cytosol (Figures 1.9A and B) and superoxide production in the mitochondria (Figures 1.9C and D).

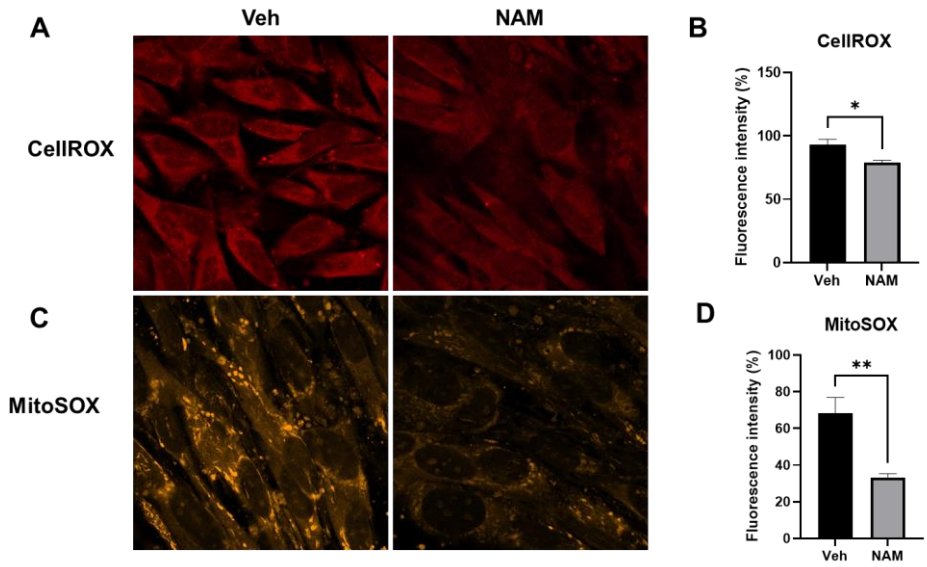

Figure 1.9. NAM reduces cellular and mitochondrial ROS.

(A) The oxidative stress in MC3T3-E1 cells was determined by CellROX^{TM} reagent after 10 μM NAM treatment with osteogenic media for 7 d. (B) The fluorescence intensity of (A) was calculated via ImageJ. (C) Mitochondrial superoxide was detected by MitoSOX^{TM} mitochondrial superoxide indicator in MC3T3-E1 cells after 10 μM NAM treatment in osteogenic media. (D) The fluorescence intensity of (C) was measured by ImageJ. Data are expressed as mean ± SD. NAM, nicotinamide. *P<0.05. **P<0.01. ***P<0.001. ****P<0.0001. ns, not significant.

PGC1-α is a transcriptional coactivator that plays a central role in the expression of genes acting against oxidative stress in combination with FOXO3a (Olmos, Valle et al. 2009). PGC1α is also known to promote mitochondrial biogenesis and enhances the capacity of cells to detoxify ROS, allowing cells to efficiently produce ATP and respire with less oxidative stress (Austin and St-Pierre 2012). For this reason, we measured the mRNA levels of *Pgc1-α* and its downstream detoxifying genes in MC3T3-E1 cells treated with NAM for 4 and 7 days. NAM increased the expression levels of *Pgc1-α*, *Ucp2*, *Trx2*, *Sod1* and *Sod2* in differentiating MC3T3-E1 cells (Figures 1.10A-E). NAM also significantly increased the enzymatic activity of SOD2, a key mitochondrial antioxidant enzyme, in differentiating MC3T3-E1 osteoblast cells (Figure 1.10F).

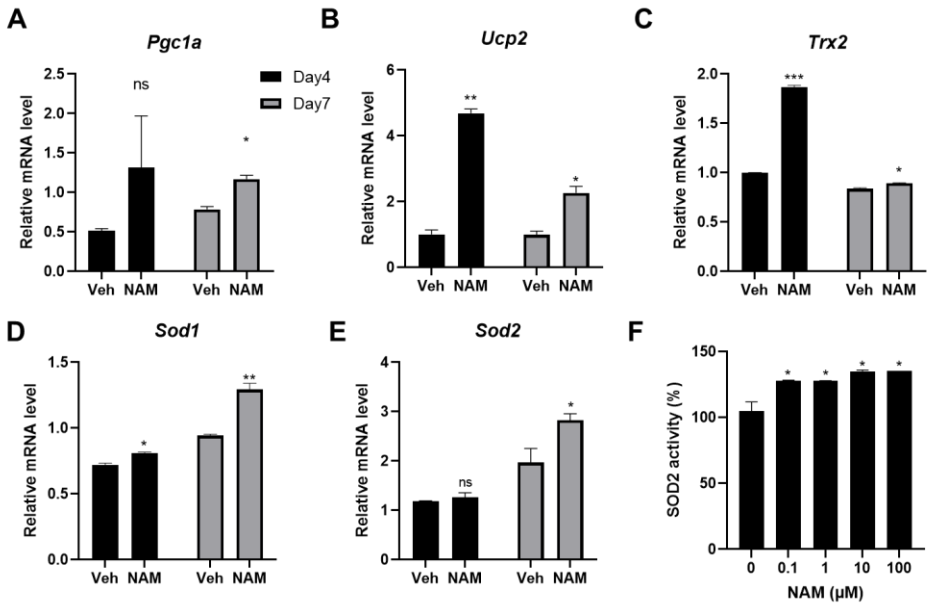

Figure 1.10. NAM stimulated the expression of antioxidant enzymes. (A–E) The mRNA expression level of *Pgc1-α* and ROS scavenger enzymes in MC3T3-E1 cells cultured in osteogenic medium supplemented with or without 10 μM NAM for 4 and 7 d was determined by RT-qPCR. (F) The mitochondrial fraction was isolated from the culture of the same condition to measure SOD2 enzymatic activity. Data are expressed as mean ± SD. NAM, nicotinamide. *P<0.05. **P<0.01. ***P<0.001. ****P<0.0001. ns, not significant.

To investigate whether NAM upregulates the expression of ROS-detoxifying enzymes through Pgc1-α, MC3T3-E1 cells were treated with small interfering RNAs (siRNAs) targeting *Pgc1-α* were treated in MC3T3-E1 cells. siPgc1α efficiently knocked down the expression of *Pgc1-α* and NAM increased *Pgc1-α* expression in both siCtrl- and siPgc1-α-transfected MC3T3-E1 cells (Figure 1.11A). As previously reported, *Pgc1-α* knockdown significantly decreased the mRNA levels of *Ucp2*, *Trx2*, *Sod1* and *Sod2* (Figures 1.11B-E). The increase of the expression of mRNAs encoding ROS-detoxifying enzyme by NAM in siPgc1α-transfected cells was much lower than that in siCtrl-transfected cells.

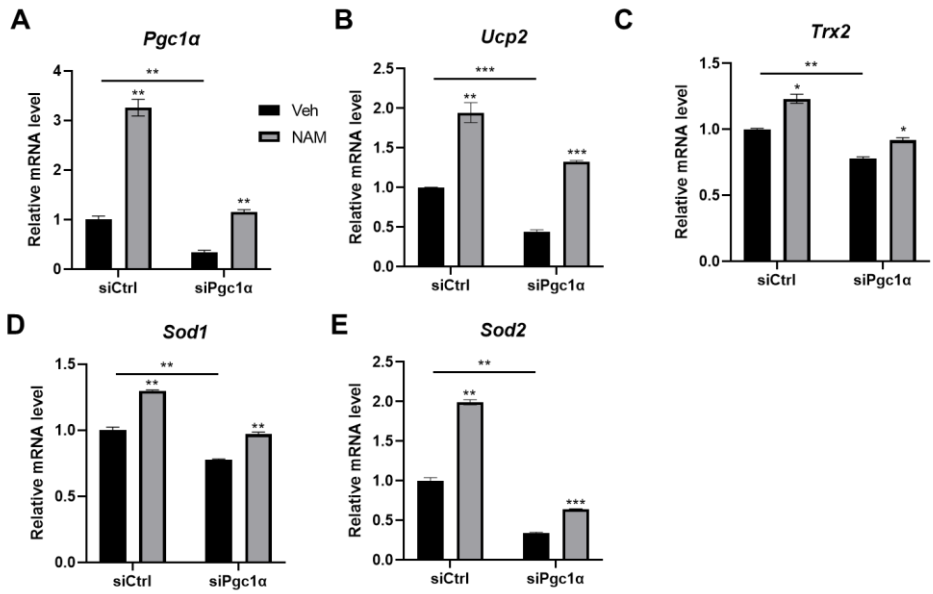

Figure 1.11. *Pgc1−α* knockdown decreased the expression of ROS scavenger enzymes.

(A−E) To understand the influence of Pgc1−α to the ROS scavenger enzyme gene expression, MC3T3−E1 cell transfected with siCtrl or siPgc1α were cultured in osteogenic media with or without 10 μM NAM for 4 d. Data are expressed as mean ± SD. NAM, nicotinamide. *P<0.05. **P<0.01. ***P<0.001. ****P<0.0001. ns, not significant.

Consistent with this, the protein levels of ROS-detoxifying enzymes were increased by NAM treatment in MC3T3-E1 osteoblast cells (Figure 1.12). These results suggest that NAM relieves mitochondrial oxidative stress by inducing the expression of antioxidant enzymes.

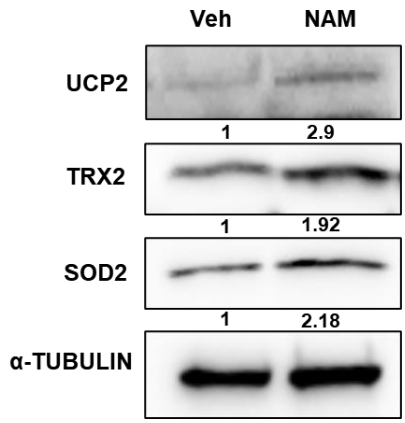

Figure 1.12. NAM increased the protein expression level of antioxidant enzymes.

MC3T3-E1 cells were cultured in osteogenic media with or without 10 μM NAM for 7 d. The protein expression level of ROS scavenger enzymes was determined by immunoblot analysis. NAM, nicotinamide.

NAM induces antioxidant enzymes expression through SIRT3/FOXO3a axis.

Treatment with nicotinamide riboside (NR), one of the NAD^+ precursors, is known to increase NAD^+ levels and activate SIRT3, an NAD^+-dependent protein deacetylase (Brown, Maqsood et al. 2014). NAM was also found to activate SIRT1, resulting in improved liver function. (Wan, Li et al. 2018). Because SIRT3 is located in the mitochondria and regulates mitochondrial functions (Zhang, Xiang et al. 2020), we tested whether NAM treatment also promotes SIRT3 activity in osteoblast cells. MC3T3-E1 osteoblast cells were treated with NAM and the mitochondrial fraction was isolated to determine mitochondrial SIRT3 activity. The results showed that such activity was increased by NAM treatment in a dose-dependent manner in MC3T3-E1 cells (Figure 1.13A). The mRNA level of *Sirt3* was also significantly upregulated by treatment with 10 μM NAM in MC3T3-E1 cells (Figure 1.13B).

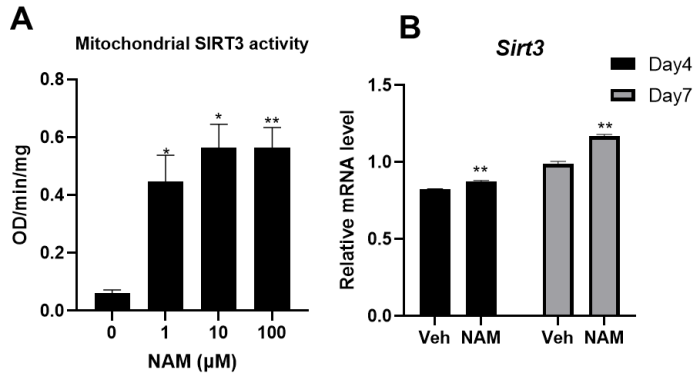

Figure 1.13. NAM stimulated the activity and expression of *Sirt3*. (A) Mitochondrial fraction was isolated after 10 μM NAM treatment with osteogenic media. SIRT3 activity was determined with the mitochondrial fraction via SIRT activity assay kit. (B) MC3T3-E1 cells were treated with 10 μM NAM in osteogenic media for 4 and 7 d. The mRNA level of *Sirt3* was determined by RT-qPCR. Data are expressed as mean ± SD. NAM, nicotinamide. *P<0.05. **P<0.01. ***P<0.001. ****P<0.0001. ns, not significant.

SIRT3 promotes the transcription-activating activity of FOXO3a, by decreasing the latter ' s acetylation and phosphorylation, which in turn induces the expression of genes encoding anti-oxidant enzymes (Kenny and Germain 2017, Sidorova-Darmos, Sommer et al. 2018). We investigated whether NAM regulates the activity of FOXO3a by using FOXO3a reporter, FHRE-Luc plasmids. NAM significantly increased both the endogenous FOXO3a transactivation activity (Figure 1.14A), and the activity of exogenous transfected FOXO3a transcription-activating activity in MC3T3-E1 osteoblast cells (Figure 1.14B).

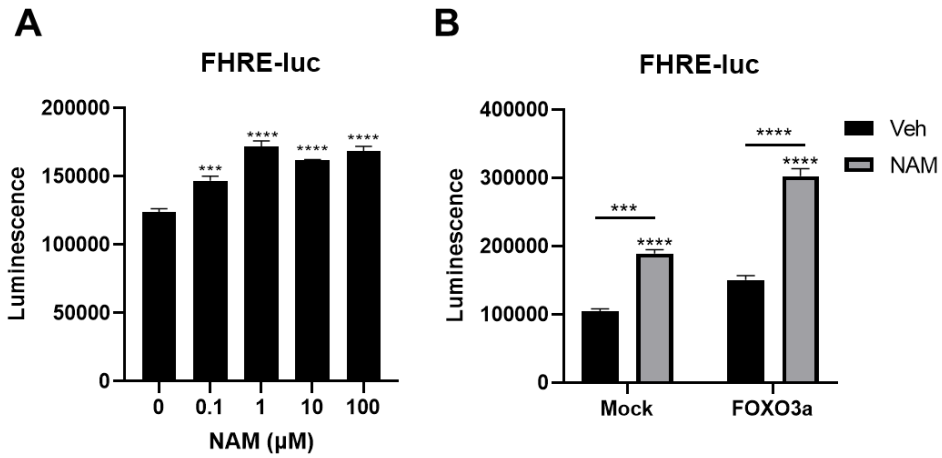

Figure 1.14. NAM increased transcriptional activity of FOXO3a.

(A) The transacting activity of FOXO3a was measured in MC3T3-E1 cells transfected with a FHRE-Luc after NAM treatment. (B) The luciferase activity was determined followed by co-transfection of a FHRE-Luc and a control plasmid (pcDNA3.1) or with plasmids expressing FOXO3a and treatment of NAM. Data are expressed as mean ± SD. NAM, nicotinamide. *P<0.05. **P<0.01. ***P<0.001. ****P<0.0001. ns, not significant.

SIRT3 physically interacts with FOXO3 in mitochondria and promotes the transcriptional activity of FOXO3a(Jacobs, Pennington et al. 2008). SIRT3 regulates the deacetylation of FOXO3a, followed by the reduction of its phosphorylation, ubiquitination, and degradation (Tseng, Wu et al. 2014). Moreover, the FOXO3a-dependent mitochondrial enzymes, such as SOD2, Prx3, Prx5 and Trx2, are involved in ROS detoxification. The acetylation of FOXO3a was diminished by NAM treatment in MC3T3-E1 cells (Figure 1.15A). The de-phosphorylation of FOXO3a at S253 was also reported to stimulate the translocation of FOXO3a from the cytoplasm to the nucleus (Tseng, Wu et al. 2014, Kim, Lee et al. 2017). The phosphorylation level of FOXO3a (S253) was decreased by NAM in a dose-dependent manner without affecting the FOXO3a protein level (Figure 1.15B). Next, we examined whether NAM regulates the subcellular localization of FOXO3a. The NAM treatment increased the translocation of FOXO3a from the cytoplasm to the nucleus in MC3T3-E1 cells (Figure 1.15C). Taking these findings together, NAM activates SIRT3 and FOXO3a, which in turn promotes the expression of mitochondrial antioxidant enzymes to facilitate ROS detoxification in osteoblasts.

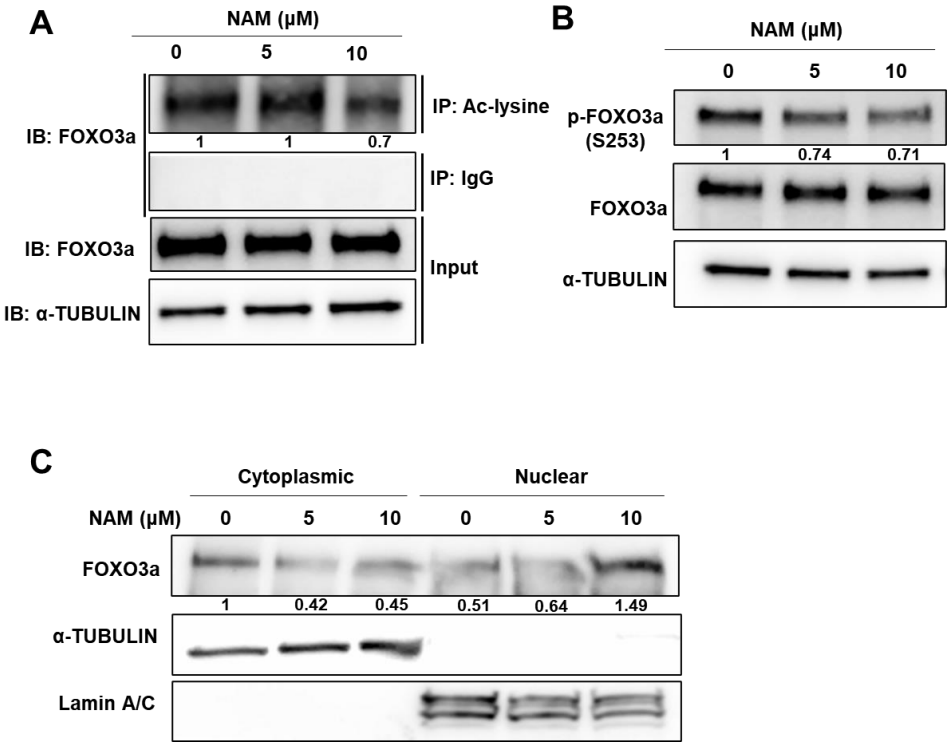

Figure 1.15. NAM increased the activity of FOXO3a by regulating its post-translational modification.

(A) The acetylation level of FOXO3a was determined by immunoprecipitation (IP) with acetylated-lysine antibody followed by immunoblot analysis with FOXO3a antibody. (B) MC3T3-E1 cells were treated with the indicated concentrations of NAM in osteogenic media and cell lysates were immunoblotted with the p-FOXO3a (S253) and FOXO3a antibody. (C) MC3T3-E1 cells were treated with NAM in osteogenic media for 4 d, followed by subcellular fractionation. The subcellular localization of FOXO3a was determined by immunoblot analysis. NAM, nicotinamide.

NAM improved mitochondrial function during osteoblast differentiation.

Excessive oxidative stress reduces mitochondrial function in osteoblasts (Ding, Zhao et al. 2016). Therefore, we tested whether NAM also regulates mitochondrial function in osteoblasts. First, to investigate the effect of osteoblast differentiation on mitochondrial respiration, we measured the oxygen consumption rate (OCR) before differentiation (day 0) and on days 4, 7, and 14 of differentiation of MC3T3-E1 cells. OCR significantly increased during the differentiation period (Figures 1.16A-H).

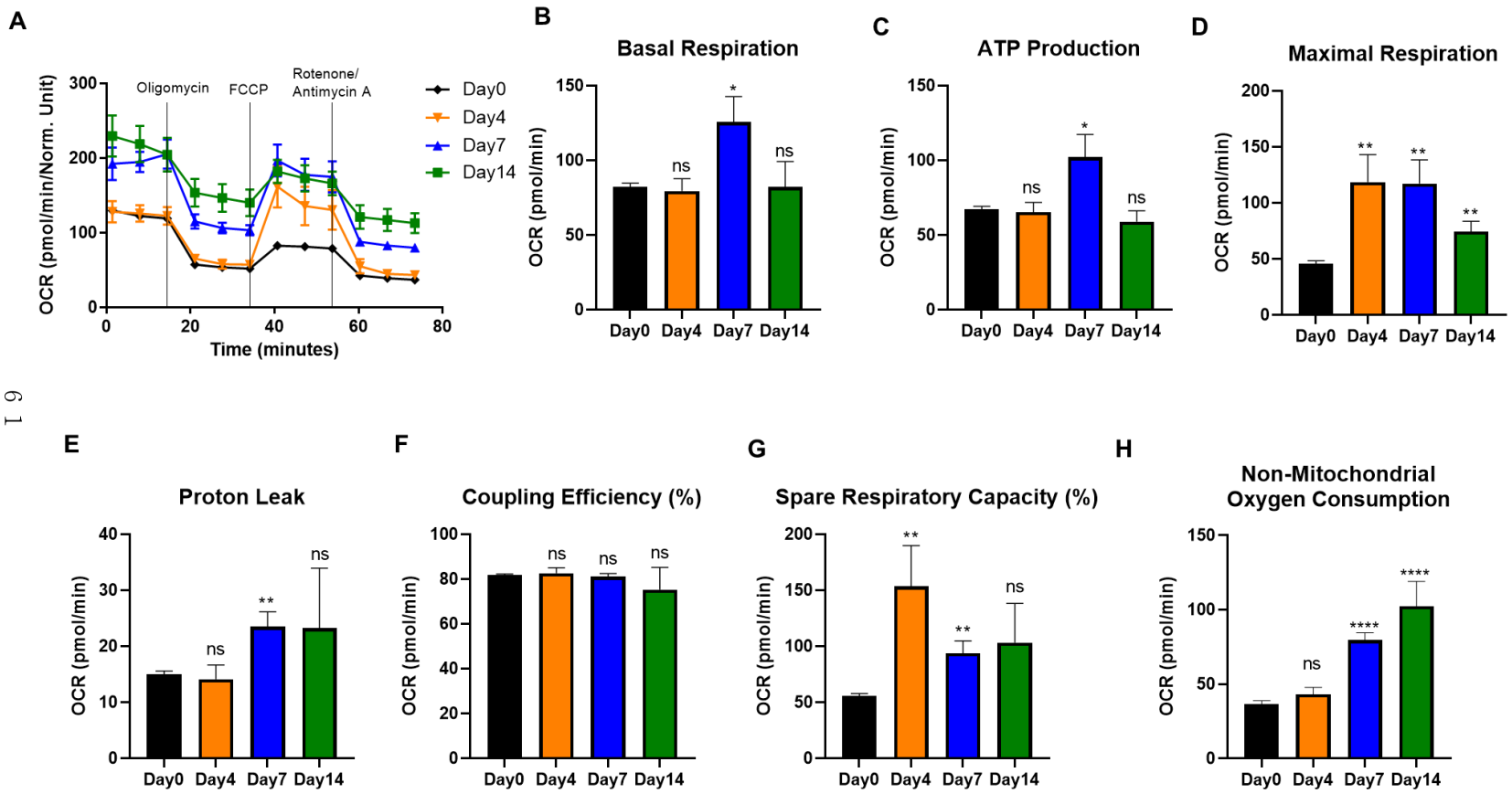
A
OCR (pmol/min/Norm. Unit)
Oligomycin
FCCP
Rotenone/
Antimycin A
Day0
Day4
Day7
Day14
Time (minutes)
B
Basal Respiration
C
ATP Production
D
Maximal Respiration
OCR (pmol/min)
E
Proton Leak
F
Coupling Efficiency (%)
G
Spare Respiratory Capacity (%)
H
Non-Mitochondrial
Oxygen Consumption
ns

Figure 1.16. The measurement of mitochondrial respiration during osteoblast differentiation using XF96 Extracellular Flux Analyzer.

(A) MC3T3-E1 cells were cultivated in osteogenic medium for indicated days and the Oxygen Consumption Rate (OCR) was measured with an XF96 Extracellular Flux Analyzer ($n \geq 3$). The summary of curved OCR plot (A) was calculated and displayed with bar plots (B-H). Data are expressed as mean ± SD. NAM, nicotinamide. $*P<0.05$. $**P<0.01$. $***P<0.001$. $****P<0.0001$. ns, not significant.

As NAM improved mitochondrial respiration in undifferentiated osteoblasts (Figures 1.17A–H), we investigated whether it can reinforce it in differentiating osteoblast cells. NAM was applied to MC3T3–E1 cells during osteogenic differentiation. NAM increased the OCR in differentiating MC3T3–E1 cells cultured in differentiation medium for 7 days (Figures 1.18A–H).

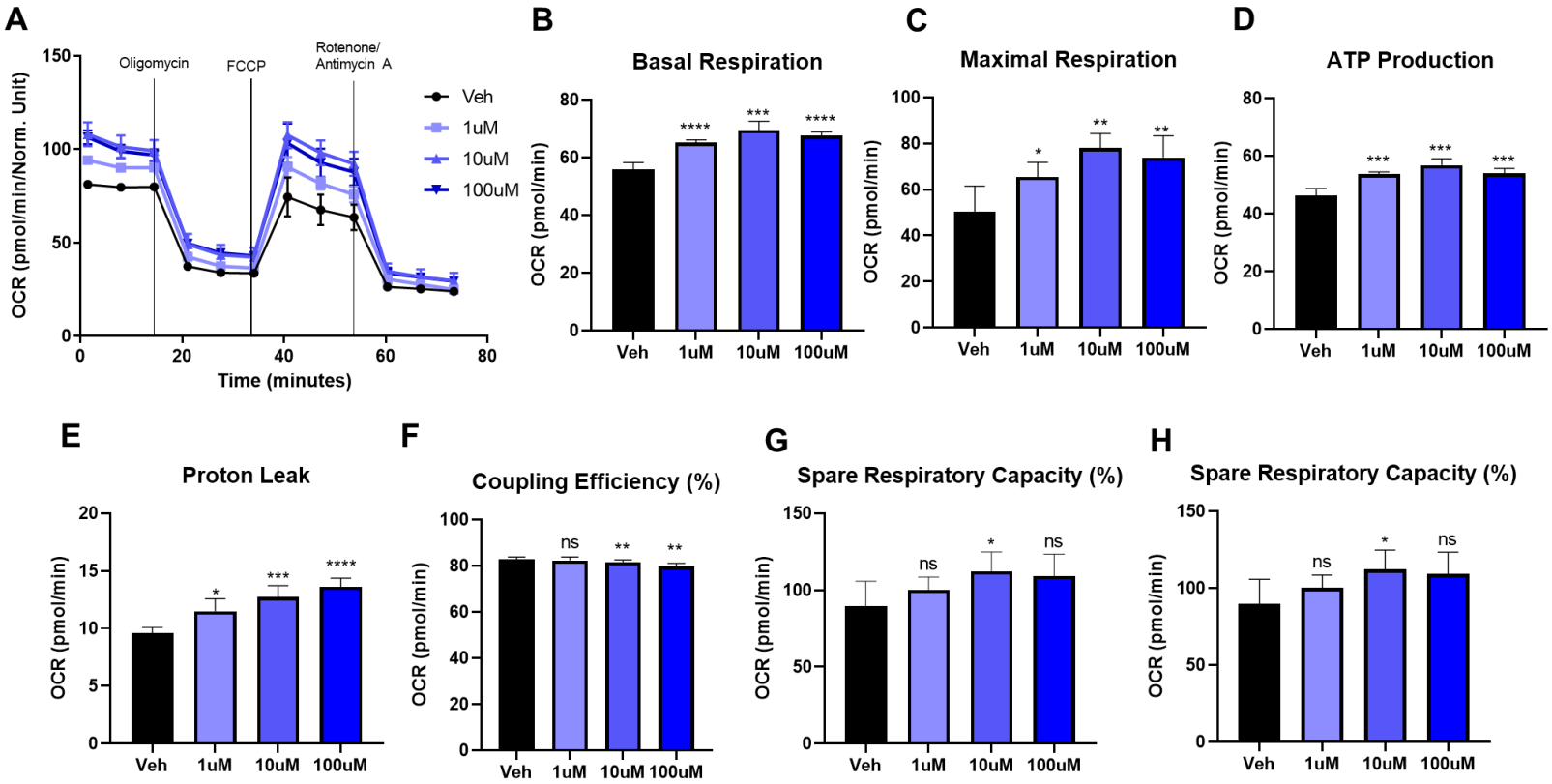
A
OCR (pmol/min/Norm. Unit)
Oligomycin
FCCP
Rotenone/
Antimycin A
Veh
1uM
10uM
100uM
Time (minutes)
B
Basal Respiration
C
Maximal Respiration
D
ATP Production
OCR (pmol/min)
Veh
1uM
10uM
100uM
E
Proton Leak
F
Coupling Efficiency (%)
G
Spare Respiratory Capacity (%)
H
Spare Respiratory Capacity (%)
ns

Figure 1.17. NAM enhances mitochondrial function in undifferentiated osteoblasts.

(A) MC3T3-E1 cells were cultivated in growth medium for 1 day and the OCR was measured with an XF96 Extracellular Flux Analyzer ($n \geq 3$). The summary of curved OCR plot (A) was calculated and displayed with bar plots (B-H). Data are expressed as mean ± SD. NAM, nicotinamide. $*P<0.05$. $**P<0.01$. $***P<0.001$. $****P<0.0001$. ns, not significant.

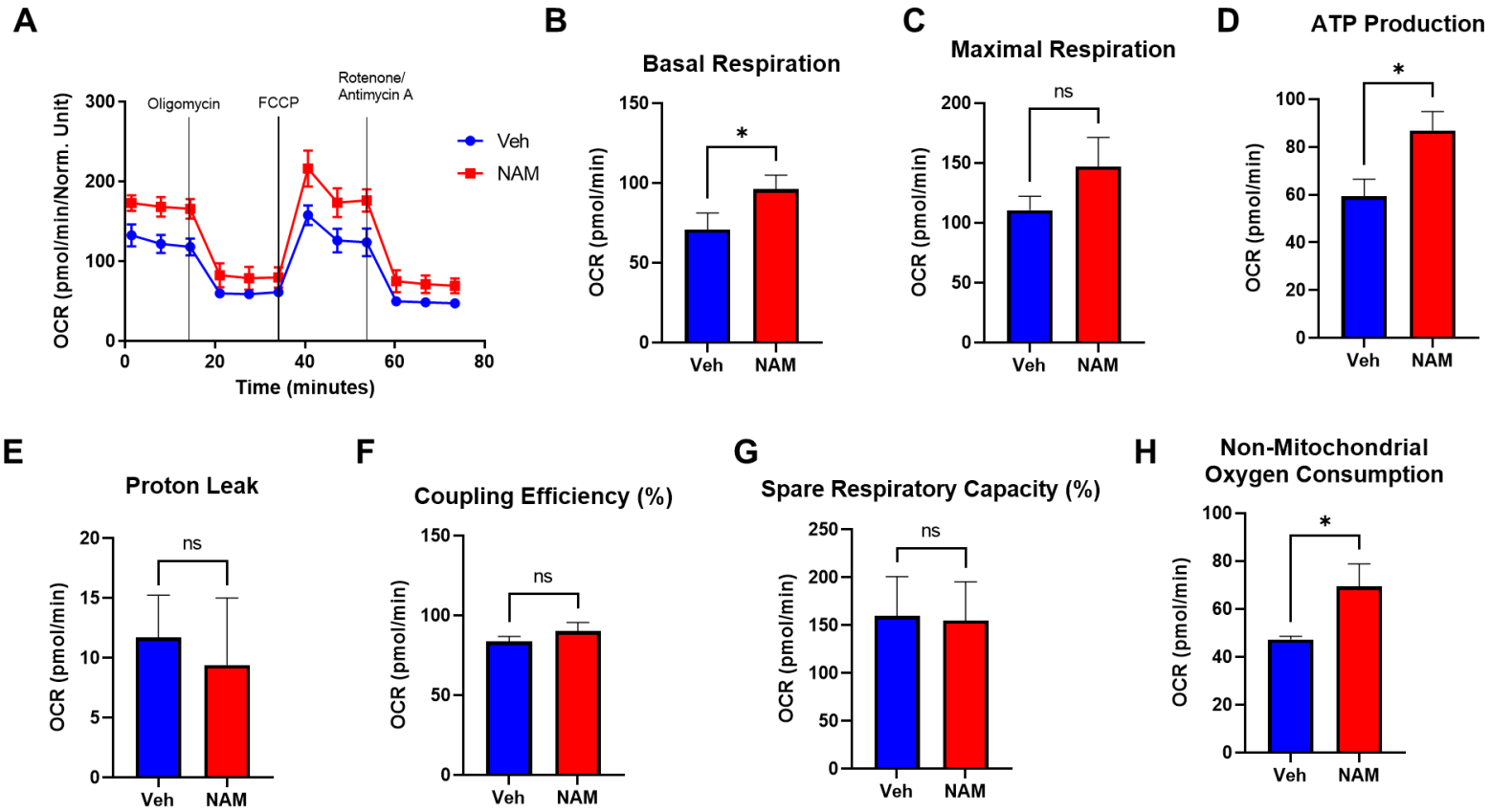
A
OCR (pmol/min/Norm. Unit)
Oligomycin
FCCP
Rotenone/
Antimycin A
Veh
NAM
Time (minutes)
B
Basal Respiration
OCR (pmol/min)
C
Maximal Respiration
ns
D
ATP Production
E
Proton Leak
F
Coupling Efficiency (%)
G
Spare Respiratory Capacity (%)
H
Non-Mitochondrial
Oxygen Consumption

Figure 1.18. NAM enhances mitochondrial function in osteoblast differentiation.

MC3T3-E1 cells were cultured in the osteogenic medium supplemented with or without 10 uM NAM for 7 days, and OCR was measured and the meaning of which was analyzed with the bar plots. The summary of curved OCR plot (A) was calculated and displayed with bar plots (B-H). Data are expressed as mean ± SD. NAM, nicotinamide. $*P<0.05$. $**P<0.01$. $***P<0.001$. $****P<0.0001$. ns, not significant.

Because the mitochondrial OCR was increased by NAM treatment, we investigated the changes in expression of mitochondrial biogenesis-related marker proteins. The protein levels of cytochrome c and peroxisome proliferator-activated receptor γ coactivator-1α (PGC-1α) were increased by treatment with 10 μM NAM during the differentiation of MC3T3-E1 cells for 7 days (Figure 1.19A). In addition, the levels of other oxidative phosphorylation-related proteins were examined using an antibody cocktail that recognizes subunits of each mitochondrial respiratory chain complex, Complex I subunit NDUF88, Complex II SDHB, Complex III UQCRC2, Complex IV MTCO1, and Complex V ATP5a. NAM increased the protein levels of all subunits of complexes I-V compared with the findings from vehicle-treated cells (Figure 1.19B). We further quantified the ratio of mtDNA:nDNA after amplification of the mitochondrial and nuclear genomes, as another representative marker of mitochondrial biogenesis (Malik, Czajka et al. 2016, Quiros, Goyal et al. 2017, Popov 2020). The results showed that NAM significantly increased this ratio (Figure 1.19C). Consistent with this, NAM treatment also significantly increased the ATP level in MC3T3-E1 osteoblast cells (Figure 1.19D). These results indicate that NAM enhances mitochondrial function, which plays an important role in supplying the energy necessary for osteogenic differentiation.

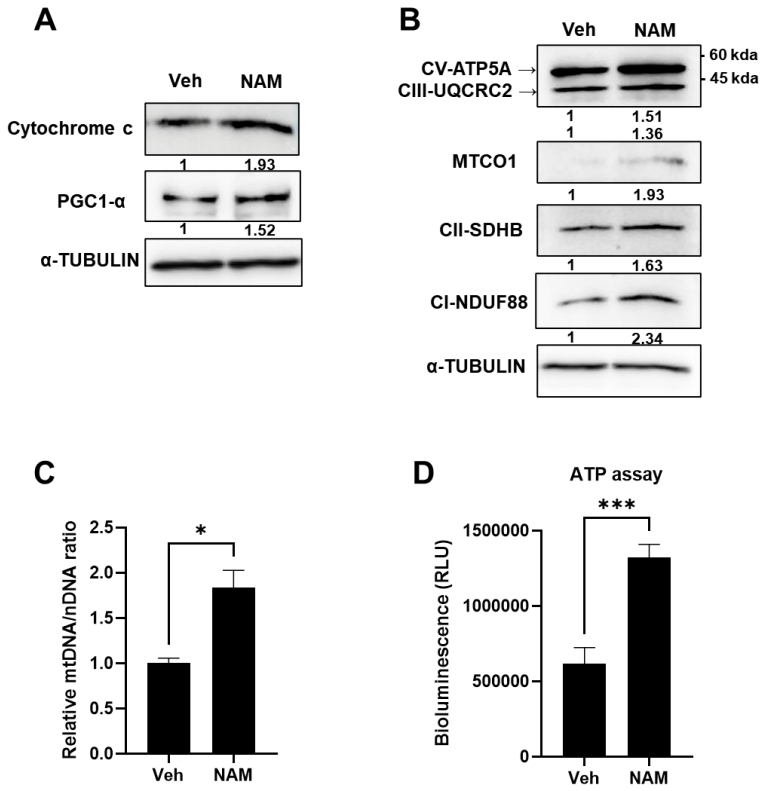

Figure 1.19. NAM enhances mitochondrial function in osteoblast differentiation.

(A) The protein expression level of Cytochrome C and PGC1-α in the same culture condition was assessed by immunoblot analysis. (B) The protein levels of OXPHOS mitochondrial complexes were measured by immunoblot analysis using total OXPHOS Rodent WB antibody cocktail. (C) The relative copy number of mitochondrial DNA (mtDNA) and nuclear DNA (nDNA) from the same culture condition was evaluated by RT-qPCR. The mtDNA/nDNA ratio was calculated by comparing the ΔΔCt values. (D) MC3T3-E1 cells cultured under the same condition was measured the ATP levels. Data are expressed as mean ± SD. NAM, nicotinamide. *P<0.05. **P<0.01. ***P<0.001. ****P<0.0001. ns, not significant.

NAM prevents osteoblast damage induced by H_2O_2 oxidative stress.

The accumulation of oxidative stress is strongly related to reduced bone mineral density and impaired osteoblast differentiation (Basu, Michaëlsson et al. 2001, Kim, Kim et al. 2022). Because we observed that NAM induced the expression of mitochondrial antioxidant enzymes in osteoblasts, we tested whether NAM treatment relieves the ROS-damaged osteoblasts. MC3T3-E1 cells were treated with NAM in the presence or absence of 100 μM H_2O_2 during osteogenic differentiation for 4 or 10 days. ALP and ARS staining results showed that NAM prevented the impairment of osteoblast differentiation caused by chronic exposure to 100 μM H_2O_2 (Figures 1.20A-C).

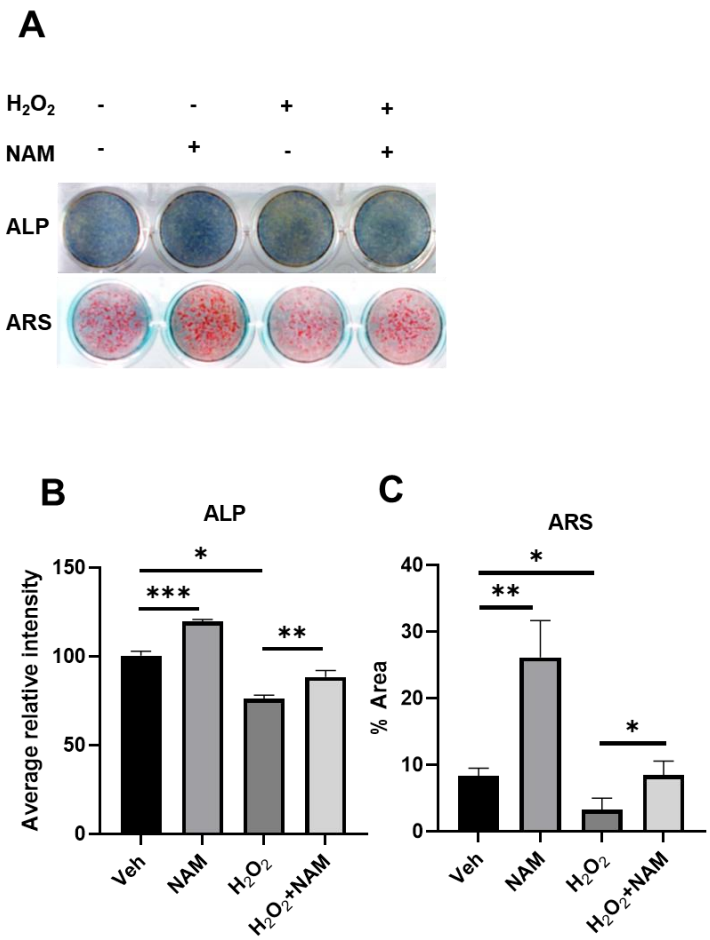

Figure 1.20. NAM prevents ROS-impaired osteoblast differentiation. (A) ALP and ARS stainings were performed after 10 μM NAM treatment with osteogenic media in the presence or absence of 100 μM H_2O_2 for 5 and 12 days, respectively. (B-C) Quantification of each staining was performed by ImageJ. Data are expressed as mean ± SD. NAM, nicotinamide. *P<0.05. **P<0.01. ***P<0.001. ****P<0.0001. ns, not significant.

RNA-seq analysis was performed to identify the effect of NAM on osteoblasts-damaged by H_2O_2. When the cells were treated with only H_2O_2 for 4 days, 405 genes were upregulated and 228 genes were downregulated (Figures 1.21A and B). Meanwhile, on day 10, 247 genes were upregulated and 298 genes were downregulated by H_2O_2 treatment (Figures 1.22A and B). The genes downregulated by H_2O_2 were associated with GO terms related to osteoblast differentiation on both day 4 and day 10, particularly on day 10 (Figures 1.21B and 1.22B).

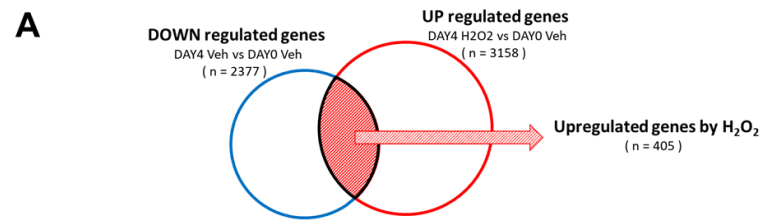
A
DOWN regulated genes
DAY4 Veh vs DAY0 Veh
(n = 2377)
UP regulated genes
DAY4 H2O2 vs DAY0 Veh
(n = 3158)
Upregulated genes by H2O2
(n = 405)

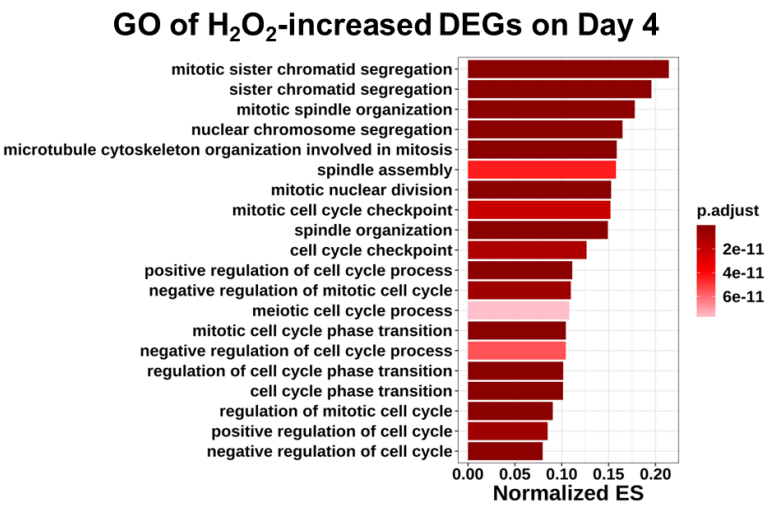
GO of H2O2-increased DEGs on Day 4
mitotic sister chromatid segregation
sister chromatid segregation
mitotic spindle organization
nuclear chromosome segregation
microtubule cytoskeleton organization involved in mitosis
spindle assembly
mitotic nuclear division
mitotic cell cycle checkpoint
spindle organization
cell cycle checkpoint
positive regulation of cell cycle process
negative regulation of mitotic cell cycle
meiotic cell cycle process
mitotic cell cycle phase transition
negative regulation of cell cycle process
regulation of cell cycle phase transition
cell cycle phase transition
regulation of mitotic cell cycle
positive regulation of cell cycle
negative regulation of cell cycle
0.00
0.05
0.10
0.15
0.20
Normalized ES
p.adjust
2e-11
4e-11
6e-11

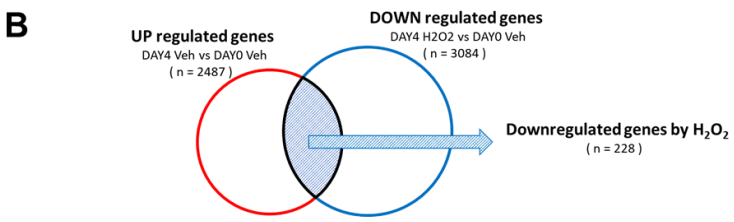
B
UP regulated genes
DAY4 Veh vs DAY0 Veh
(n = 2487)
DOWN regulated genes
DAY4 H2O2 vs DAY0 Veh
(n = 3084)
Downregulated genes by H2O2
(n = 228)

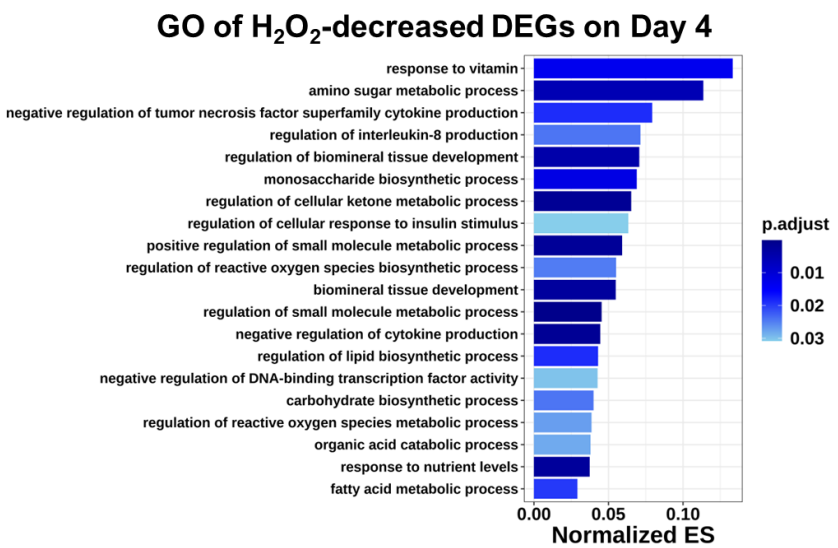
GO of H2O2-decreased DEGs on Day 4
response to vitamin
amino sugar metabolic process
negative regulation of tumor necrosis factor superfamily cytokine production
regulation of interleukin-8 production
regulation of biomineral tissue development
monosaccharide biosynthetic process
regulation of cellular ketone metabolic process
regulation of cellular response to insulin stimulus
positive regulation of small molecule metabolic process
regulation of reactive oxygen species biosynthetic process
biomineral tissue development
regulation of small molecule metabolic process
negative regulation of cytokine production
regulation of lipid biosynthetic process
negative regulation of DNA-binding transcription factor activity
carbohydrate biosynthetic process
regulation of reactive oxygen species metabolic process
organic acid catabolic process
response to nutrient levels
fatty acid metabolic process
0.00
0.05
0.10
Normalized ES
p.adjust
0.01
0.02
0.03

Figure 1.21. RNA-seq analysis of H_2O_2-induced gene expression in osteoblasts on day 4.

(A-B) GO analysis of upregulated or downregulated DEGs by 100 μM H_2O_2 on day 4. The top 20 GO terms are selected based on adjusted p-value and sorted by enrichment score.

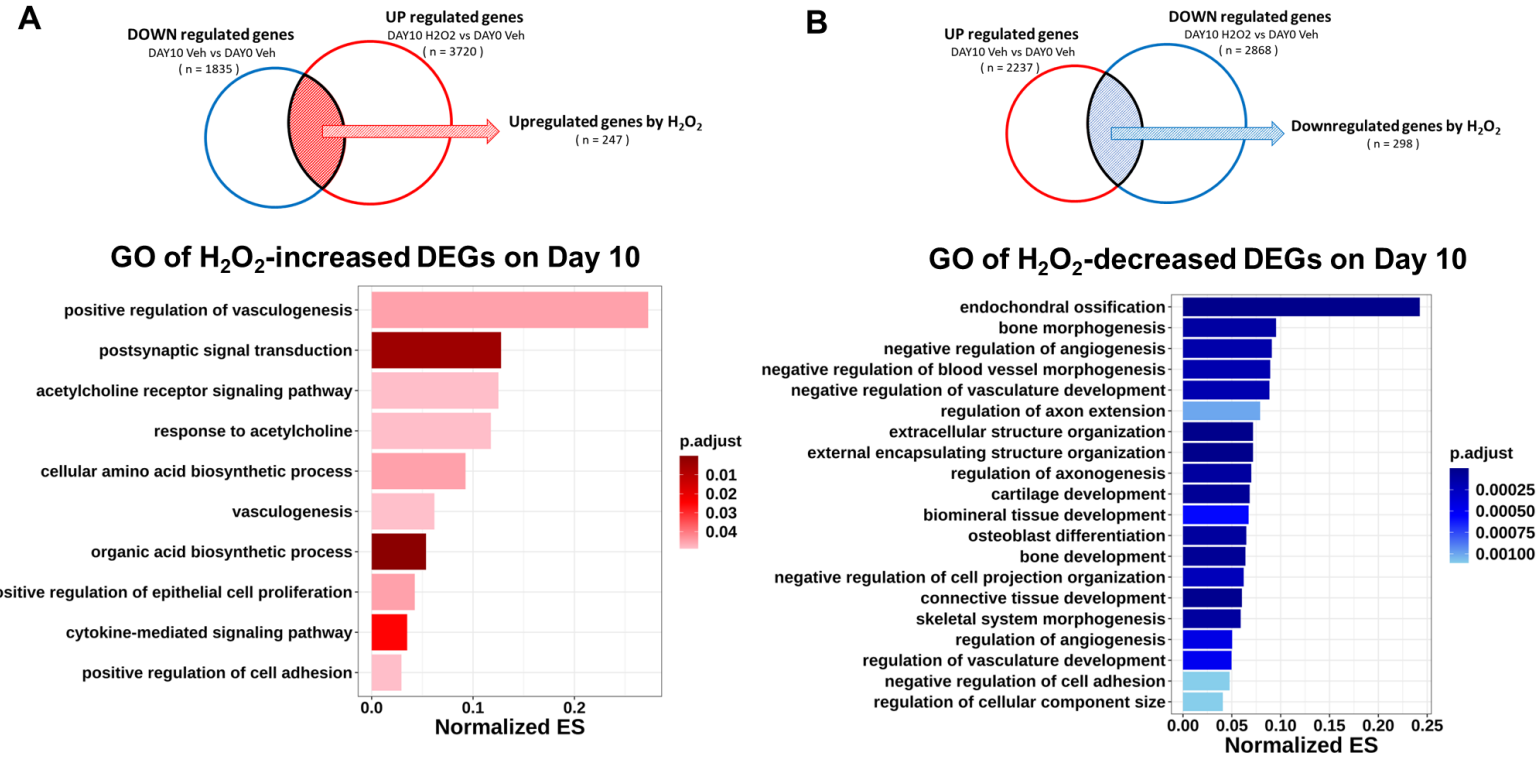
A
DOWN regulated genes
DAY10 Veh vs DAY0 Veh
(n = 1835)
UP regulated genes
DAY10 H2O2 vs DAY0 Veh
(n = 3720)
Upregulated genes by H2O2
(n = 247)
GO of H2O2-increased DEGs on Day 10
positive regulation of vasculogenesis
postsynaptic signal transduction
acetylcholine receptor signaling pathway
response to acetylcholine
cellular amino acid biosynthetic process
vasculogenesis
organic acid biosynthetic process
positive regulation of epithelial cell proliferation
cytokine-mediated signaling pathway
positive regulation of cell adhesion
0.0
0.1
0.2
Normalized ES
p.adjust
0.01
0.02
0.03
0.04
B
UP regulated genes
DAY10 Veh vs DAY0 Veh
(n = 2237)
DOWN regulated genes
DAY10 H2O2 vs DAY0 Veh
(n = 2868)
Downregulated genes by H2O2
(n = 298)
GO of H2O2-decreased DEGs on Day 10
endochondral ossification
bone morphogenesis
negative regulation of angiogenesis
negative regulation of blood vessel morphogenesis
negative regulation of vasculature development
regulation of axon extension
extracellular structure organization
external encapsulating structure organization
regulation of axonogenesis
cartilage development
biomineral tissue development
osteoblast differentiation
bone development
negative regulation of cell projection organization
connective tissue development
skeletal system morphogenesis
regulation of angiogenesis
regulation of vasculature development
negative regulation of cell adhesion
regulation of cellular component size
0.00
0.05
0.10
0.15
0.20
0.25
Normalized ES
p.adjust
0.00025
0.00050
0.00075
0.00100

Figure 1.22. RNA-seq analysis of H_2O_2-induced gene expression in osteoblasts on day 10.

(A-B) GO analysis of upregulated or downregulated DEGs by 100 μM H_2O_2 on day 10. The top 20 GO terms are selected based on adjusted p-value and sorted by enrichment score.

To determine whether NAM enables osteoblasts to recover from ROS-induced damage, GO analysis was performed on genes whose expression was decreased by H_2O_2 but restored by NAM. On day 4, the expression of only six genes was restored by NAM (Figure 1.23A). However, on day 10, the expression of 114 genes was significantly restored by NAM, these genes were particularly associated with GO terms related to osteoblast differentiation or bone formation (Figure 1.23B).

A

H_2O_2-decreased DEGs restored by NAM

	Genes
Day4	Gab2, Cd200, Larp1b, Sgk3, Ptpn3, Col22a1

B

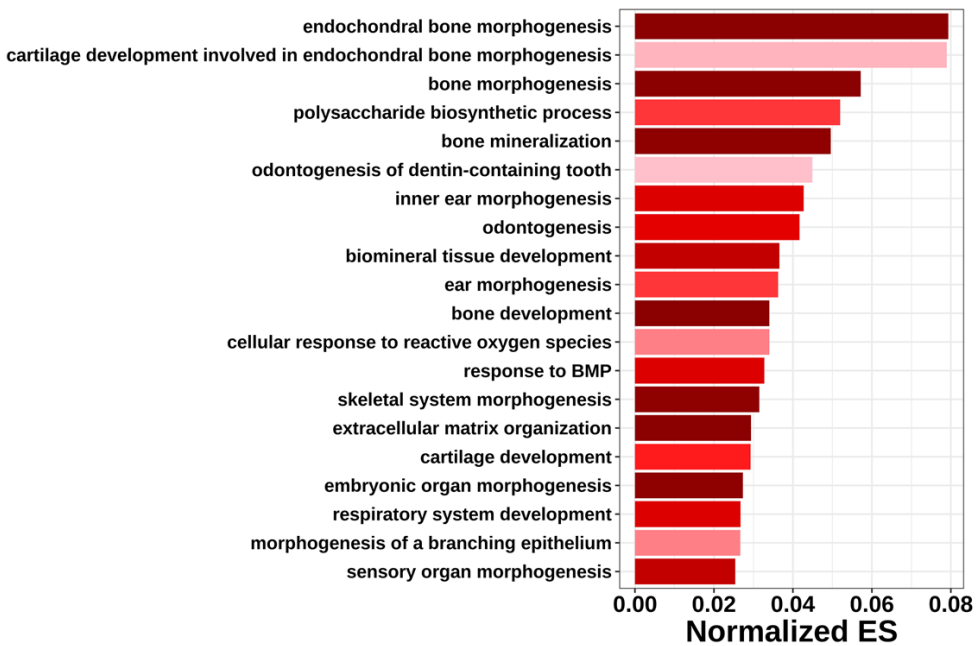

Figure 1.23. GO analysis of H_2O_2-decreased DEGs restored by NAM in osteoblasts.

(A) H_2O_2-decreased DEGs restored by NAM on day 4 are listed in table. (B) H_2O_2-decreased DEGs restored by NAM were investigated by GO analysis in biological process on day 10. Top 20 GOs are selected and listed based on adjusted *P*-value and enrichment score, respectively.

A correlation test was performed on the DEGs whose expression was decreased by H_2O_2 but restored by NAM, included in the top 20 GOs (Figure 1.24). Next, we listed the top 10 ranked GO in each cluster (Figures 1.25–27). Interestingly, cellular response to reactive oxygen species and bone mineralization were related in the first cluster (Figure 1.25). Overall, the expression of 80% of genes involved in cellular response to reactive oxygen species was decreased by H_2O_2 but restored by co-treatment with H_2O_2 and NAM. In addition, cluster 1 contained *Runx2* and *Wnt10b*, which are crucial factors in osteoblast differentiation. Cluster 2, included genes associated with many GO categories related to bone development and cartilage development (Figure 1.26), such as *Mmp13*, *Vdr* and *Dlx5*. Genes in cluster 3 were related to GO categories, including cartilage development, bone development, and extracellular matrix organization (Figure 1.27).

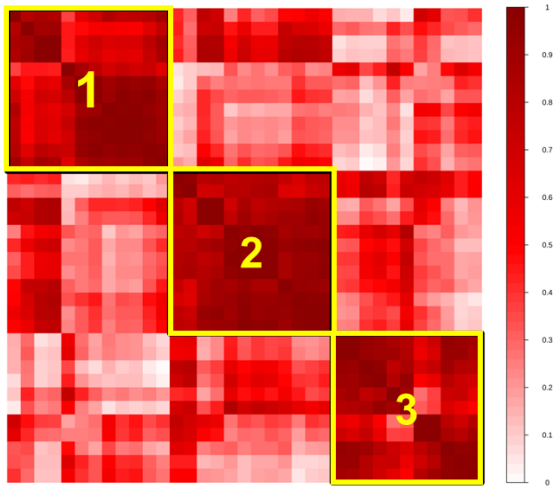

Figure 1.24. Correlation matrix plot on the DEGs whose expression was decreased by H_2O_2–restored by NAM. Related to Figure 1.23B.

Correlation analysis of DEGs, included in the top 20 GOs (Figure 1.23B) decreased by 100 μM H_2O_2 and restored by 10 μM NAM on day 10. A normalized correlation matrix was performed to show correlation among genes.

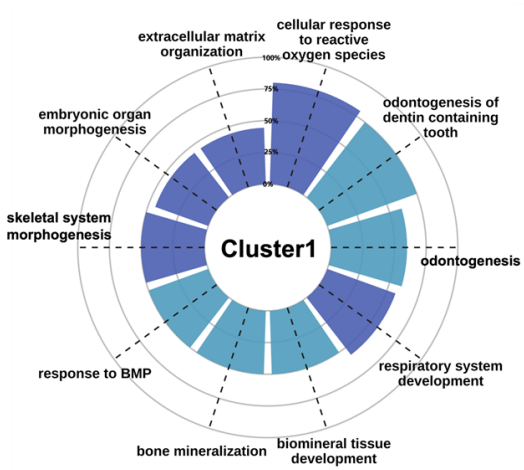
Cluster1
cellular response to reactive oxygen species
odontogenesis of dentin containing tooth
odontogenesis
respiratory system development
biomineral tissue development
bone mineralization
response to BMP
skeletal system morphogenesis
embryonic organ morphogenesis
extracellular matrix organization
100%
75%
50%
25%
0%

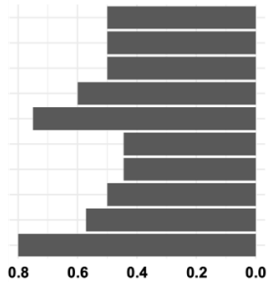
0.8
0.6
0.4
0.2
0.0

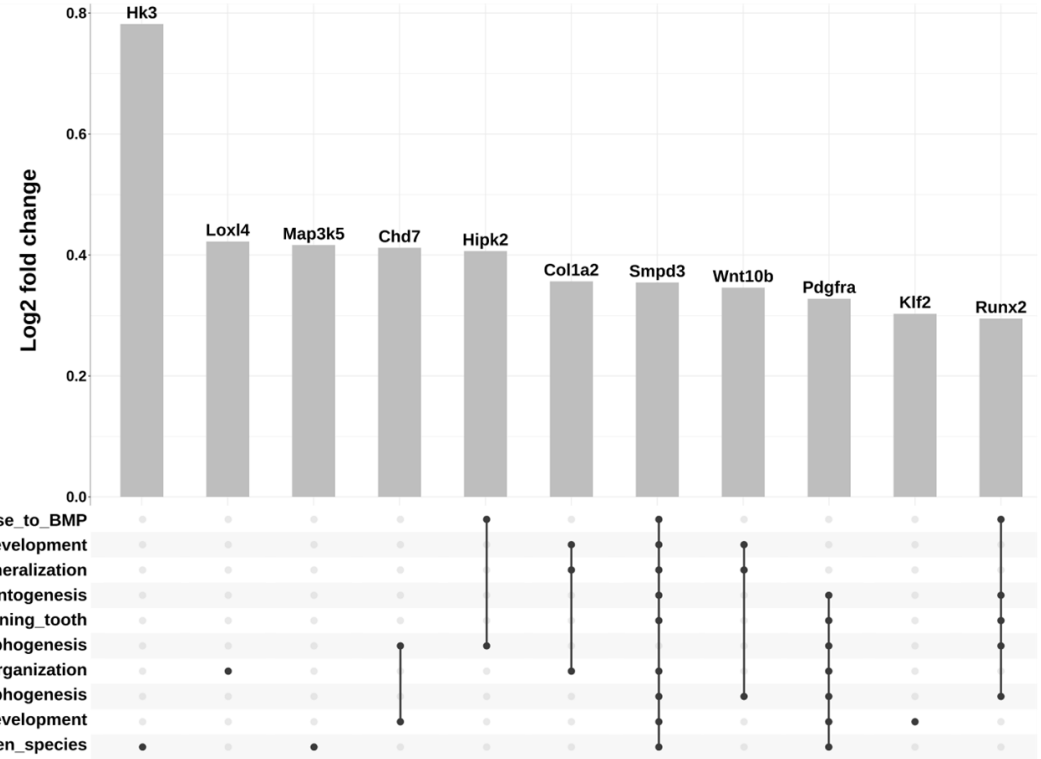
Log2 fold change
0.8
0.6
0.4
0.2
0.0
Hk3
Loxl4
Map3k5
Chd7
Hipk2
Col1a2
Smpd3
Wnt10b
Pdgfra
Klf2
Runx2
response_to_BMP
biomineral_tissue_development
bone_mineralization
odontogenesis
odontogenesis_of_dentin_containing_tooth
embryonic_organ_morphogenesis
extracellular_matrix_organization
skeletal_system_morphogenesis
respiratory_system_development
cellular_response_to_reactive_oxygen_species

Figure 1.25. The correlated GO terms and gene list of cluster 1. Related to Figure 1.24.

H_2O_2-decreased DEGs restored by NAM were investigated by GO analysis on day 10 (Figure 1.21.B). The circular bar plot (left top) showed GO terms correlated in cluster 1. The UpSet plot (right bottom) indicated the genes included in cluster 1 of Figure 1.22..

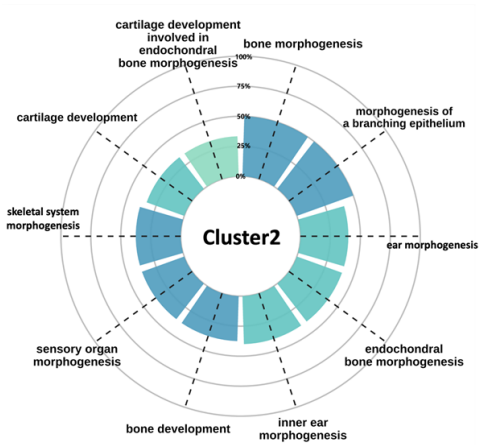
cartilage development involved in endochondral bone morphogenesis
bone morphogenesis
morphogenesis of a branching epithelium
ear morphogenesis
endochondral bone morphogenesis
inner ear morphogenesis
bone development
sensory organ morphogenesis
skeletal system morphogenesis
cartilage development
Cluster2
100%
75%
50%
25%
0%

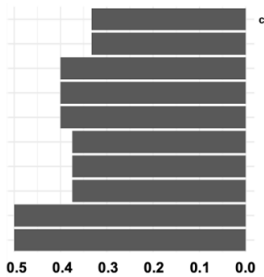
0.5
0.4
0.3
0.2
0.1
0.0

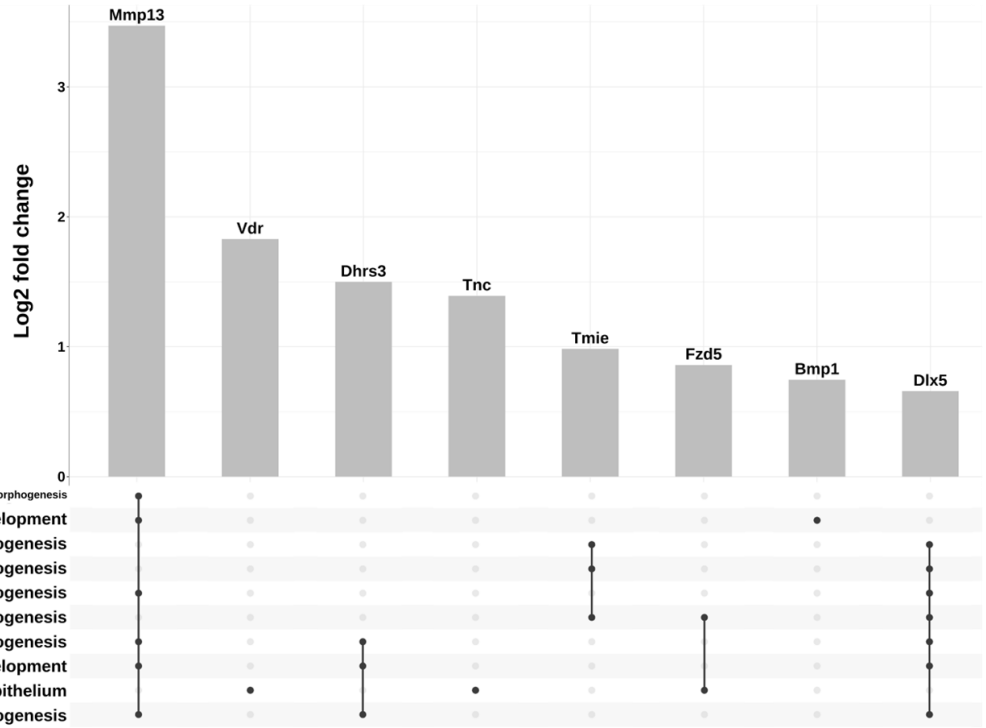
Log2 fold change
0
1
2
3
Mmp13
Vdr
Dhrs3
Tnc
Tmie
Fzd5
Bmp1
Dlx5
cartilage_development_involved_in_endochondral_bone_morphogenesis
cartilage_development
ear_morphogenesis
inner_ear_morphogenesis
endochondral_bone_morphogenesis
sensory_organ_morphogenesis
skeletal_system_morphogenesis
bone_development
morphogenesis_of_a_branching_epithelium
bone_morphogenesis

Figure 1.26. The correlated GO terms and gene list of cluster 2. Related to Figure 1.24.

H_2O_2-decreased DEGs restored by NAM were investigated by GO analysis on day 10 (Figure 1.21.B). The circular bar plot (left top) showed GO terms correlated in cluster 2. The UpSet plot (right bottom) indicated the genes included in cluster 2 of Figure 1.22..

Log2 fold change
3
2
1
0
Phex
B3galt2
Ppp1r3c
Col22a1
Foxd1
Col2a1
Sema5a
Clic5
Sgms2
Cfh
cartilage_development_involved_in_endochondral_bone_morphogenesis
cartilage_development
response_to_BMP
biomineral_tissue_development
bone_mineralization
ear_morphogenesis
inner_ear_morphogenesis
polysaccharide_biosynthetic_process
extracellular_matrix_organization
sensory_organ_morphogenesis
0.5
0.4
0.3
0.2
0.1
0.0
Cluster3
100%
75%
50%
25%
0%
response to BMP
polysaccharide biosynthetic process
ear morphogenesis
inner ear morphogenesis
sensory organ morphogenesis
biomineral tissue development
bone mineralization
cartilage development
cartilage development involved in endochondral bone morphogenesis
extracellular matrix organization

Figure 1.27. The correlated GO terms and gene list of cluster 3. Related to Figure 1.24.

H_2O_2-decreased DEGs restored by NAM were investigated by GO analysis on day 10 (Figure 1.21.B). The circular bar plot (left top) showed GO terms correlated in cluster 3. The UpSet plot (right bottom) indicated the genes included in cluster 3 of Figure 1.22..

Our RNA-seq results, showed that the expression of *Col1A1*, *Col1A2*, and *Vdr* genes associated with osteoporosis (as revealed by OMIM disease enrichment analysis) was decreased by H_2O_2 (Table 2). Interestingly, NAM restored the H_2O_2-decreased expression of *Col1A1* and *Vdr* (Table 3). These results suggest that NAM can prevent osteoblast dysfunction caused by oxidative stress.

Table 2. Enrichment analysis based on OMIM disease libraries for H_2O_2-decreased DEGs

Term	Overlap	Adjusted P-value	Combined Score	Genes
osteoporosis	3/11	0.007417265	190.5643617	COL1A1;COL1A2;VDR
ehlers-danlos	3/11	0.007417265	190.5643617	COL1A1;COL1A2;TNXB
hypertension	2/29	0.459410905	13.16195516	PTGIS;AGT
alopecia	1/11	0.459410905	12.47958022	HR
hypothyroidism	1/11	0.459410905	12.47958022	TG
skin/hair/eye pigmentation	1/12	0.459410905	10.86386938	MC1R
long qt syndrome	1/12	0.459410905	10.86386938	KCNH2
anomalies	1/13	0.459410905	9.555886574	RUNX2
rheumatoid arthritis	1/13	0.459410905	9.555886574	PTPN22

Table 3. Enrichment analysis based on OMIM disease libraries for H_2O_2-decreased DEGs restored by NAM

Term	Overlap	Adjusted P-value	Combined Score	Genes
osteoporosis	2/11	0.017127866	251.2087451	COL1A2;VDR
hypothyroidism	1/11	0.136997884	49.20758107	TG
ehlers-danlos	1/11	0.136997884	49.20758107	COL1A2
anomalies	1/13	0.136997884	38.63591875	RUNX2
myopia	1/15	0.136997884	31.38589486	COL2A1
hypogonadism	1/15	0.136997884	31.38589486	CHD7
lymphoma	1/22	0.165094954	17.87363593	BCL7A
deafness	2/111	0.165094954	6.558998122	TMIE;COL2A1
obesity	1/31	0.1805597	10.64289988	SDC3
neuropathy	1/35	0.181466527	8.818608039	SLC12A6

ROS are known to impede mitochondrial function (Peoples, Saraf et al. 2019). Therefore, we determined whether NAM could regulate ROS-damaged mitochondrial function. We observed that NAM prevented the reductions of mitochondrial respiration and oxygen consumption rate caused by treating MC3T3-E1 osteoblast cells with H_2O_2 (Figures 1.28A-H).

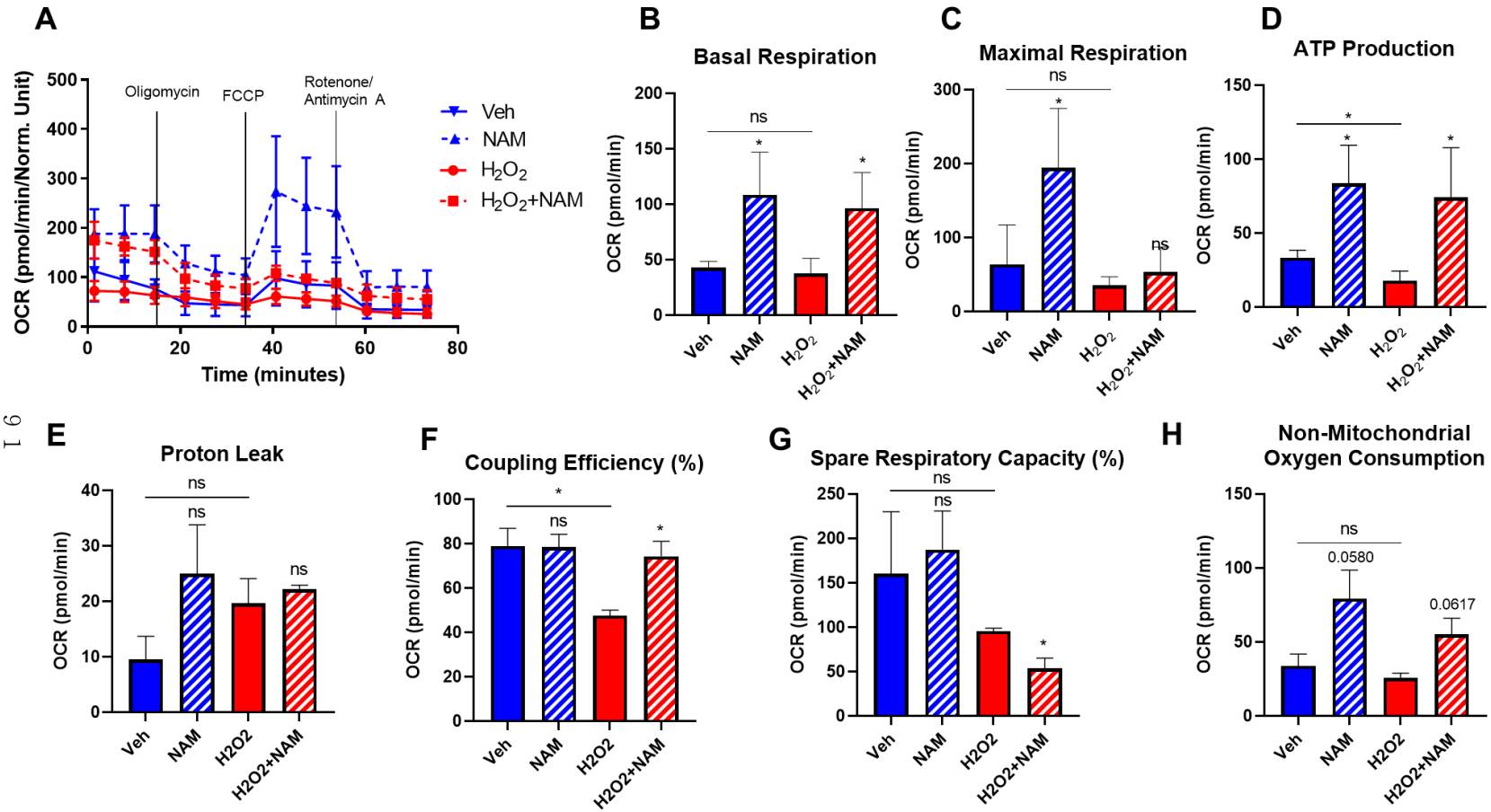
A
OCR (pmol/min/Norm. Unit)
Oligomycin
FCCP
Rotenone/
Antimycin A
Veh
NAM
H2O2
H2O2+NAM
Time (minutes)
B
Basal Respiration
C
Maximal Respiration
D
ATP Production
E
Proton Leak
F
Coupling Efficiency (%)
G
Spare Respiratory Capacity (%)
H
Non-Mitochondrial
Oxygen Consumption
OCR (pmol/min)
ns
0.0580
0.0617
Veh
NAM
H2O2
H2O2+NAM

Figure 1.28. NAM prevents ROS-induced mitochondrial impairment in osteoblasts.

The mitochondrial OCR was evaluated after the treatment of 10 μM NAM together with or without 100 μM H_2O_2 containing osteogenic medium for 7 d in MC3T3-E1 cells using an XF96 Extracellular Flux Analyzer. The parameters calculated from the curved OCR plot (A) were described into bar plots (B-H). Data are expressed as mean ± SD. NAM, nicotinamide. $*P<0.05$. $**P<0.01$. $***P<0.001$. $****P<0.0001$. ns, not significant.

The accumulation of γH2AX foci, involving histone H2A.X phosphorylation, is a biomarker for DNA damage and genotoxicity accompanying the DNA damage response (DDR) (Stope 2021). As previously reported (Kim, Kim et al. 2022), H_2O_2 treatment increased the number of MC3T3-E1 osteoblast cells with γH2AX foci (Figures 1.29A and B). NAM significantly ameliorated the accumulation of γH2AX foci that occurred at the basal level as well as that induced by H_2O_2 treatment.

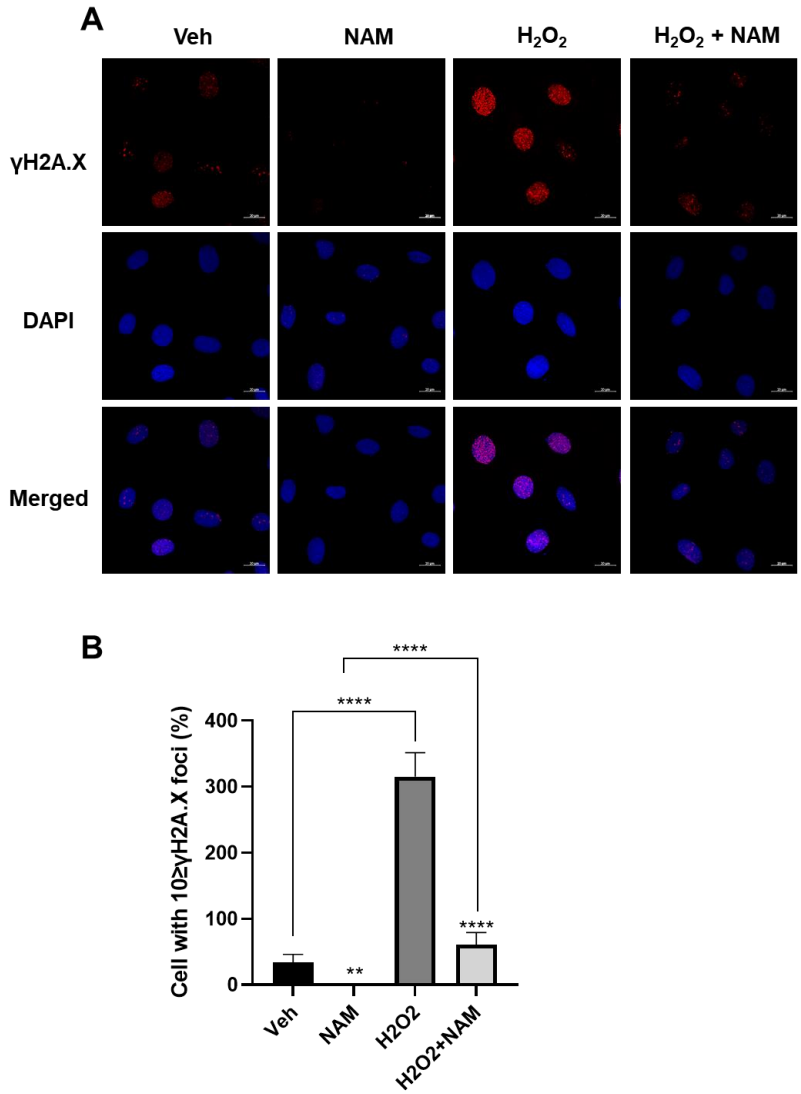

Figure 1.29. NAM protects ROS-induced DNA damage in osteoblasts.

MC3T3-E1 cells were treated with 100 μM of H_2O_2 in combination with or without 10 μM of NAM for 24 h. (A) Immunostaining was performed using γH2AX antibody (red) and DAPI (blue). (B) To quantify the number of cells with γH2AX foci, the cells containing ≥10 foci were counted. Data are expressed as mean ± SD. NAM, nicotinamide. *P<0.05. **P<0.01. ***P<0.001. ****P<0.0001. ns, not significant.

Excessive ROS can result in cellular apoptosis accompanied by the release of cytochrome c from damaged mitochondria, which in turn disrupts redox homeostasis in tissues (Kannan and Jain 2000, Arfin, Jha et al. 2021). We investigated whether NAM alleviates the apoptosis of osteoblasts damaged by acute exposure to excessive H_2O_2. Treatment with 300 μM H_2O_2 caused acute oxidative damages that significantly decreased the population of Annexin V− and propidium iodide (PI)−negative healthy live cells, but significantly increased both Annexin V− and PI−positive late apoptotic cells, and PI−positive and Annexin V−negative necrotic cells (Figures 1.30A−E). Co−treatment with H_2O_2 and NAM significantly increased the population of live cells compared with that upon H_2O_2–treatment alone.

Taking these findings together, NAM prevents osteoblasts from suffering H_2O_2−induced acute or chronic oxidative damage to mitochondria and DNA.

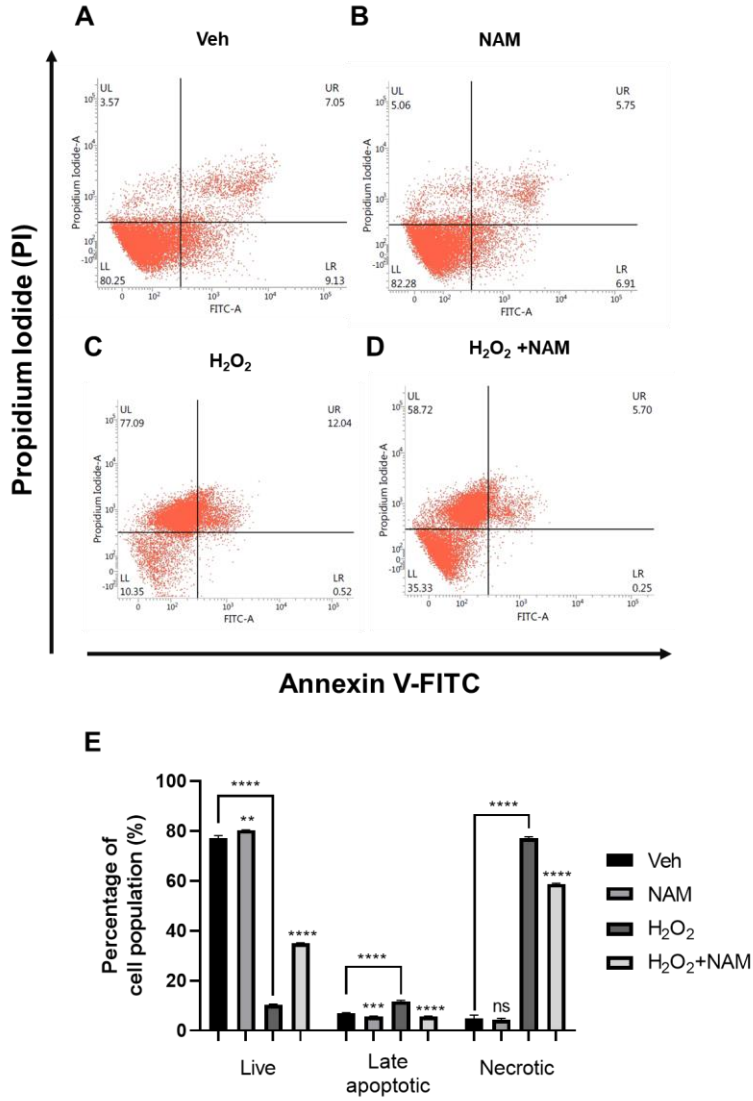

Figure 1.30. NAM prevents ROS-induced cell death in osteoblasts.

(A-D) MC3T3-E1 cells were treated with 300 μM of H_2O_2 in combination with or without10 μM of NAM. To detect H_2O_2-induced cell death, flow cytometry analysis after Annexin V and PI double staining was performed. (E) The percentages of each cell population were presented by bar plot (n=3). Data are expressed as mean ± SD. *P<0.05. **P<0.01. ***P<0.001. ****P<0.0001. ns, not significant.

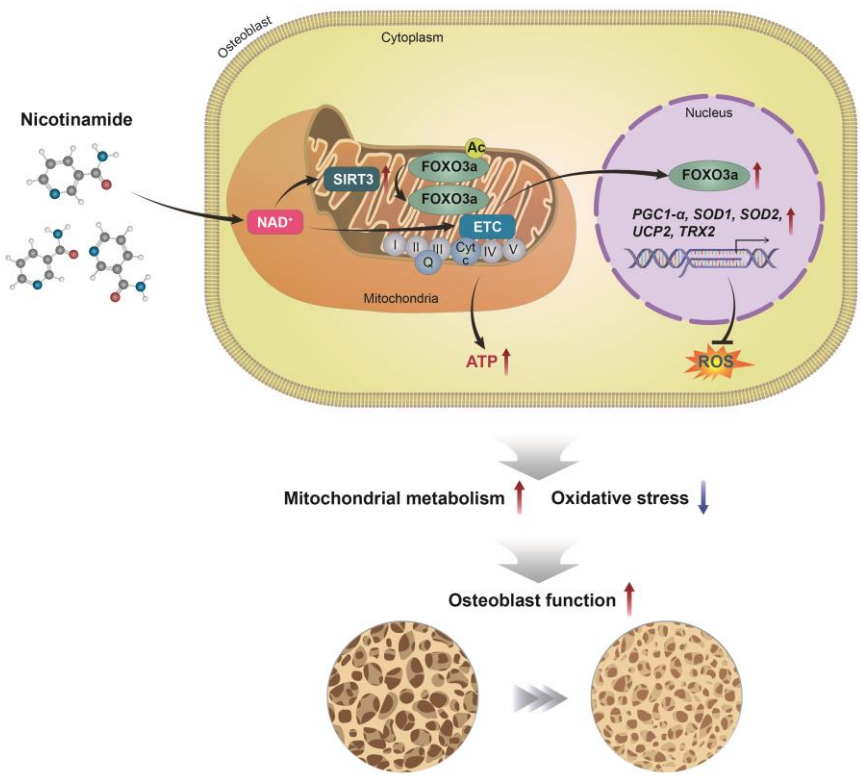

Figure 1.31. Schema of mechanisms of the improvement of osteoblast differentiation by NAM.

This study demonstrates that NAM greatly improved osteoblast differentiation by reducing mitochondrial oxidative stress. NAM promotes osteogenic differentiation by increasing mitochondrial respiration and the production of antioxidant enzymes via SIRT3, FOXO3a, and PGC1−α activation.

Discussion

Mitochondria are key intracellular organelles for the generation and regulation of cellular bioenergetics, producing the majority of ATP molecules via the oxidative phosphorylation system (OXPHOS). Mitochondrial metabolism normally produces ROS as a byproduct. Although intracellular ROS are necessary for regular function (Sena and Chandel 2012), when they are present at excess levels, they can lead to intracellular stress and numerous bone disorders including osteoporosis (Goettsch, Babelova et al. 2013) and osteoarthritis (Zahan, Serban et al. 2020). To maintain an appropriate level of ROS, antioxidant enzymes play a crucial role in the antioxidant system. A previous study reported that osteoblast lineage-specific *Sod2*-deficient mice showed decreased osteoblast activity accompanying an osteoporosis-like phenotype (Schoppa, Chen et al. 2022). The antioxidant *N*-acetylcysteine, a precursor of glutathione (GSH), also increased osteoblast differentiation in mouse calvarial cells (Jun, Lee et al. 2008). In this study, we showed that the stimulation of osteoblast differentiation by NAM was related to genes involved in the regulation of oxidative stress by RNA-seq. In addition, via in vitro analysis, we confirmed that NAM alleviated the ROS level in osteoblasts by regulating antioxidant enzymes. Moreover, NAM effectively eliminated ROS that arose under physiological conditions as well as those that emerged acutely through the activation of these enzymes. As a result, the induction of antioxidant enzymes by NAM not only strengthened the function of osteoblasts under normal conditions, but also significantly prevented the decrease in osteoblast function caused by excessive ROS.

Mitochondria generate ATP through respiration, which is the energy needed for cell metabolism. Therefore, when cells need more energy for their function, mitochondrial respiration is stimulated to supply more ATP (Russell, Foletta et al. 2014). Bioenergetic demand and capacity alter as cell function changes (Li, Gao et al. 2017). In order to satisfy this, the mitochondrial capacity and efficiency increase in differentiating cells. The mitochondrial respiration of osteoblasts is elevated during differentiation in order to provide the required energy. When bone marrow stromal cells (BMSCs) undergo osteogenic differentiation, the mitochondrial OXPHOS reaction is upregulated in BMSCs in order to fulfill the energetic demands of the process (Forni, Peloggia et al. 2016, Shum, White et al. 2016). The suppression of mitochondrial respiration using a mitochondrial complex inhibitor (e.g., rotenone) was reported to inhibit osteoblast differentiation (Gao, Feng et al. 2018). Our results also showed that mitochondrial respiration was increased during osteoblast differentiation (Figure 1.16). Furthermore, NAM was found to boost mitochondrial respiration during osteoblast differentiation (Figure 1.18). These results indicate that NAM activates the energy generation required for osteoblast differentiation through increased mitochondrial respiration. The administration of NMN, similar to the exogenous addition of NAD^+, led to increases in OCR and mitochondrial function in neuroblastoma cells (Long, Owens et al. 2015). Thus, NAM has the potential to be used as a medication for the prevention and treatment of bone disorders because it can improve the physiological function of osteoblasts through the metabolic activation of mitochondria.

In bone, osteogenesis is a sequential process of

mesenchymal stem cells (MSCs) recruitment, pre-osteoblast proliferation, lineage commitment, collagen secretion, and extracellular matrix mineralization (Infante and Rodríguez 2018). During this process, the proliferation of MSCs and pre-osteoblasts is a prerequisite for osteoblast differentiation (Qiao, Nie et al. 2016). According to our results of GO analysis of DEGs whose expression was increased by NAM on day 4, the early stage of differentiation, these genes were particularly associated with the cell cycle and chromosome segregation, indicating that NAM might play an important role in ensuring a sufficient population of osteoblast precursors for osteogenesis by regulating genes involved in cell proliferation in the early stage of differentiation. When NAM was applied in an osteogenic medium for 10 days (the maturation stage of osteoblast differentiation), RNA-seq analysis revealed that along with those related to osteoblast differentiation, a set of genes related to oxidative stress were also significantly affected (Figure 1). Our data also confirmed that NAM reduced the mitochondrial ROS levels during osteoblast differentiation (Figure 2) and mitigated mitochondrial and cellular damage caused by excessive ROS (Figure 5). These results suggest that the supply of NAM is advantageous for improving the functionality of osteoblasts and maintaining bone homeostasis by reducing intracellular ROS levels.

HDACs, including both class I (Lee, Suh et al. 2006) and class II HDACs (Jensen, Schroeder et al. 2008), inhibit osteoblast differentiation and bone formation. Meanwhile, MS-275, a class I HDAC inhibitor, has been reported to promote bone formation (Kim, Lee et al. 2011, Bae, Yoon et al. 2017). However, Sirt3, a major deacetylase of mitochondrial Sirts, was shown to be crucial for bone development and metabolism (Ho, Wang et al. 2017). Although

SIRT3-deficient mice showed bone loss and SIRT3 has been linked to the production of osteoclasts (Huh, Shin et al. 2016, Ling, Krager et al. 2021), its function and importance in osteoblasts incompletely understood. In this study, we showed that NAM promotes osteoblast differentiation by inducing the expression of antioxidant enzymes through the activation of Sirt3 (Figure 4). In addition, Sirt3, together with FOXO3a, was shown to play an important role in increasing antioxidant enzymes in osteoblasts. FOXO3a induces the expression of antioxidant enzymes under oxidative stress or hypoxia (Olmos, Valle et al. 2009, Tseng, Wu et al. 2014). FOXO3a inhibits the differentiation of osteoblast precursors by inhibiting Wnt signaling (Iyer, Ambrogini et al. 2013), while inhibiting ROS in mature osteoblasts to reduce apoptosis and promote bone formation (Ambrogini, Almeida et al. 2010). In our study, we showed that NAM promotes osteoblast differentiation by activating FOXO3a and increasing the levels of antioxidant enzymes (Figure 4). Ultimately, NAM is thought to play an important role in maintaining homeostasis by promoting the expression of antioxidant enzymes in mature osteoblasts. Taking the obtained findings together, NAM promotes the differentiation of osteoblasts and maintains homeostasis by increasing the levels of antioxidant enzymes through SIRT3 activation and sequential FOXO3a activation.

Oxidative stress is one of the most important factors accelerating aging of the musculoskeletal system (Thoma, Akter-Miah et al. 2020). NAD^+, the level of which is known to decrease with aging (Mouchiroud, Houtkooper et al. 2013), promotes mitochondrial function and prolongs the lifespan of mice when it is increased through NAD precursors such as NR (Zhang, Ryu et al. 2016). In this study, we revealed that NAM plays an important role

in maintaining mitochondrial homeostasis by regulating antioxidant enzymes to ensure appropriate levels of intracellular ROS. In addition, oxidative stress can cause DNA damage and cell death. If DNA requiring the DNA damage response (DDR) continues to accumulate in cells, it cannot be removed through the DNA repair mechanism, leading to cellular senescencevia irreversible cell-cycle arrest (Sedelnikova, Horikawa et al. 2004, Sedelnikova, Redon et al. 2010). In our study, NAM prevented osteoblast DNA damage and cell death caused by oxidative stress. Therefore, NAM can prevent the acceleration of musculoskeletal aging caused by oxidative stress.

In summary, the present study shows that NAM significantly enhanced osteoblast differentiation by relieving mitochondrial oxidative stress. NAM increases mitochondrial respiration and the expression of antioxidant enzymes via SIRT3, FOXO3a and PGC1-α activation, facilitating osteoblast differentiation both in normal physiological conditions and under oxidative stress. On the basis of this study, NAM could be a therapeutic or prophylactic drug to improve bone health.

IV. Part 2

Nicotinamide improves delayed tooth eruption in *Runx2*$^{+/-}$ mice

This research was originally published in Journal of Dental Research.

Journal of Dental Research, 2021 Vol.100 Issue 4 Page 423-431

Abstract

Patients with cleidocranial dysplasia (CCD) caused by mutations in RUNX2 have severe dental anomalies, including delayed or absent eruption of permanent teeth. This requires painful and expensive surgical/orthodontic intervention because of the absence of medicine for this condition. Here, we demonstrate that nicotinamide, a vitamin B3 and class III histone deacetylase inhibitor, significantly improves delayed tooth eruption in *Runx2*$^{+/-}$ mice, a well-known CCD animal model, through the restoration of decreased osteoclastogenesis. We also found that *Csf1* mRNA and protein levels were significantly reduced in *Runx2*$^{+/-}$ osteoblasts compared to WT whereas RANKL and OPG levels had no significant difference between both WT and *Runx2*$^{+/-}$ osteoblasts. The nicotinamide-induced restoration of osteoclastogenesis of bone-marrow-derived macrophages (BMMs) in *Runx2*$^{+/-}$ mice was due to the increased expression of RUNX2 and CSF1 and increased RANKL/OPG ratio. RUNX2 directly regulated *Csf1* mRNA expression via binding to the promoter region of the *Csf1* gene. In addition, nicotinamide enhanced the RUNX2 protein level and transacting activity posttranslationally with Sirt2 inhibition. Taken together, our study shows the potential and underlying molecular mechanism of nicotinamide for the treatment of delayed tooth eruption using the *Runx2*$^{+/-}$ murine model, suggesting nicotinamide as a candidate therapeutic drug for dental abnormalities in CCD patients.

Introduction

RUNX2 is a master transcription factor for skeletal development (Komori, Yagi et al. 1997). Mutations of *Runx2* gene cause cleidocranial dysplasia (CCD), exhibiting premature closure of cranial sutures, hypoplastic clavicles, and dental anomalies (Otto, Kanegane et al. 2002). The chief complaint of CCD patients is functional and esthetic impairment due to delayed or unerupted permanent dentition (Farrow, Nicot et al. 2018). However, the only therapeutic intervention has been a combination of surgical and orthodontic treatments during the confined period of the eruption stage of permanent dentition, requiring the establishment of therapeutic drugs to treat the symptoms.

Tooth eruption is a tightly regulated process that involves cells of the tooth and the surrounding alveolar bone. Osteoclasts are essential for the development of the eruption pathway through reciprocal interactions with osteoblasts and stromal cells (Wise, Frazier-Bowers et al. 2002, Wise and King 2008). Colony-stimulating factor 1 (CSF1), receptor activator of nuclear factor-kappa B ligand (RANKL), and osteoprotegerin (OPG), which are secreted by osteoblast-lineage cells and key regulatory factors for osteoclastogenesis, play critical roles in forming the eruption pathway (Heinrich, Bsoul et al. 2005). *Csf1*$^{-/-}$ mice, known as osteopetrotic (*op/op*) mice, exhibit arrested tooth eruption (Ida-Yonemochi, Noda et al. 2002). *Rankl*-deficient mice also show the defect in tooth eruption due to the lack of osteoclasts (Kong, Yoshida et al. 1999). OPG as a soluble decoy receptor inhibits osteoclast differentiation by interrupting the interaction between

RANKL and RANK. Also, the timely expression of these molecules regulating osteoclast differentiation is crucial to control tooth eruption.

Nicotinamide is a form of vitamin B3 and also acts as one of class III histone deacetylase (HDAC) inhibitor which suppresses the activity of Sirtuins by promoting nicotinamide exchange (Avalos, Bever et al. 2005). Several studies have revealed that the acetyl residues on the lysine side chains of histone or nonhistone proteins can be deacetylated by nicotinamide (Kim, Lee et al. 2011, Park, Lee et al. 2012). As HDACs inhibit the stability and activity of RUNX2 through deacetylation, HDAC inhibitors (HDIs) may be applicable to the treatment of bone diseases associated with RUNX2 deficiency (Kim, Kim et al. 2020). We have shown this proof of concept in our previous study that exhibited MS-275, a class I HDI, prevented delayed cranial suture closure in *Runx2*$^{+/-}$ mice (Bae, Yoon et al. 2017). However, as most HDIs, including MS-275, are approved as anticancer drugs, the adverse effects of HDIs preclude clinical trials to children (aged 7~12 years) for the treatment of delayed tooth eruption in CCD patients. We hypothesized that nicotinamide can ameliorate the CCD symptoms through the activation of RUNX2 with little toxicity. In this study, we demonstrate that nicotinamide significantly improved delayed tooth eruption in *Runx2*$^{+/-}$ mice and reveal the underlying mechanism of action.

Materials and Methods

Animal experiments

Runx2-deficient mice were kindly provided by Dr. Komori (Komori, Yagi et al. 1997) and maintained under specific pathogen-free conditions. Nicotinamide (1%, w/v) (Sigma Aldrich, St. Louis, MO, USA), added in drinking water, was provided *ad libitum* to pregnant and nursing mice until sacrifice. All animal studies were conducted according to Institutional Animal Care and Use Committee (IACUC) policies and reviewed by the Special Committee on Animal Welfare, Seoul National University, Seoul, Republic of Korea.

Micro-CT analysis

Mice were sacrificed and fixed with 4% PFA at 4° C overnight. Micro-CT analysis was performed using an inspeXio SMX-100CT system and TriBONTM software (RATOC, Tokyo, Japan).

Cell culture

Wild type (WT) and *Runx2*$^{+/-}$ calvarial cells were isolated from newborn mice. Primary calvarial cells, MC3T3-E1 cells, and human dental follicle cells were cultured in α-MEM with 10% fetal bovine serum (FBS) containing 100 U/mL penicillin and 100 μg/mL streptomycin. *Runx2*$^{-/-}$ calvarial cells were cultured as previously described (Kim, Kim et al. 2003). For nicotinamide treatment, the osteoblast differentiation medium supplemented with 10 mM β-

glycerophosphate and 50 μg/mL ascorbic acid was used. Bone marrow cells were isolated from the tibias of 4-week-old WT and *Runx2*$^{+/-}$ mice to differentiate into osteoclast. See the Appendix for details.

Osteoclast differentiation and co-cultures

BMMs were seeded (3 x 104 cells/300 μl/well in a 96-well plate) and differentiated into osteoclasts with 20 ng/mL CSF1 and 80 ng/mL recombinant murine sRANKL (PeproTech, Rocky Hill, NJ, USA) for 5 days. Multinucleated osteoclasts were identified by tartrate-resistant acid phosphate (TRAP) staining and counted under light microscopy. For co-culture of osteoblasts and osteoclasts, primary calvarial osteoblasts were plated in 48-well plates (1 x 104 cells/well). After 24 hours, BMMs were added and cultured in α-MEM supplemented with 10% FBS, 10 mM β-glycerophosphate, 50 μg/mL ascorbic acid, 10 nM 1 α,25(OH)2D3 (PeproTech, Rocky Hill, NJ, USA) and 1μM prostaglandin E2 (Tocris bioscience, Bristol, UK) for 7 days. The medium was changed every two days using the same composition. TRAP-positive multinucleated cells were detected using TRAP staining. Co-culture of human dental follicle cells (hDFCs) and human peripheral blood mononuclear cells (hPBMCs) was performed in α-MEM containing 10% FBS and 10 nM 1 α,25(OH)2D3 for 7 days as described above for co-culture of osteoblasts and osteoclasts. To assess bone resorption activity, pit formation assays were performed using a bone resorption assay kit (Cosmo Bio, Tokyo, Japan) according to the manufacture's protocol.

Alkaline Phosphate (ALP) staining

An ALP staining kit was purchased from Cosmo Bio (Tokyo, Japan). Human dental follicle cells were cultured in osteogenic medium containing 10 mM β-glycerophosphate, 50 μg/mL ascorbic acid for 5 days, washed with PBS, and stained according to the manufacturer's instructions. The ALP staining level was quantified by using Image J software.

Reverse transcription and quantitative real-time PCR (RT-qPCR)

Isolated RNAs using Qiazol Lysis Reagent (Qiagen, Mannheim, Germany) were reverse-transcribed using the PrimeScriptTM RT-reagent kit (Takara Bio, Shiga, Japan). The Takara SYBR premix Ex Taq (Takara Bio) was used for qPCR in an Applied Biosystems 7500 RT-PCR system (Foster city, CA, USA), and the results were normalized to Gapdh expression. The primers are listed in Appendix Table 1. The procedures were described previously (Cho et al. 2014).

Immunoblot analysis

Cellular proteins were obtained using lysis buffer and used for immunoblot (IB) as described previously (Yoon et al. 2013). IB was conducted with specific antibody binding RUNX2 (MBLI, Woburn, MA, USA), CSF1, OPG (abcam, Cambridge, UK) and RANKL (Thermo scientific, MA, USA). Quantitative analysis was performed using Image J software (NIH, USA).

Transient Transfection

Primary calvarial osteoblasts and MC3T3-E1 cells were transfected by electroporation using the Neon transfection system (Invitrogen, CA, USA) according to manufacturer's instructions. HA-tagged Sirt2 expression vector was generously provided by Prof. Suk-Chul Bae (Chungbuk National University, Cheongju, Korea).

Luciferase reporter assay

RUNX2 transacting activity was evaluated using the 6XOSE2-Luc reporter gene (Shin, Bae et al. 2018). Passive lysis buffer, the Bright-Glo™ Luciferase Assay System, and the GloMax-Multi Detection System (Promega, WI, USA) were used to measure luciferase activity. See the Appendix for details of the transient transfection and *Csf1* reporter vector.

Construction of the Csf1 reporter vector

The +74 to +260 region of the Csf1 promoter sequence was obtained from National Center for Biotechnology Information (NC_000069.5:c107563320-107563202 Mus musculus strain C57BL/6J chromosome 3, MGSCv37 C57BL/6J). The indicated promoter region was generated using PCR (forward 5'-CGA CGA GCT AGC GGG CCT CTG GGG TGT AGT AT-3' and reverse 5'-CGA CGA AAG CTT CCG AGG CAA ACT TTC ACT TT-3'). The PCR product was ligated into the NheI and HindIII sites of the pGL4.23 reporter vector. To produce a reporter vector having a mutation in the putative RUNX2 binding sites, site-directed

mutagenic PCR was performed. The primers used were as follows: forward 5’-GAT TTC CCA TAA ACC TTA TGC CCC GCC AGC C-3’ and reverse 5’-GGC TGG CGG GGC ATA AGG TTT ATG GGA AAT C-3’.

Preparation of probes for in situ hybridization

To assess the expression patterns of the Csf1, a complementary DNA construct was used as described previously (Choi et al. 2002). A 455-base pair Csf1-specific sequence was digested with NotI and SalI and sublconed into pCMV-SPORT6. Plasmid linearized with SmaI was transcribed for antisense probe synthesis. In vitro transcription was performed with linearized DNA template, RNase inhibitor, DIG RNA labeling mix and T7 RNA polymerase (Roche, Basel, Switzerland) for 2 hrs at 37° C. After 2 hrs, RNase free DNase (Roche) was added and incubated for 15min at 37° C. To stop the reaction, 0.5 M EDTA pH 8.0 was added. LiCl (4 M) and pre-chilled ethanol were added and incubated overnight at −20° C. After centrifugation, the pellet was washed, dried and dissolved in nuclease free water.

Histology analysis

For histological analysis, P5 and P8 mice were fixed in 4% PFA at 4° C for 24 hours and decalcified in 10% Ethylene Diamine Tetra Acetic Acid (EDTA) for 7 days. Dehydration and paraffin embedding was performed according to the standard procedure (Kim et al. 2020b). Serial sections of paraffin blocks (7 μM in ISH, 10 μM in IHC) were subjected to TRAP staining (Cosmo Bio, Tokyo,

Japan), immunohistochemistry (IHC) and in situ hybridization (ISH). TRAP staining was performed according to the manufacturer's protocol. IHC was performed using the VECTASTAIN® ABC-HRP kit (VECTOR LABORATORIES, Inc., CA, USA) and CSF1 antibody (Abcam, Cambridge, UK). For ISH, digoxigenin-11-UTP-labeled single-stranded antisense RNA probes to detect Csf1 (Appendix Table 3) were prepared using the DIG RNA labeling kit (Roche, Basel, Switzerland). Deparaffinization and rehydration were performed using xylene and ethanol, respectively. Permeabilization was performed with 20 μg/ml proteinase-K for 12 min at 37° C and acetylation with 0.1 M triethanolamine-HCl (pH 8.0) for 3 min at RT. Hybridization was performed at 42° C for 16h. Slides were washed sequentially with 2x SSC, 0.5X SSC and 0.2X SSC for 15 min each and incubated with anti-DIG antibody (Roche, Basel, Switzerland) overnight at 4° C. The next day, NBT/BCIP stock (Roche, Basel, Switzerland) was applied for color development at RT in the dark for 2-3 hrs. Background staining was conducted using methyl-green before mounting. Slides were imaged with a DP72 digital camera (Olympus, Tokyo, Japan) and analyzed with OsteomeasureTM (OsteoMetrics, Inc., Decatur, GA, USA).

Chromatin Immunoprecipitation (ChIP) Assay

The ChIP assay was performed by using the SimpleChIP® Enzymatic Chromatin IP kit (Cell Signaling Technology, MA, USA). HA-Runx2- or empty vector-transfected MC3T3-E1 cells were harvested and used for the ChIP assay according to the manufacturer's instruction. The PCR primer pairs used to detect

DNA segments for the ChIP assay are listed in Appendix Table 2.

Bioinformatic data analysis

We downloaded RUNX2-ChIP-seq data during various differentiation periods of MC3T3-E1 preosteoblast cells (Day 0, 9, 28) (Wu et al. 2014). The detailed annotation of ChIP-seq peaks is provided in electronic supplementary material and the raw files have been deposited in the Gene Expression Omnibus (GEO) database (GSE54013). DNase-seq data set were downloaded from the GEO database (GSE55046) which represents DNase hypersensitivity (DHS) during MC3T3-E1 differentiation (Tai et al. 2017). The peak-related WIG files were analyzed and visualized using Integrative Genomics Viewer 2.8.2 (IGV 2.8.2). RNA-seq procedure and data analysis were performed as described previously (Bae et al. 2017).

Statistics

Data are presented as means ± S.E. Each experiment was performed at least three times, and representative results are shown in the figures. The significance of differences was evaluated using either Student's *t* test or one-way analysis of variance, followed by Bonferroni's test using the Prism 8.0 software (GraphPad Software, San Diego, CA, USA).

Table 4. Primer sequences for RT−qPCR

gene	sequence
Runx2	F: 5'-CCGCACGACAACCGCACCAT-3'
	R: 5'-CGCTCCGGCCCACAAATCTC-3'
Csf1	F: 5'-GACCCTCGAGTCAACAGAGC-3'
	R: 5'-TGTCAGTCTCTGCCTGGATG-3'
Rankl	F: 5'-CAGCCATTTGCACACCTCACCAT-3'
	R: 5'-TTTCGTGCTCCCTCCTTTCATCAG-3'
Opg	F: 5'-ACCCAGAAACTGGTCATCAGC-3'
	R: 5'-CTGCAATACACACACTCATCACT-3'
Spi1	F: 5'-AGAAGCTGATGGCTTGGAGC-3'
	R: 5'-GCGAATCTTTTTCTTGCTGCC-3'
Mmp9	F: 5'-CTGGACAGCCAGACACTAAAG-3'
	R: 5'-CTCGCGGCAAGTCTTCAGAG-3'
Nfatc1	F: 5'-GGTGCCTTTTGCGAGCAGTATC-3'
	R: 5'-CGTATGGACCAGAATGTGACGG-3'
Acp5	F: 5'-GCGACCATTGTTAGCCACATACG-3'
	R: 5'-CGTTGATGTCGCACAGAGGGAT-3'
Ctsk	F: 5'-AGCAGAACGGAGGCATTGACTC-3'
	R: 5'-ATCGCAGTCTGGGCACTTGTGA-3'
Ctr	F: 5'-CAAACCGAAGATGAGGTTCCT-3'
	R: 5'- TGGGCTCACTAGGAGCAGG-3'
Gapdh	F: 5'-CATGTTCCAGTATGACTCCACTC-3'
	R: 5'-GGCCTCACCCCATTTGATGT-3'

Table 5. Primer sequences for ChIP assay

Csf1	F: 5'-GGGCCTCTGGGGTGTAGTAT-3'
	R: 5'-CCGAGGCAAACTTTCACTTT-3'

Table 6. Primer sequences for *in situ* hybridization RNA probes to detect *Csf1*

Csf1	F: 5'-CGACGAGTCGACCCTGATTGCAACTGCCTGTA-3'
	R: 5'-CGACGAGCGGCCGCTGTCAGTCTCTGCCTGGATG-3'

Results

Delayed tooth eruption in CCD mice is rescued by the treatment with nicotinamide

To investigate whether nicotinamide can rescue delayed tooth eruption, we analyzed the mandibular first molar of WT and *Runx2*$^{+/-}$ mice with nicotinamide treatment at postnatal day 10 (P10) using micro-CT. Nicotinamide provided as a 1% solution in drinking water to pregnant or nursing mice did not show any toxicities including lethality, loss of body weight, or miscarriage (data not shown). *Runx2*$^{+/-}$ mice showed delayed eruption of the mandibular first molar compared to WT mice as was previously reported (Yoda, Suda et al. 2004). Images from multiple views (Figures 2.1A-C) show that most of the cusps of the maxillary and mandibular first molars were exposed in WT mice whereas those of *Runx2*$^{+/-}$ were mostly covered by the alveolar bone. The nicotinamide significantly restored tooth eruption in *Runx2*$^{+/-}$ mice to the level of WT (Figures. 2.1A-C). To quantitatively assess tooth eruption, we measured the eruption distance (red line in Figure 2.3). Compared to WT mice, the eruption distance in *Runx2*$^{+/-}$ was significantly decreased and was rescued by nicotinamide (Figure 2.1D). However, nicotinamide did not accelerate tooth eruption in WT mice.

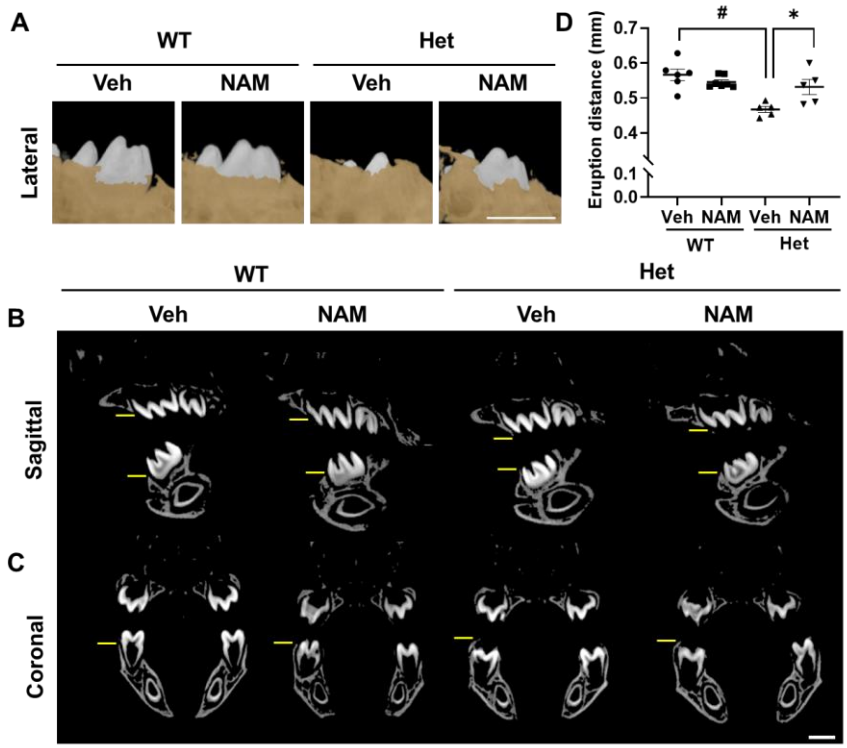

Figure 2.1. Nicotinamide improves the delayed first molar eruption

(A) Representative lateral view images of the erupting mandibular first molar of NAM-treated or untreated WT and *Runx2*$^{+/-}$ pups at postnatal day 10 (P10) (n ≥ 5 in each group; scale bar = 1 mm). (B-C) Sagittal and coronal views of maxillary and mandibular first molars at P10. Thin yellow lines indicate the edge of the alveolar bone (n ≥ 5 in each group; scale bar = 1 mm). (D) The eruption distance from the line connecting the most concave points anterior and posterior of the first molar alveolar bone to the highest vertical point of the cusp. Quantitative data were obtained using TriBON^{TM} software (n≥5 in each group). Data are expressed as the mean ± SE. WT, wild type; Het, *Runx2*$^{+/-}$; NAM, nicotinamide. * $P < 0.05$, ** $P < 0.01$, # $P < 0.005$, ## $P < 0.001$; ns, not significant.

Next, to investigate whether nicotinamide can affect the recruitment and differentiation of osteoclasts around eruption path, we performed TRAP staining on tissue sections of P5 and P8 mice. TRAP-positive osteoclasts in *Runx2*$^{+/-}$ mice were remarkably diminished compared to those in WT mice (Figure 2.2A), which is in agreement with a previous report (Yoda, Suda et al. 2004). The administration of nicotinamide dramatically increased the number of TRAP-positive osteoclasts in *Runx2*$^{+/-}$ mice compared to untreated *Runx2*$^{+/-}$ mice. Quantitative analyses showed that both the number and area of osteoclasts were significantly decreased in *Runx2*$^{+/-}$ mice, and both were recovered to the levels of WT with nicotinamide treatment (Figures 2.2B-E). These results suggest that nicotinamide rescue delayed tooth eruption in *Runx2*$^{+/-}$ mice through the stimulation of osteoclastogenesis.

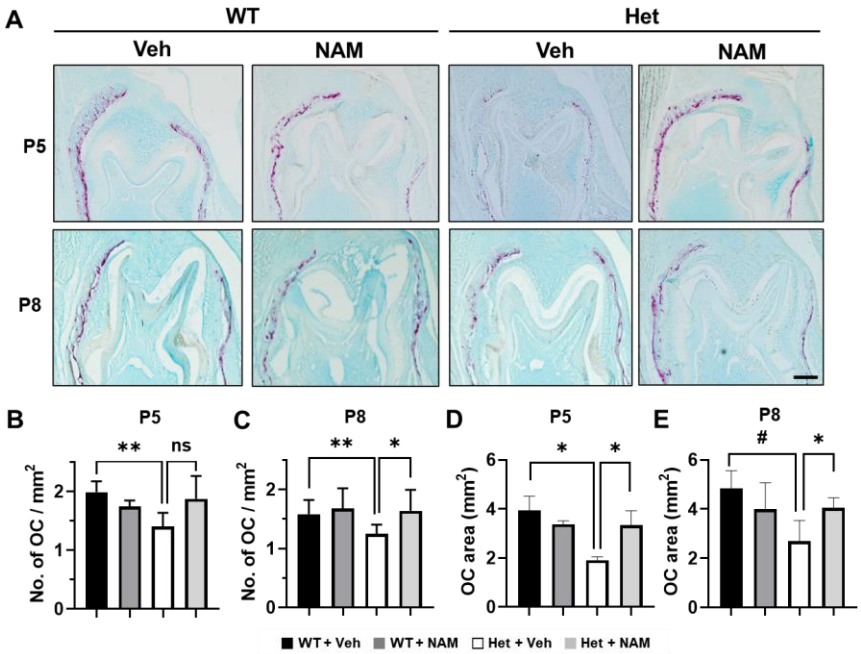

Figure 2.2. Nicotinamide improves the decreased osteoclast differentiation in *Runx2*$^{+/-}$ mice.

(A) TRAP-positive osteoclasts as determined by TRAP staining of the mandible covering the first molar in P5 (top row) and P8 (bottom row) mice (scale bar = 200 μm). Osteoclast (OC) number (B-E) and coverage area (I-J) (n > 5 in each group). Data are expressed as the mean ± SE. WT, wild type; Het, *Runx2*$^{+/-}$; NAM, nicotinamide. * $P < 0.05$, ** $P < 0.01$, # $P < 0.005$, ## $P < 0.001$; ns, not significant.

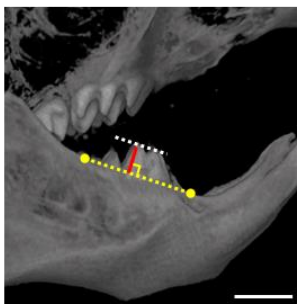

Figure 2.3. The measurement of eruption distance.

To quantitatively assess tooth eruption, we measured the eruption distance (red line), which was defined as the length of the vertical line from the highest point of the middle cusp to an arbitrary line (white dotted line) connecting anterior and posterior downwardly concave points (scale bar = 1 mm).

Nicotinamide restores osteoclastogenesis in *Runx2*$^{+/-}$ mice by acting on bone-forming cells

Since *Runx2*$^{+/-}$ mice showed decreased osteoclast differentiation, we examined the possibility of impaired differentiation of BMMs to osteoclasts. Unexpectedly, the osteoclastogenic capacity of *Runx2*$^{+/-}$ mouse-derived BMMs was not significantly different from that of BMMs derived from WT mice in the presence of CSF1 and RANKL. Differentiation assays on BMMs from these mice showed a similar number of osteoclasts (Figures 2.4A and B) and TRAP activity (Figure 2.4C), suggesting that *Runx2* haploinsufficiency in BMMs themselves does not affect their differentiation to osteoclasts. Interestingly, however, co-culture of WT BMMs with *Runx2*$^{+/-}$ osteoblasts resulted in significantly lower osteoclast differentiation than did co-culture with WT osteoblasts (Figures 2.4D and E). However, the osteoclast differentiation of *Runx2*$^{+/-}$ BMMs by co-culture with WT osteoblasts was similar to that of WT BMMs co-cultured with WT osteoblasts. These observations suggest that the reduced osteoclast differentiation in *Runx2*$^{+/-}$ mice may be caused by RUNX2 deficiency in osteoblasts rather than that in osteoclasts.

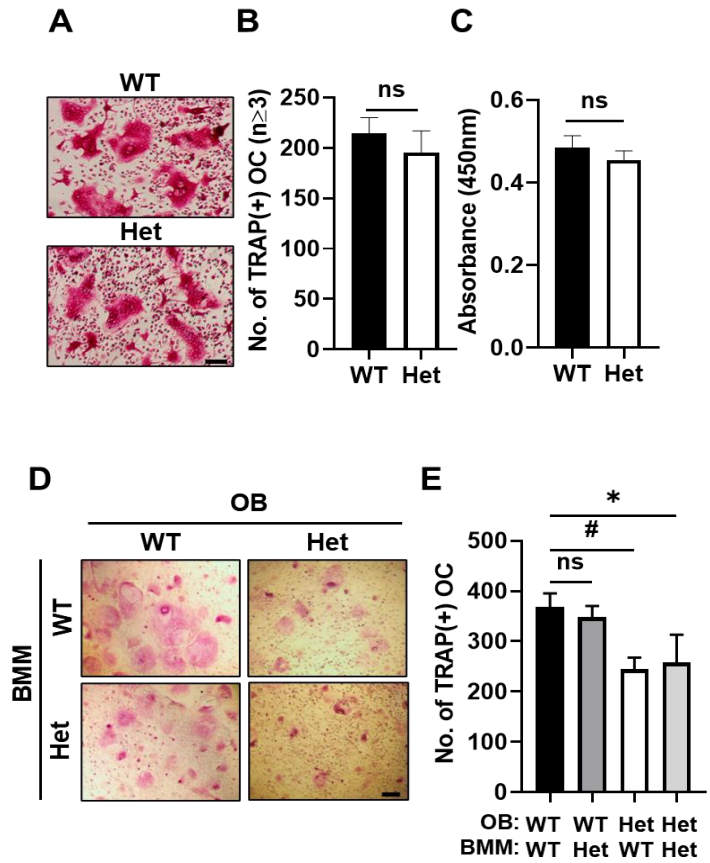

Figure 2.4. Impaired osteoclast differentiation in *Runx2*$^{+/-}$ mice was attributed to the impairment of osteoblast-lineage cells.

(A) Osteoclasts identification by TRAP staining. Bone-marrow-derived mononuclear cells (BMMs) isolated from WT and *Runx2*$^{+/-}$ mice were differentiated into osteoclasts in the presence of CSF1 (20 ng/mL) and RANKL (80 ng/mL) for 5 days (scale bar = 100 μm). (B) Counting of TRAP-positive osteoclasts with more than three nuclei. (C) TRAP activity was measured from cell lysates from (A). (D) TRAP staining of BMMs from WT and *Runx2*$^{+/-}$ mice co-cultured with primary calvarial osteoblasts from WT and *Runx2*$^{+/-}$, respectively, for 7 days with vitamin D3 (10 nM) for osteoclast differentiation. (E) Counting of TRAP-positive

osteoclasts. Data are expressed as the mean ± SE. WT, wild type; Het, *Runx2*$^{+/-}$; NAM, nicotinamide. * $P < 0.05$, ** $P < 0.01$, # $P < 0.005$, ## $P < 0.001$; ns, not significant.

Since nicotinamide restored osteoclast differentiation in *Runx2*$^{+/-}$ mice (Figure. 2.4), we investigated whether this restoration occurs through an effect of nicotinamide on osteoblasts. Co-culture of *Runx2*$^{+/-}$ BMMs with nicotinamide-treated *Runx2*$^{+/-}$ osteoblasts increased osteoclast differentiation compared to co-culture with vehicle-treated *Runx2*$^{+/-}$ osteoblasts (Figures. 2.5A and B). We also confirmed increased osteoclast pit formation by *Runx2*$^{+/-}$ osteoblasts treated with nicotinamide (Figures. 2.8A and B). It is known that dental follicle cells recruit monocytes, which differentiate into mature osteoclasts to resorb the alveolar bone surrounding the eruption path (Camilleri and McDonald 2006, Wang, Sun et al. 2016). Thus, to examine the effect of nicotinamide on human dental follicle cells (hDFCs) and osteoclast differentiation of monocytes, *Runx2*-depleted hDFCs were treated with nicotinamide, followed by co-culture with human peripheral blood mononuclear cells (hPBMCs) for 7 days. The efficiency of *Runx2* knockdown was confirmed by western blot analysis (Figures 2.8C and D). Although the co-culture of *Runx2*-depleted hDFCs with hPBMCs resulted in fewer TRAP-positive cells, nicotinamide treatment of *Runx2*-depleted hDFCs restored osteoclast differentiation of hPBMCs (Figures. 2.6A and B). The expression levels of osteoclast marker genes including *Spi1, Mmp9, Nfatc1, Acp5, Ctsk,* and *Ctr* were significantly decreased in co-culture of *Runx2*$^{+/-}$ BMMs with *Runx2*$^{+/-}$ osteoblasts compared to co-culture with WT osteoblasts (Figures. 2.7A-F). Concordantly, co-cultured with nicotinamide-treated *Runx2*$^{+/-}$ osteoblasts show elevated mRNA levels of *Spi1*, *Mmp9*, *Acp5* and *Ctr* although it did not affect *Nfatc1* and *Ctsk*.

Altogether, these results indicate that nicotinamide restores the osteoclastogenesis of BMMs by acting on *Runx2*–depleted osteoblast–lineage cells.

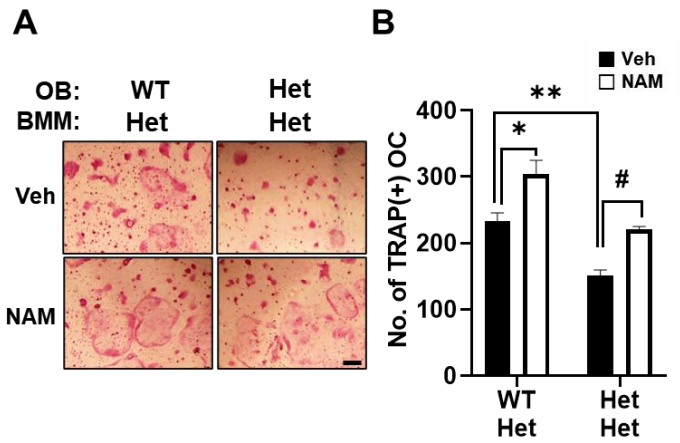

Figure 2.5. Impaired osteoclast differentiation was recovered by nicotinamide treated osteoblasats.

(A–B Primary calvarial osteoblasts were treated with 5mM NAM, followed by co–culture with BMMs. Data are expressed as the mean ± SE. WT, wild type; Het, *Runx2*$^{+/-}$; NAM, nicotinamide. * $P < 0.05$, ** $P < 0.01$, # $P < 0.005$, ## $P < 0.001$; ns, not significant. 5 mM NAM, followed by co–culture with BMMs.

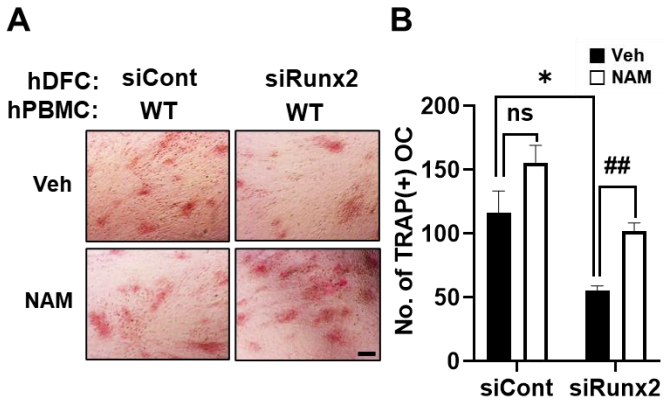

Figure 2.6. Nicotinamide-treated Runx2 deficient human dental follicle cells restored reduced osteoclast differentiation in co-culture with human primary blood monocytes.

(A-B) Identification of osteoclasts using TRAP staining. Human dental follicle cells (hDFCs) transfected with siRunx2 or siCont (40 nM), incubated with 5 mM NAM, and co-cultured with hPBMCs for 1 week (scale bar = 100 μm). Data are expressed as the mean ± SE. WT, wild type; Het, *Runx2*$^{+/-}$; NAM, nicotinamide. * $P < 0.05$, ** $P < 0.01$, # $P < 0.005$, ## $P < 0.001$; ns, not significant.

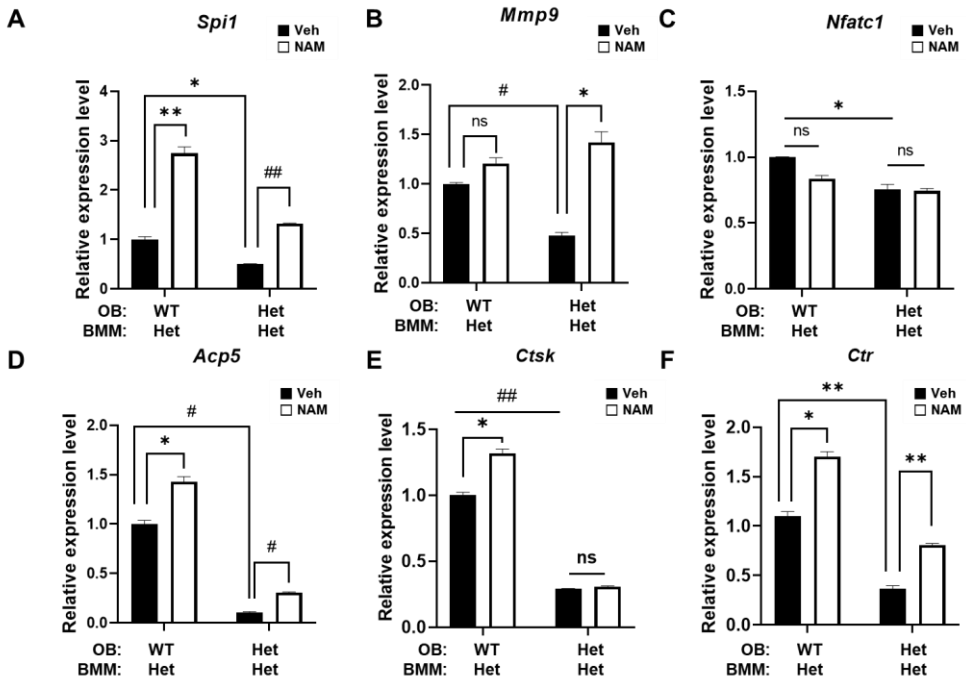

Figure 2.7. Nicotinamide increased the expression of osteoclast marker genes in co-culture of primary osteoblasts and BMMs.

(A-F) Nicotinamide or vehicle treated primary calvarial osteoblast and *Runx2*$^{+/-}$ BMMs were co-cultured. The mRNA levels of osteoclast marker genes were determined by RT-qPCR. Data are expressed as the mean ± SE. WT, wild type; Het, *Runx2*$^{+/-}$; NAM, nicotinamide. * $P < 0.05$, ** $P < 0.01$, # $P < 0.005$, ## $P < 0.001$; ns, not significant.

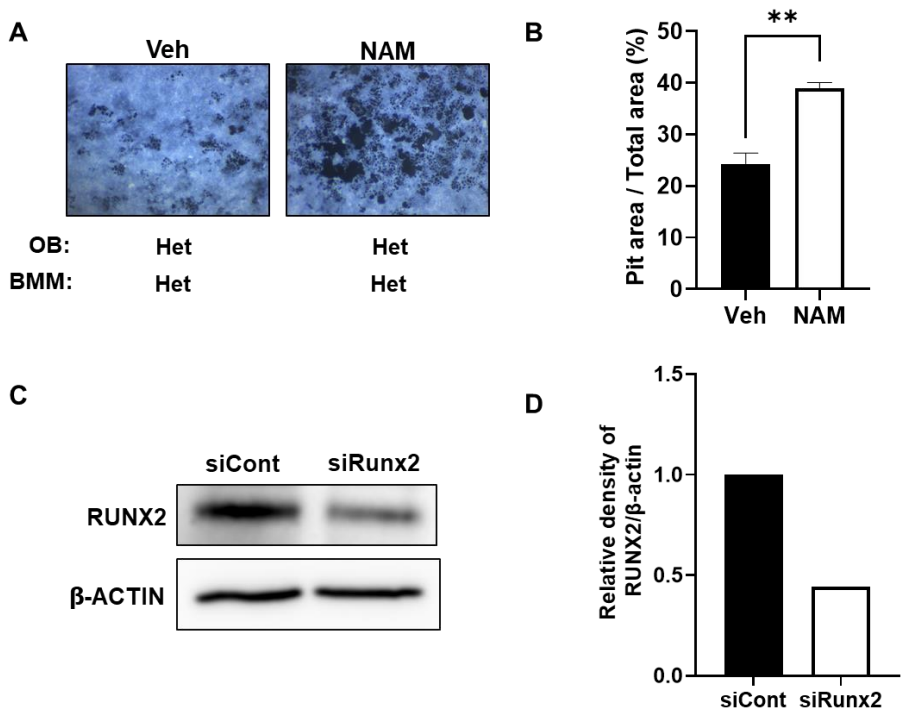

Figure 2.8. Co-culture of *Runx2*$^{+/-}$ BMM cells with *Runx2*$^{+/-}$ osteoblasts pre-treated with nicotinamide increased osteoclast pit formation

(A) Bone resorptive activity of BMMs isolated from *Runx2*$^{+/-}$ mice was assessed using an optical microscope after 7 days of co-culture with primary *Runx2*$^{+/-}$ calvarial osteoblasts with or without NAM on a calcium phosphate coated plate. (B) The pit area was measured by Image J with an inverted microscopic image. (C-D) Transfection efficiency of siRunx2- or siCont-transfected hDFCs was evaluated by immunoblot. Data are expressed as the mean ± SE. WT, wild type; Het, *Runx2*$^{+/-}$; NAM, nicotinamide. * $P < 0.05$, ** $P < 0.01$, # $P < 0.005$, ## $P < 0.001$; ns, not significant. 5 mM NAM, followed by co-culture with BMMs.

Nicotinamide restores RUNX2 and CSF1 levels in *Runx2*$^{+/-}$ osteoblasts

As HDIs increase RUNX2 expression by enhancing the protein's stability (Jeon, Lee et al. 2006), we tested for the effects of nicotinamide on *Runx2* mRNA and protein levels. Although nicotinamide did not change the *Runx2* mRNA levels (Figure. 2.9A), it restored the RUNX2 protein level in *Runx2*$^{+/-}$ osteoblasts to that found in untreated WT osteoblasts (Figure. 2.9B). Nicotinamide also increased the RUNX2 protein levels in WT osteoblasts. These results indicate that nicotinamide regulates RUNX2 at the posttranslational level but not at the transcriptional level. Correlatively, nicotinamide dose-dependently enhanced the RUNX2 transactivation function in MC3T3-E1 pre-osteoblast cells (Figure. 2.9C).

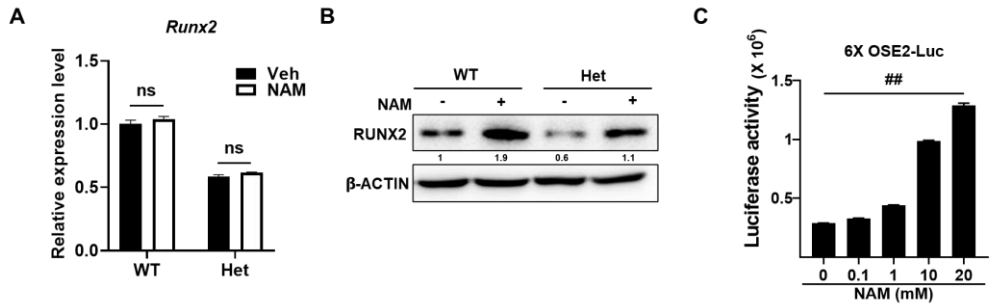

Figure 2.9. Nicotinamide increases the expression and transacting activity of RUNX2 in osteoblasts

(A–B) The mRNA level and protein level of Runx2 in WT and *Runx2*$^{+/-}$ mouse calvarial cells cultured in the presence or absence of 5 mM NAM for 3 days as determined by RT–qPCR (A) and immunoblot analysis (B). (C) The relative transactivation activity of RUNX2 as assessed using the 6XOSE2–luciferase reporter construct. Following transfection with 6XOSE2 reporter construct in the MC3T3–E1 pre–osteoblast cell line, cells were treated with NAM for 24 h. Data are expressed as the mean ± SE. WT, wild type; Het, *Runx2*$^{+/-}$; NAM, nicotinamide. * $P < 0.05$, ** $P < 0.01$, # $P < 0.005$, ## $P < 0.001$; ns, not significant.

Next, we examined the effects of nicotinamide in osteogenic differentiation of hDFCs. *Runx2*-depleted hDFCs showed lower ALP staining level than scrambled siRNA-treated cells (Figures. 2.10A and B). Although nicotinamide slightly increased ALP staining in both groups, we confirmed that the staining level of *Runx2*-depleted cells treated 10 mM nicotinamide was similar to that of vehicle-treated control cells, quantitatively (Figures. 2.10A and B).

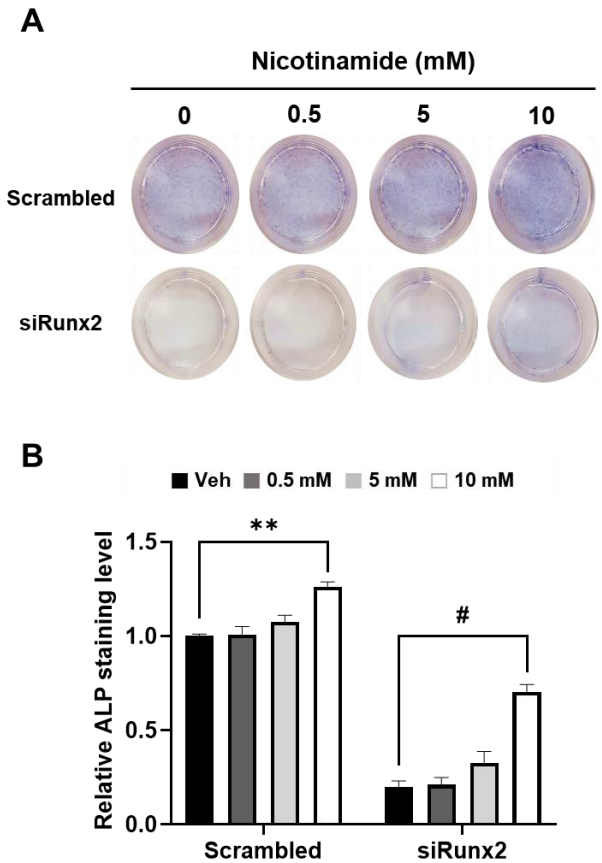

Figure 2.10. Nicotinamide increases osteogenic differentiation in siRunx2-treated human dental follicle cells.

(D) ALP staining was performed after scrambled or siRunx2-treated hDFCs were cultured in osteogenic media with the indicated concentration of NAM for 5 days. (E) ALP staining level was quantified by using Image J (n=2). Data are expressed as the mean ± SE. WT, wild type; Het, *Runx2*$^{+/-}$; NAM, nicotinamide. * $P < 0.05$, ** $P < 0.01$, # $P < 0.005$, ## $P < 0.001$; ns, not significant.

When examining our previously published RNA-seq data from WT and *Runx2*$^{+/-}$ calvarial osteoblasts (GSE87608) (Bae et al. 2017), we found that *Csf1* transcript was robustly decreased in *Runx2*$^{+/-}$ osteoblasts in comparison to WT osteoblasts, though the significance of this difference was weak. However, *Rankl* and *Opg* showed low basal expression level and no significant difference between WT and *Runx2*$^{+/-}$ cells, respectively (Figures. 2.11A-C).

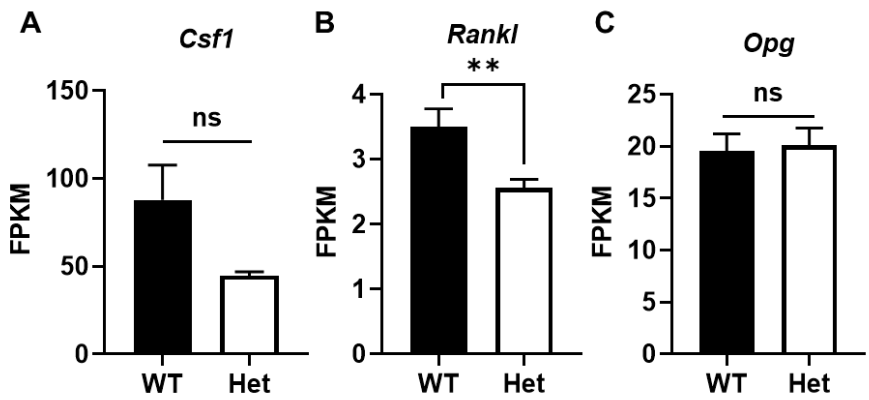

Figure 2.11. The expression levels of osteoclastogenicfactors in WT and *Runx2*$^{+/-}$ calvarial osteoblast cells

(A–C) Based on analysis of RNA–seq data, *Csf1*, *Rankl*, and *Opg* mRNA levels were compared in WT and *Runx2*$^{+/-}$ calvarial osteoblast cells. Data are expressed as the mean ± SE. FPKM, Fragments Per Kilobase of transcript per Million mapped reads; WT, wild type; Het, *Runx2*$^{+/-}$; NAM, nicotinamide. * $P < 0.05$, ** $P < 0.01$, # $P < 0.005$, ## $P < 0.001$; ns, not significant.

To confirm the results, we examined the mRNA levels by RT-qPCR. *Csf1* level was significantly reduced in *Runx2*$^{+/-}$ osteoblast cells compared to WT (Figure. 2.12A) while the levels of *Rankl* and *Opg* showed no significant difference between them (Figures. 2.12B and C), indicating that Csf1 might be a key regulator in the impairment of osteoclastogenesis shown in *Runx2*$^{+/-}$ CCD patients. Nicotinamide significantly increased *Csf1* mRNA level in both WT and *Runx2*$^{+/-}$ cells (Figure. 2.12D). *Rankl* was slightly increased by nicotinamide in *Runx2*$^{+/-}$ osteoblasts but not in WT (Figure. 2.12E). *Opg* mRNA level was significantly decreased by nicotinamide in both WT and *Runx2*$^{+/-}$ cells (Figure. 2.12F). This eventually led to the increase in the *Rankl/Opg* mRNA ratio (Figure. 2.12G). Additionally, the expression patterns of these proteins were similar to their mRNA expression patterns (Figure. 2.12H and I). These results suggest that nicotinamide can increase the protein level and transcriptional activity of RUNX2 and regulate the expression of critical osteoclastogenic factors, especially, Csf1 in osteoblasts.

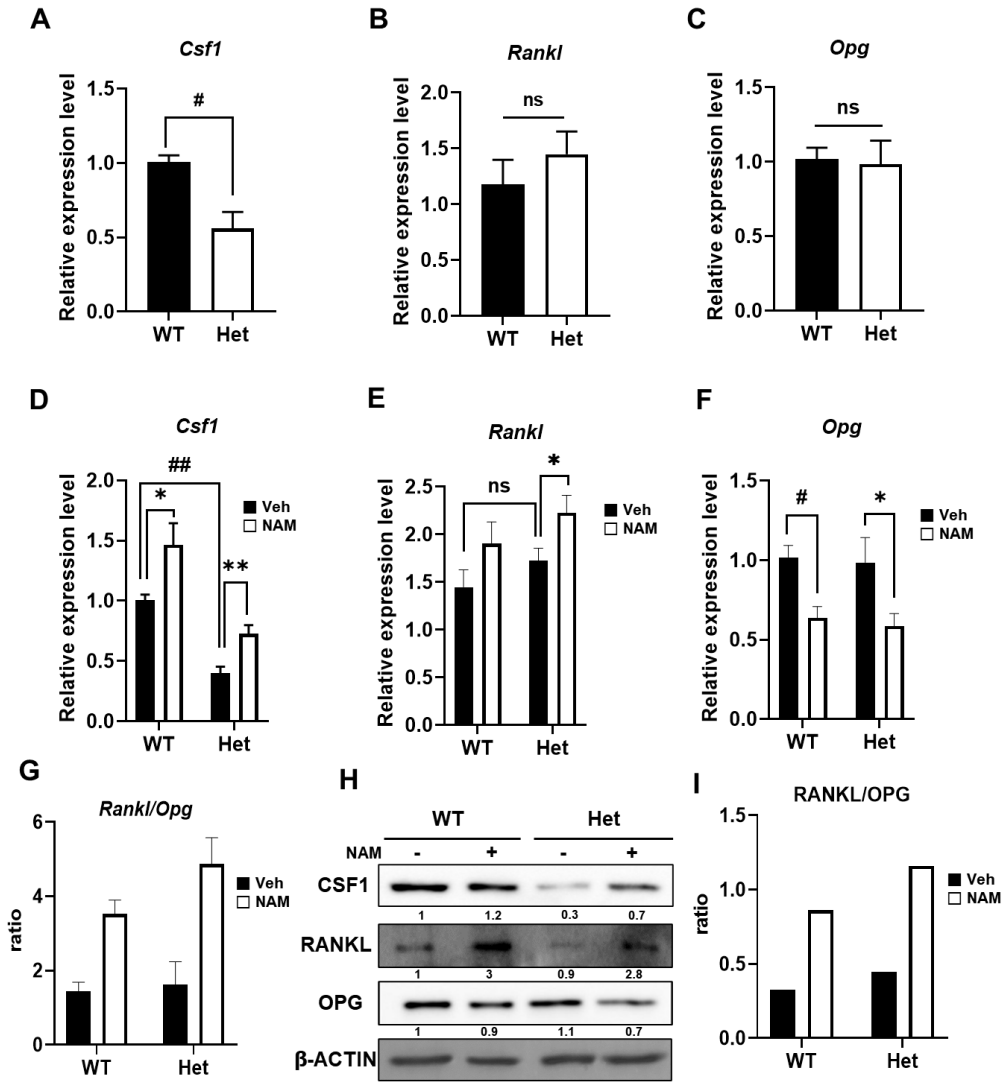

Figure 2.12. Nicotinamide increases the expression level of RUNX2 and CSF1 in *Runx2*$^{+/-}$ osteoblasts.

(A–C) Expression level of osteoclast differentiation–regulating genes in WT and *Runx2*$^{+/-}$ mouse calvarial cells as determined by RT–qPCR (n = 4). (D–F) The relative mRNA expression level of osteoclast differentiation factors in WT and *Runx2*$^{+/-}$ osteoblasts treated with vehicle or 5 mM NAM for 3 days as measured by RT–qPCR and the relative ratio of Rankl/Opg (G) (n ≥ 3). The protein

expression level of osteoclast differentiation-regulating genes as assessed by immunoblot analysis (H) and the RANKL/OPG ratio as calculated by densitometry using ImageJ (I). Data are expressed as the mean ± SE. WT, wild type; Het, *Runx2*$^{+/-}$; NAM, nicotinamide. * $P < 0.05$, ** $P < 0.01$, # $P < 0.005$, ## $P < 0.001$; ns, not significant.

RUNX2 directly up-regulates *Csf1* expression at the transcriptional level

Since we observed that the *Csf1* expression level was significantly decreased in *Runx2*$^{+/-}$ osteoblasts, we investigated whether *Csf1* expression was directly regulated by RUNX2. Both the mRNA and protein levels of Csf1 were significantly stimulated by forced RUNX2 expression in *Runx2*$^{-/-}$ cells (Figures. 2.13A and B). To see whether RUNX2 regulates *Csf1* expression at the transcriptional level, we investigated whether RUNX2 binding motifs exist in the promoter region of the *Csf1* gene using JASPAR (Fornes, Castro-Mondragon et al. 2020). We also analyzed both DNase-seq and RUNX2 ChIP-seq data using the MC3T3-E1 osteoblast differentiation model, which were downloaded from the GEO public functional genomics data repository (Wu, Whitfield et al. 2014, Tai, Wu et al. 2017). Surprisingly, we discovered that the DNase-seq and RUNX2 ChIP-seq results displayed the same peaks corresponding to the +68 to +186 bp downstream region from the transcription start site of the *Csf1* gene (boxed region in Figure. 2.14A). Moreover, a RUNX2 binding motif exists in this peak region (+173 to +178). ChIP assay verified that RUNX2 binds at the peak region containing the putative RUNX2 response elements of the *Csf1* gene (+74 to +260) (Figure. 2.13C). To further analyze whether RUNX2 directly regulates *Csf1* gene expression via this binding motif of the *Csf1* gene, we generated two reporter constructs with this response element containing region (+74 to +260) of the *Csf1* gene and with one having site-directed mutations at the RUNX2 binding motif. As shown in Figure.

2.13D, RUNX2 enhanced the transcriptional activity of the *Csf1* reporter gene, and the mutation of the putative RUNX2 binding motif abrogated the RUNX2-mediated stimulation.

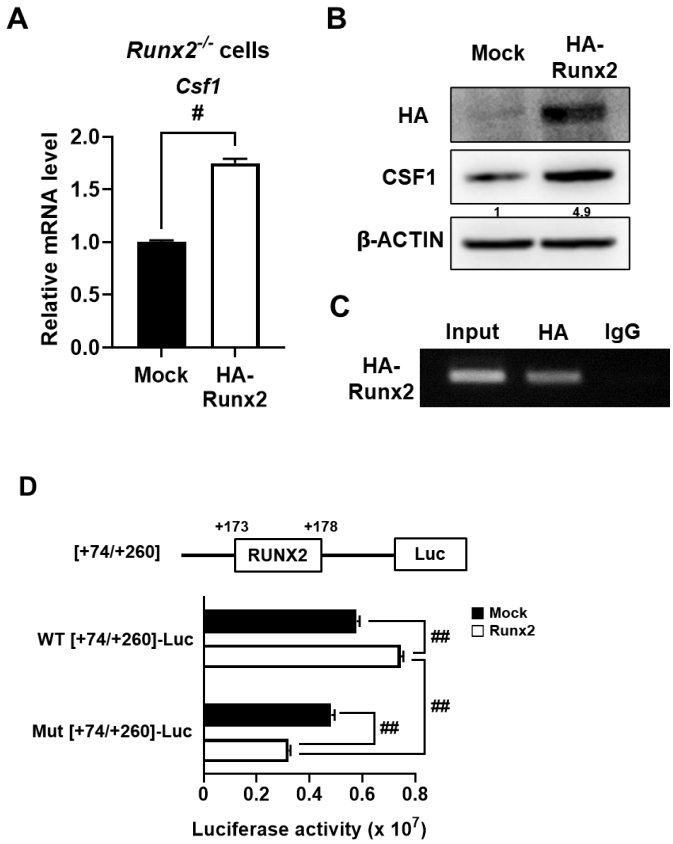

Figure 2.13. RUNX2 directly regulates *Csf1* expression via binding on the promoter region of the *Csf1* gene.

(A–B) The mRNA and protein levels of Csf1 in HA–tagged Runx2 plasmid–transfected *Runx2*$^{-/-}$ calvarial cell lines as assessed by RT–qPCR (A) and immunoblot analyses (B), respectively. (C) Chromatin immunoprecipitation (ChIP) assays performed on MC3T3–E1 cells transiently transfected with HA–Runx2. (D) Luciferase activities in HEK293 cells transfected with the Csf1 reporter vector and Runx2 expression vector. Data are expressed as the mean ± SE. WT, wild type; Het, *Runx2*$^{+/-}$; NAM, nicotinamide. * $P < 0.05$, ** $P < 0.01$, # $P < 0.005$, ## $P < 0.001$; ns, not significant.

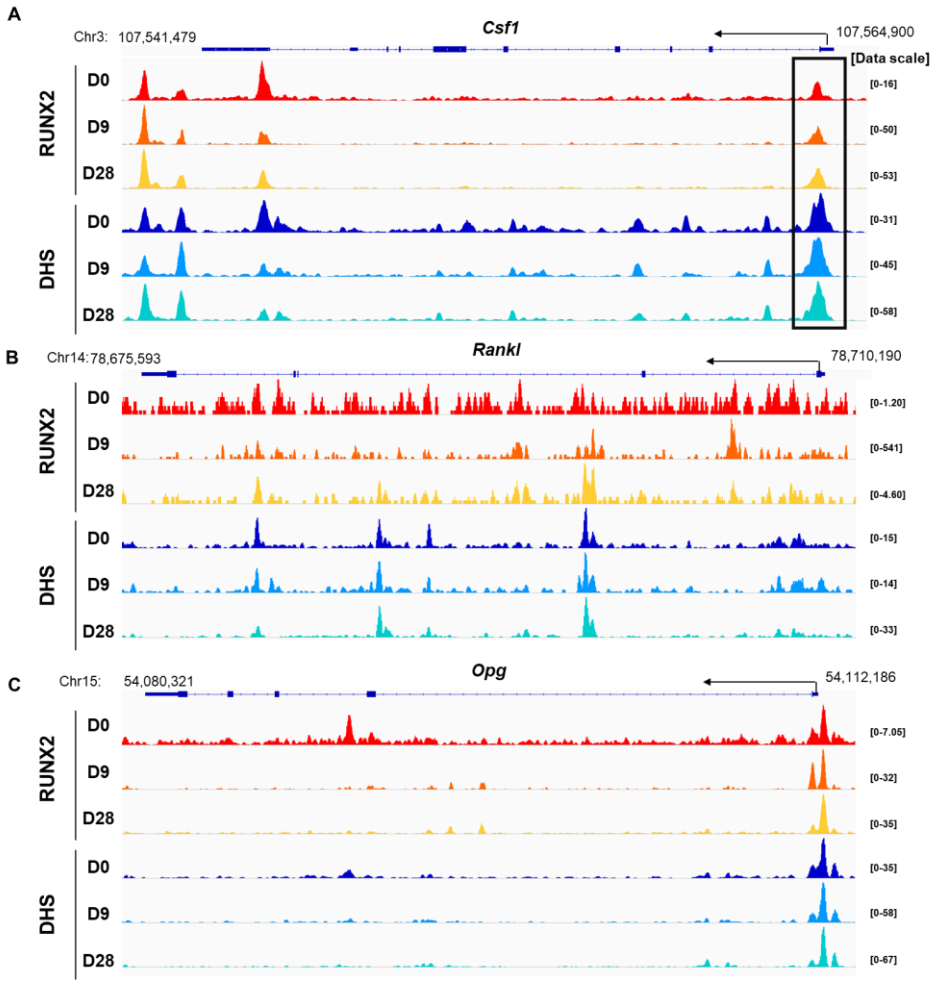

Figure 2.14. RUNX2 chromatin accessibility analysis during osteoblast differentiation in the promoter regions of *Csf1*, *Rankl* and *Opg* genes

(A-C) Analysis of RUNX2 occupancy and Genome-wide DNase hypersensitivity near or within *Csf1*, *Rankl* and *Opg* during MC3T3-E1 preosteoblast cell differentiation using the GO public genomics data repository (GSE54013 and GSE55046). The ChIP-seq and DNase-seq data were visualized using Integrative Genomics Viewer 2.8.2 (IGV 2.8.2).

Histological analyses confirmed attenuated CSF1 expression

in osteoblasts within the alveolar bone, DFCs, and dental pulp in *Runx2*$^{+/-}$ mice at P5 compared to WT mice (Figures. 2.15A and B). Like the data shown in Figures. 2.15A and B, nicotinamide administration restored the *Csf1* mRNA and protein levels in *Runx2*$^{+/-}$ mice. Taken together, these data indicate that nicotinamide-enhanced RUNX2 protein accumulation directly regulates Csf1 expression.

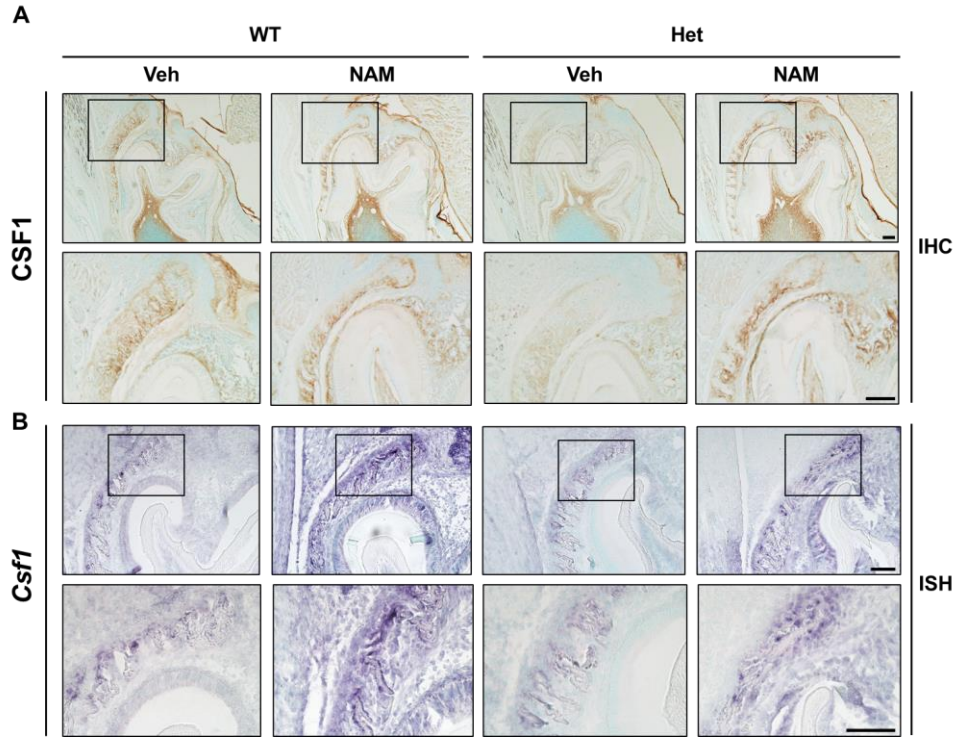

Figure 2.15. RUNX2 directly regulates Csf1 expression via binding on the promoter region of the *Csf1* gene.

(A) Immunohistochemistry (IHC) for CSF1 protein expression with histological sections of nicotinamide-treated or untreated P5 mice. The boxed areas in the top row are shown at a higher magnification in the bottom row. (B) *Csf1* mRNA expression with histological sections as detected by in situ hybridization (ISH). The boxed areas of the first row are displayed in the bottom row at a higher magnification (scale bar = 100 μm). Data are expressed as the mean ± SE. WT, wild type; Het, *Runx2*$^{+/-}$; NAM, nicotinamide. * $P < 0.05$, ** $P < 0.01$, # $P < 0.005$, ## $P < 0.001$; ns, not significant.

Nicotinamide activates RUNX2 through the inhibition of Sirt2

Sirt2 is the NAD^+-dependent deacetylases acting on a variety of histone and nonhistone substrates. Sirt2 activity is regulated by nicotinamide, a noncompetitive inhibitor that promotes a base-exchange reaction at the expense of deacetylation (Avalos, Bever et al. 2005). Therefore, we investigated whether Sirt2 is involved in the nicotinamide regulation of RUNX2 expression. To this end, primary osteoblasts were transfected with the Sirt2 expression vector at increasing concentrations. Immunoblot analysis showed that RUNX2 expression was decreased upon Sirt2 expression in a dose-dependent manner (Figure. 2.16A). Sirt2-dependent decrease of RUNX2 expression was significantly restored upon nicotinamide treatment (Figure. 2.16B). Taken together, these results indicate that nicotinamide can increase RUNX2 protein levels by inhibiting Sirt2 (Figure. 2.16C).

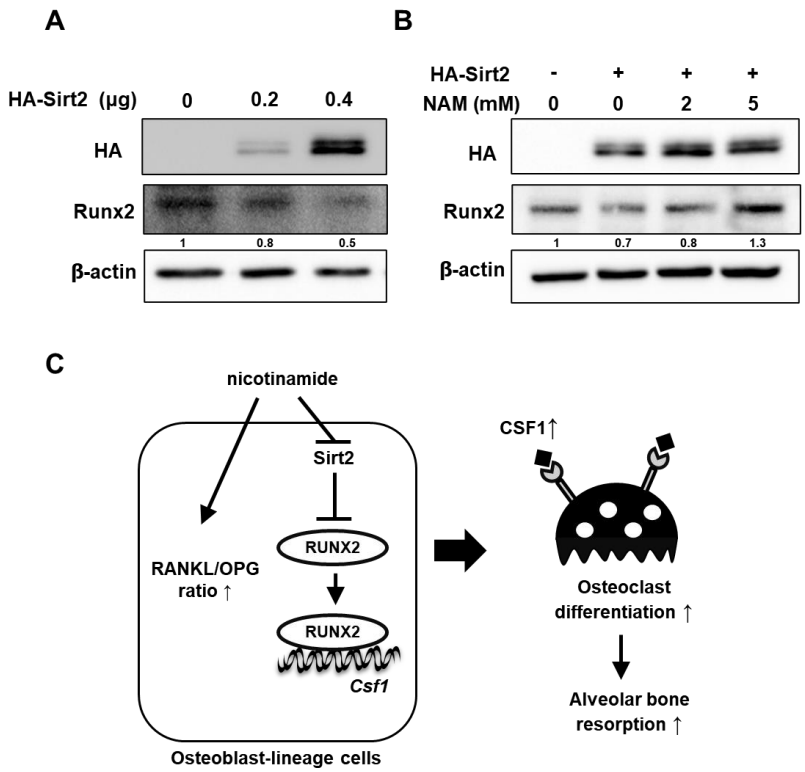

Figure 2.16. Nicotinamide enhances RUNX2 protein level by Sirt2 inhibition.

(A) Endogenous RUNX2 protein level in WT primary calvarial cells transiently transfected with HA-tagged Sirt2 plasmid as assessed by immunoblot analysis. (B) Nicotinamide treatment for 2 days following transfection of HA-tagged Sirt2 plasmid (0.4 μg). (C) Schema of mechanisms of RUNX2-Csf1 axis activation by nicotinamide. Nicotinamide treatment enhances RUNX2 protein level and transacting activity by Sirt2 inhibition. RUNX2 activated by nicotinamide directly increases Csf1 expression via Csf1 gene promoter binding and increased RANKL/OPG ratio in bone-forming cells, facilitating alveolar bone resorption via stimulation of osteoclast differentiation. NAM, nicotinamide.

Discussion

CCD patients suffer from abnormal skeletal development, especially dental anomalies, including delayed or unerupted permanent teeth. Timely surgical and orthodontic intervention are essential for dental management in CCD (Roberts, Stephen et al. 2013). Avoiding this painful, and expensive conventional treatment would be a present clinical unmet need. Our recent review suggested that RUNX2 modifying enzymes could be therapeutic targets for bone diseases (Kim, Kim et al. 2020, Kim, Shin et al. 2020). In this study, we demonstrate that nicotinamide improves impaired tooth eruption in CCD mice and reveal the underlying molecular mechanism.

Based on our *in vivo* proof of concept that an HDI alleviates CCD phenotypes (Bae, Yoon et al. 2017), we here tested whether nicotinamide could restore the delayed tooth eruption in *Runx2*$^{+/-}$ mice. When considering long-term dental treatment in young CCD patients, the safety is the most important issue together with therapeutic effect of the drug. In terms of the safety, unlike other HDIs, nicotinamide has been classified as a food additive rather than a drug and shows a low incidence of side effects and toxicities (Rolfe 2014). Also, nicotinamide has an established safety profile even at high dose in human (8 g/day) (Damian 2017). In our study, 1% nicotinamide (w/v) in drinking water provided to pregnant and nursing mice (1.19 g/kg), which equates to a 5.76 g dose of nicotinamide for a 60 kg person, did not show any notable toxic effects. When the dosage is converted to human equivalent dose (HED), it is within the range of safety profile. For this reason, it is

thought that nicotinamide is well suited for this indication. The current study showed that nicotinamide increases the expression and transactivation activity of RUNX2 via Sirt2 inhibition. Nicotinamide-activated RUNX2 enhances *Csf1* expression in bone-forming osteoblasts and subsequently stimulates osteoclast differentiation, leading to the rescue of delayed tooth eruption in *Runx2*$^{+/-}$ mice. On the basis of a proven safety profile and our current findings, nicotinamide may be considered for the treatment of dental abnormalities of CCD patients in the clinic as a RUNX2 activator.

CSF1 is a critical factor for osteoclastogenesis. *Op/op* mice, which lack *Csf1*, exhibit impacted teeth because of a deficiency in osteoclast activity (Ida-Yonemochi, Noda et al. 2002). It has been reported that the impairment of osteoclast differentiation in CCD patients is due to the decreased RANKL expression and RANKL/OPG ratio in bone-forming cells by the loss of RUNX2 (Enomoto et al. 2003; Wang et al. 2016). However, our study clearly indicates that CSF1 is the crucial target for the defect in osteoclast differentiation and the delayed tooth eruption in *Runx2*$^{+/-}$ mouse. The Csf1 mRNA and protein level were downregulated in *Runx2*$^{+/-}$ osteoblasts, while there were no significant differences in *Rankl* or *Opg* mRNA levels or *Rankl/Opg* ratio between WT and *Runx2*$^{+/-}$ osteoblasts. This discrepancy may be attributed to differences of the spatiotemporal expression of *Csf1*, *Rankl*, and *Opg* in tissue samples and primary cell systems tested between our and other groups. However, nicotinamide significantly increased the *Rankl/Opg* ratio in both WT and *Runx2*$^{+/-}$ osteoblasts via an

increase in *Rankl* expression and a decrease in *Opg* expression (Figure 3). It has been reported that *Csf1* downregulates *Opg* expression in DFCs for the alveolar bone resorption needed for tooth eruption (Wise, Yao et al. 2005). Our results showed increased *Csf1* and decreased *Opg* expression upon nicotinamide treatment (Figures 3I and K). These results suggest that the decreased *Opg* expression can be affected by nicotinamide-induced *Csf1 expression*. In addition, the increase in *Rankl/Opg* ratio may have maximized the effect of the nicotinamide restoration of delayed tooth eruption in CCD mice. Nicotinamide has been reported to upregulate RUNX3 expression through epigenetic activation and post-translation modification by Sirt2 inhibition (Kim, Lee et al. 2011). In this study, we confirmed that nicotinamide increases the expression and transacting activity of RUNX2 either. Moreover, the decreased RUNX2 level by the forced Sirt2 expression was rescued by nicotinamide. Although further study would be required to conclude that Sirt2 is indispensable factor in the nicotinamide-induced Runx2 expression, our current study shows that Sirt2 is involved in nicotinamide-induced Runx2 expression.

In summary, the present study shows for the first time that CSF1 level, not RANKL and OPG, is significantly reduced in *Runx2*$^{+/-}$ osteoblasts compared to WT and nicotinamide restores delayed tooth eruption in *Runx2*$^{+/-}$ mice with CCD phenotypes. We summarized its underlying mechanism in Figure 5C, which nicotinamide increases *Csf1* expression in *Runx2*-haploinsufficient osteoblasts via RUNX2 accumulation induced by Sirt2 inhibition, facilitating osteoclast differentiation for alveolar bone resorption for

tooth eruption. On the basis of this study, we propose nicotinamide as a candidate therapeutic drug for delayed or unerupted teeth in CCD patients. As nicotinamide stimulates bone remodeling via stimulation of both osteoblasts and osteoclasts, it may also facilitate orthodontic tooth movement by enhancing bone remodeling.

V. Conclusion

In this study, we aimed to determine the effect of NAM on the regulation of bone homeostasis. In part1, NAM not only promoted mitochondrial metabolism but also induced osteogenic differentiation by regulating intracellular ROS levels in osteoblasts. In part2, the delayed tooth eruption in *Runx2*$^{+/-}$ mice was due to the decreased osteoclast differentiation caused by *Runx2* deficient osteoblasts accompanying reduced *Csf1* level, an important osteoclast differentiation inducing factor.

NAM, a water-soluble vitamin B3, has been used for a long time to treat various diseases due to its safety profile. However, the effect of NAM on bone metabolism remains unclear. In this study, we established that NAM plays an important role in the regulation of both osteoblasts and osteoclasts. The results showed that various NAM concentrations either indirectly stimulated osteoclast differentiation by regulating osteoblasts or directly promoted osteoblast differentiation by targeting different Sirt. However, osteoblasts and osteoclasts always interact together in the process of bone remodeling, and a tightly regulated balance between the two is crucial. Thus, further studies are required to determine how NAM affect the communication between osteoblasts and osteoclasts.

VI. References

Ahuja, N., B. Schwer, S. Carobbio, D. Waltregny, B. J. North, V. Castronovo, P. Maechler and E. Verdin (2007). "Regulation of insulin secretion by SIRT4, a mitochondrial ADP-ribosyltransferase." J Biol Chem **282**(46): 33583-33592.

Alfadda, A. A. and R. M. Sallam (2012). "Reactive Oxygen Species in Health and Disease." Journal of Biomedicine and Biotechnology **2012**: 936486.

Ambrogini, E., M. Almeida, M. Martin-Millan, J.-H. Paik, R. A. DePinho, L. Han, J. Goellner, R. S. Weinstein, R. L. Jilka, C. A. O'Brien and S. C. Manolagas (2010). "FoxO-Mediated Defense against Oxidative Stress in Osteoblasts Is Indispensable for Skeletal Homeostasis in Mice." Cell Metabolism **11**(2): 136-146.

Andreyev, A. Y., Y. E. Kushnareva and A. A. Starkov (2005). "Mitochondrial metabolism of reactive oxygen species." Biochemistry (Mosc) **70**(2): 200-214.

Arakaki, N., A. Yamashita, S. Niimi and T. Yamazaki (2013). "Involvement of reactive oxygen species in osteoblastic differentiation of MC3T3-E1 cells accompanied by mitochondrial morphological dynamics." Biomedical Research **34**(3): 161-166.

Arfin, S., N. K. Jha, S. K. Jha, K. K. Kesari, J. Ruokolainen, S. Roychoudhury, B. Rathi and D. Kumar (2021). "Oxidative Stress in Cancer Cell Metabolism." Antioxidants (Basel) **10**(5).

Austin, S. and J. St-Pierre (2012). "PGC1α and mitochondrial metabolism – emerging concepts and relevance in ageing and neurodegenerative disorders." Journal of Cell Science **125**(21): 4963-4971.

Auten, R. L. and J. M. Davis (2009). "Oxygen Toxicity and Reactive Oxygen Species: The Devil Is in the Details." Pediatric Research **66**(2): 121-127.

Avalos, J. L., K. M. Bever and C. Wolberger (2005). "Mechanism of sirtuin inhibition by nicotinamide: altering the NAD(+) cosubstrate specificity of a Sir2 enzyme." Mol Cell **17**(6): 855-868.

Avalos, J. L., K. M. Bever and C. Wolberger (2005). "Mechanism of Sirtuin Inhibition by Nicotinamide: Altering the NAD+ Cosubstrate Specificity of a Sir2 Enzyme." Molecular Cell **17**(6): 855-868.

Ayer, D. E. (1999). "Histone deacetylases: transcriptional repression with SINers and NuRDs." Trends Cell Biol **9**(5): 193-198.

Bae, H.-S., W.-J. Yoon, Y.-D. Cho, R. Islam, H.-R. Shin, B.-S. Kim, J.-M. Lim, M.-S. Seo, S.-A. Cho, K.-Y. Choi, S.-H. Baek, H.-G. Kim, K.-M. Woo, J.-H. Baek, Y.-S. Lee and H.-M. Ryoo (2017). "An HDAC Inhibitor, Entinostat/MS-275, Partially

Prevents Delayed Cranial Suture Closure in Heterozygous Runx2 Null Mice." Journal of Bone and Mineral Research **32**(5): 951-961.

Bae, H. S., W. J. Yoon, Y. D. Cho, R. Islam, H. R. Shin, B. S. Kim, J. M. Lim, M. S. Seo, S. A. Cho, K. Y. Choi, S. H. Baek, H. G. Kim, K. M. Woo, J. H. Baek, Y. S. Lee and H. M. Ryoo (2017). "An HDAC Inhibitor, Entinostat/MS-275, Partially Prevents Delayed Cranial Suture Closure in Heterozygous Runx2 Null Mice." J Bone Miner Res **32**(5): 951-961.

Balaban, R. S., S. Nemoto and T. Finkel (2005). "Mitochondria, Oxidants, and Aging." Cell **120**(4): 483-495.

Bannister, A. J. and T. Kouzarides (2011). "Regulation of chromatin by histone modifications." Cell Research **21**(3): 381-395.

Basu, S., K. Michaëlsson, H. Olofsson, S. Johansson and H. Melhus (2001). "Association between oxidative stress and bone mineral density." Biochem Biophys Res Commun **288**(1): 275-279.

Begum, R., S. Howlader, A. N. M. M. Or-Rashid, R. S M, G. Ashraf, G. Albadrani, A. Sayed, I. Peluso, M. Abdel Daim and M. Uddin (2021). "Antioxidant and Signal Modulating Effects of Brown Seaweed Derived Compounds against Oxidative Stress-Associated Pathology." Oxidative Medicine and Cellular Longevity **2021**.

Blander, G. and L. Guarente (2004). "The Sir2 family of protein deacetylases." Annu Rev Biochem **73**: 417-435.

Bradley, E. W., L. R. Carpio, A. J. v. Wijnen, M. E. McGee-Lawrence and J. J. Westendorf (2015). "Histone Deacetylases in Bone Development and Skeletal Disorders." Physiological Reviews **95**(4): 1359-1381.

Brown, Kevin D., S. Maqsood, J.-Y. Huang, Y. Pan, W. Harkcom, W. Li, A. Sauve, E. Verdin and Samie R. Jaffrey (2014). "Activation of SIRT3 by the NAD+ Precursor Nicotinamide Riboside Protects from Noise-Induced Hearing Loss." Cell Metabolism **20**(6): 1059-1068.

Callaway, D. A. and J. X. Jiang (2015). "Reactive oxygen species and oxidative stress in osteoclastogenesis, skeletal aging and bone diseases." Journal of Bone and Mineral Metabolism **33**(4): 359-370.

Camilleri, S. and F. McDonald (2006). "Runx2 and dental development." Eur J Oral Sci **114**(5): 361-373.

Cantó, C. and J. Auwerx (2012). "Targeting sirtuin 1 to improve metabolism: all you need is NAD(+)?" Pharmacol Rev **64**(1): 166-187.

Cantó, C., R. H. Houtkooper, E. Pirinen, D. Y. Youn, M. H. Oosterveer, Y. Cen, P. J.

Fernandez-Marcos, H. Yamamoto, P. A. Andreux, P. Cettour-Rose, K. Gademann, C. Rinsch, K. Schoonjans, A. A. Sauve and J. Auwerx (2012). "The NAD(+) precursor nicotinamide riboside enhances oxidative metabolism and protects against high-fat diet-induced obesity." Cell Metab **15**(6): 838-847.

Carafa, V., D. Rotili, M. Forgione, F. Cuomo, E. Serretiello, G. S. Hailu, E. Jarho, M. Lahtela-Kakkonen, A. Mai and L. Altucci (2016). "Sirtuin functions and modulation: from chemistry to the clinic." Clinical Epigenetics **8**(1): 61.

Chang, A. R., C. M. Ferrer and R. Mostoslavsky (2019). "SIRT6, a Mammalian Deacylase with Multitasking Abilities." Physiological Reviews **100**(1): 145-169.

Chen, A. C., A. J. Martin, B. Choy, P. Fernández-Peñas, R. A. Dalziell, C. A. McKenzie, R. A. Scolyer, H. M. Dhillon, J. L. Vardy, A. Kricker, G. St. George, N. Chinniah, G. M. Halliday and D. L. Damian (2015). "A Phase 3 Randomized Trial of Nicotinamide for Skin-Cancer Chemoprevention." New England Journal of Medicine **373**(17): 1618-1626.

Chen, C.-T., Y.-R. V. Shih, T. K. Kuo, O. K. Lee and Y.-H. Wei (2008). "Coordinated Changes of Mitochondrial Biogenesis and Antioxidant Enzymes During Osteogenic Differentiation of Human Mesenchymal Stem Cells." Stem Cells **26**(4): 960-968.

Cho, Y. D., W. J. Yoon, K. M. Woo, J. H. Baek, G. Lee, J. Y. Cho and H. M. Ryoo (2009). "Molecular regulation of matrix extracellular phosphoglycoprotein expression by bone morphogenetic protein-2." J Biol Chem **284**(37): 25230-25240.

Choi, K.-Y., S.-W. Lee, M.-H. Park, Y.-C. Bae, H.-I. Shin, S.-H. Nam, Y.-J. Kim, H.-J. Kim and H.-M. Ryoo (2002). "Spatio-temporal expression patterns of Runx2 isoforms in early skeletogenesis." Experimental & Molecular Medicine **34**(6): 426-433.

Cohen, H. Y., C. Miller, K. J. Bitterman, N. R. Wall, B. Hekking, B. Kessler, K. T. Howitz, M. Gorospe, R. de Cabo and D. A. Sinclair (2004). "Calorie restriction promotes mammalian cell survival by inducing the SIRT1 deacetylase." Science **305**(5682): 390-392.

Crapo, J. D., T. Oury, C. Rabouille, J. W. Slot and L. Y. Chang (1992). "Copper,zinc superoxide dismutase is primarily a cytosolic protein in human cells." Proc Natl Acad Sci U S A **89**(21): 10405-10409.

D'Souza, R. N., T. Aberg, J. Gaikwad, A. Cavender, M. Owen, G. Karsenty and I. Thesleff (1999). "Cbfa1 is required for epithelial-mesenchymal interactions

regulating tooth development in mice." Development **126**(13): 2911-2920.
Damian, D. L. (2017). "Nicotinamide for skin cancer chemoprevention." Australas J Dermatol **58**(3): 174-180.
Derr, R. S., A. Q. van Hoesel, A. Benard, I. J. Goossens-Beumer, A. Sajet, N. G. Dekker-Ensink, E. M. de Kruijf, E. Bastiaannet, V. T. Smit, C. J. H. van de Velde and P. J. K. Kuppen (2014). "High nuclear expression levels of histone-modifying enzymes LSD1, HDAC2 and SIRT1 in tumor cells correlate with decreased survival and increased relapse in breast cancer patients." BMC Cancer **14**(1): 604.
Dikalova, A. E., A. Pandey, L. Xiao, L. Arslanbaeva, T. Sidorova, M. G. Lopez, F. T. Billings, E. Verdin, J. Auwerx, D. G. Harrison and S. I. Dikalov (2020). "Mitochondrial Deacetylase Sirt3 Reduces Vascular Dysfunction and Hypertension While Sirt3 Depletion in Essential Hypertension Is Linked to Vascular Inflammation and Oxidative Stress." Circulation Research **126**(4): 439-452.
Ding, G., J. Zhao and D. Jiang (2016). "Allicin inhibits oxidative stress-induced mitochondrial dysfunction and apoptosis by promoting PI3K/AKT and CREB/ERK signaling in osteoblast cells." Exp Ther Med **11**(6): 2553-2560.
Donmez, G., A. Arun, C. Y. Chung, P. J. McLean, S. Lindquist and L. Guarente (2012). "SIRT1 protects against α-synuclein aggregation by activating molecular chaperones." J Neurosci **32**(1): 124-132.
Drazic, A., L. M. Myklebust, R. Ree and T. Arnesen (2016). "The world of protein acetylation." Biochimica et Biophysica Acta (BBA) - Proteins and Proteomics **1864**(10): 1372-1401.
Du, J., Y. Zhou, X. Su, J. J. Yu, S. Khan, H. Jiang, J. Kim, J. Woo, J. H. Kim, B. H. Choi, B. He, W. Chen, S. Zhang, R. A. Cerione, J. Auwerx, Q. Hao and H. Lin (2011). "Sirt5 is a NAD-dependent protein lysine demalonylase and desuccinylase." Science **334**(6057): 806-809.
Edwards, J. R., D. S. Perrien, N. Fleming, J. S. Nyman, K. Ono, L. Connelly, M. M. Moore, S. T. Lwin, F. E. Yull, G. R. Mundy and F. Elefteriou (2013). "Silent information regulator (Sir)T1 inhibits NF-κB signaling to maintain normal skeletal remodeling." Journal of Bone and Mineral Research **28**(4): 960-969.
Edwards, J. R., D. S. Perrien, N. Fleming, J. S. Nyman, K. Ono, L. Connelly, M. M. Moore, S. T. Lwin, F. E. Yull, G. R. Mundy and F. Elefteriou (2013). "Silent information regulator (Sir)T1 inhibits NF-κB signaling to maintain normal skeletal remodeling." J Bone Miner Res **28**(4): 960-969.

Enomoto, H., S. Shiojiri, K. Hoshi, T. Furuichi, R. Fukuyama, C. A. Yoshida, N. Kanatani, R. Nakamura, A. Mizuno, A. Zanma, K. Yano, H. Yasuda, K. Higashio, K. Takada and T. Komori (2003). "Induction of Osteoclast Differentiation by Runx2 through Receptor Activator of Nuclear Factor-κB Ligand (RANKL) and Osteoprotegerin Regulation and Partial Rescue of Osteoclastogenesis in Runx2–/– Mice by RANKL Transgene*." Journal of Biological Chemistry **278**(26): 23971-23977.

Farrow, E., R. Nicot, A. Wiss, A. Laborde and J. Ferri (2018). "Cleidocranial Dysplasia: A Review of Clinical, Radiological, Genetic Implications and a Guidelines Proposal." J Craniofac Surg **29**(2): 382-389.

Feher, J. (2017). 2.10 - ATP Production II: The TCA Cycle and Oxidative Phosphorylation. Quantitative Human Physiology (Second Edition). J. Feher. Boston, Academic Press**:** 227-240.

Fornes, O., J. A. Castro-Mondragon, A. Khan, R. van der Lee, X. Zhang, P. A. Richmond, B. P. Modi, S. Correard, M. Gheorghe, D. Baranasic, W. Santana-Garcia, G. Tan, J. Cheneby, B. Ballester, F. Parcy, A. Sandelin, B. Lenhard, W. W. Wasserman and A. Mathelier (2020). "JASPAR 2020: update of the open-access database of transcription factor binding profiles." Nucleic Acids Res **48**(D1): D87-d92.

Forni, M. F., J. Peloggia, K. Trudeau, O. Shirihai and A. J. Kowaltowski (2016). "Murine Mesenchymal Stem Cell Commitment to Differentiation Is Regulated by Mitochondrial Dynamics." Stem Cells **34**(3): 743-755.

Fourcade, S., T. F. Outeiro and A. Pujol (2018). "SIRT2 in age-related neurodegenerative disorders." Aging (Albany NY) **10**(3): 295-296.

Fukai, T., R. J. Folz, U. Landmesser and D. G. Harrison (2002). "Extracellular superoxide dismutase and cardiovascular disease." Cardiovasc Res **55**(2): 239-249.

Fukuda, M., T. Yoshizawa, M. F. Karim, S. U. Sobuz, W. Korogi, D. Kobayasi, H. Okanishi, M. Tasaki, K. Ono, T. Sawa, Y. Sato, M. Chirifu, T. Masuda, T. Nakamura, H. Tanoue, K. Nakashima, Y. Kobashigawa, H. Morioka, E. Bober, S. Ohtsuki, Y. Yamagata, Y. Ando, Y. Oike, N. Araki, S. Takeda, H. Mizuta and K. Yamagata (2018). "SIRT7 has a critical role in bone formation by regulating lysine acylation of SP7/Osterix." Nature Communications **9**(1): 2833.

Gao, J., Z. Feng, X. Wang, M. Zeng, J. Liu, S. Han, J. Xu, L. Chen, K. Cao, J. Long, Z. Li, W. Shen and J. Liu (2018). "SIRT3/SOD2 maintains osteoblast differentiation

and bone formation by regulating mitochondrial stress." Cell Death & Differentiation **25**(2): 229-240.

Gaur, T., C. J. Lengner, H. Hovhannisyan, R. A. Bhat, P. V. N. Bodine, B. S. Komm, A. Javed, A. J. van Wijnen, J. L. Stein, G. S. Stein and J. B. Lian (2005). "Canonical WNT Signaling Promotes Osteogenesis by Directly Stimulating Runx2 Gene Expression*." Journal of Biological Chemistry **280**(39): 33132-33140.

Geoffroy, V., D. A. Corral, L. Zhou, B. Lee and G. Karsenty (1998). "Genomic organization, expression of the human CBFA1 gene, and evidence for an alternative splicing event affecting protein function." Mamm Genome **9**(1): 54-57.

Goettsch, C., A. Babelova, O. Trummer, R. G. Erben, M. Rauner, S. Rammelt, N. Weissmann, V. Weinberger, S. Benkhoff, M. Kampschulte, B. Obermayer-Pietsch, L. C. Hofbauer, R. P. Brandes and K. Schröder (2013). "NADPH oxidase 4 limits bone mass by promoting osteoclastogenesis." The Journal of Clinical Investigation **123**(11): 4731-4738.

He, L., T. He, S. Farrar, L. Ji, T. Liu and X. Ma (2017). "Antioxidants Maintain Cellular Redox Homeostasis by Elimination of Reactive Oxygen Species." Cellular Physiology and Biochemistry **44**(2): 532-553.

Heinrich, J., S. Bsoul, J. Barnes, K. Woodruff and S. Abboud (2005). "CSF-1, RANKL and OPG regulate osteoclastogenesis during murine tooth eruption." Arch Oral Biol **50**(10): 897-908.

Ho, L., L. Wang, T. M. Roth, Y. Pan, E. M. Verdin, E. C. Hsiao and R. A. Nissenson (2017). "Sirtuin-3 Promotes Adipogenesis, Osteoclastogenesis, and Bone Loss in Aging Male Mice." Endocrinology **158**(9): 2741-2753.

Hordyjewska, E., A. Jaruga, G. Kandzierski and P. Tylzanowski (2017). "Novel Mutation of the RUNX2 Gene in Patients with Cleidocranial Dysplasia." Molecular Syndromology **8**(5): 253-260.

Hu, E., Z. Chen, T. Fredrickson, Y. Zhu, R. Kirkpatrick, G. F. Zhang, K. Johanson, C. M. Sung, R. Liu and J. Winkler (2000). "Cloning and characterization of a novel human class I histone deacetylase that functions as a transcription repressor." J Biol Chem **275**(20): 15254-15264.

Huh, J.-E., J. H. Shin, E. S. Jang, S. J. Park, D. R. Park, R. Ko, D.-H. Seo, H.-S. Kim, S. H. Lee, Y. Choi, H. S. Kim and S. Y. Lee (2016). "Sirtuin 3 (SIRT3) maintains bone homeostasis by regulating AMPK-PGC-1β axis in mice." Scientific Reports **6**(1): 22511.

Hwang, E. S. and S. B. Song (2017). "Nicotinamide is an inhibitor of SIRT1 in

vitro, but can be a stimulator in cells." Cell Mol Life Sci **74**(18): 3347-3362.
Ida-Yonemochi, H., T. Noda, H. Shimokawa and T. Saku (2002). "Disturbed tooth eruption in osteopetrotic (op/op) mice: histopathogenesis of tooth malformation and odontomas." Journal of Oral Pathology & Medicine **31**(6): 361-373.
Imai, S.-i., C. M. Armstrong, M. Kaeberlein and L. Guarente (2000). "Transcriptional silencing and longevity protein Sir2 is an NAD-dependent histone deacetylase." Nature **403**(6771): 795-800.
Infante, A. and C. I. Rodríguez (2018). "Osteogenesis and aging: lessons from mesenchymal stem cells." Stem Cell Research & Therapy **9**(1): 244.
Iyer, S., E. Ambrogini, S. M. Bartell, L. Han, P. K. Roberson, R. de Cabo, R. L. Jilka, R. S. Weinstein, C. A. O'Brien, S. C. Manolagas and M. Almeida (2013). "FOXOs attenuate bone formation by suppressing Wnt signaling." J Clin Invest **123**(8): 3409-3419.
Iyer, S., L. Han, S. M. Bartell, H. N. Kim, I. Gubrij, R. de Cabo, C. A. O'Brien, S. C. Manolagas and M. Almeida (2014). "Sirtuin1 (Sirt1) promotes cortical bone formation by preventing β-catenin sequestration by FoxO transcription factors in osteoblast progenitors." J Biol Chem **289**(35): 24069-24078.
Jacobs, K. M., J. D. Pennington, K. S. Bisht, N. Aykin-Burns, H. S. Kim, M. Mishra, L. Sun, P. Nguyen, B. H. Ahn, J. Leclerc, C. X. Deng, D. R. Spitz and D. Gius (2008). "SIRT3 interacts with the daf-16 homolog FOXO3a in the mitochondria, as well as increases FOXO3a dependent gene expression." Int J Biol Sci **4**(5): 291-299.
Janciauskiene, S. (2020). "The Beneficial Effects of Antioxidants in Health And Diseases." Chronic Obstr Pulm Dis **7**(3): 182-202.
Jensen, E. D., T. M. Schroeder, J. Bailey, R. Gopalakrishnan and J. J. Westendorf (2008). "Histone deacetylase 7 associates with Runx2 and represses its activity during osteoblast maturation in a deacetylation-independent manner." J Bone Miner Res **23**(3): 361-372.
Jeon, E. J., K. Y. Lee, N. S. Choi, M. H. Lee, H. N. Kim, Y. H. Jin, H. M. Ryoo, J. Y. Choi, M. Yoshida, N. Nishino, B. C. Oh, K. S. Lee, Y. H. Lee and S. C. Bae (2006). "Bone morphogenetic protein-2 stimulates Runx2 acetylation." J Biol Chem **281**(24): 16502-16511.
Jeong, J. K., M. H. Moon, Y. J. Lee, J. W. Seol and S. Y. Park (2013). "Autophagy induced by the class III histone deacetylase Sirt1 prevents prion peptide neurotoxicity." Neurobiol Aging **34**(1): 146-156.
Jun, J. H., S. H. Lee, H. B. Kwak, Z. H. Lee, S. B. Seo, K. M. Woo, H. M. Ryoo, G. S.

Kim and J. H. Baek (2008). "N-acetylcysteine stimulates osteoblastic differentiation of mouse calvarial cells." J Cell Biochem **103**(4): 1246-1255.
Jun, J. H., W.-J. Yoon, S.-B. Seo, K.-M. Woo, G.-S. Kim, H.-M. Ryoo and J.-H. Baek (2010). "BMP2-activated Erk/MAP Kinase Stabilizes Runx2 by Increasing p300 Levels and Histone Acetyltransferase Activity." Journal of Biological Chemistry **285**(47): 36410-36419.
Kannan, K. and S. K. Jain (2000). "Oxidative stress and apoptosis." Pathophysiology **7**(3): 153-163.
Kenny, T. C. and D. Germain (2017). "From discovery of the CHOP axis and targeting ClpP to the identification of additional axes of the UPRmt driven by the estrogen receptor and SIRT3." J Bioenerg Biomembr **49**(4): 297-305.
Khalid, S., H. Yamazaki, M. Socorro, D. Monier, E. Beniash and D. Napierala (2020). "Reactive oxygen species (ROS) generation as an underlying mechanism of inorganic phosphate (Pi)-induced mineralization of osteogenic cells." Free Radical Biology and Medicine **153**: 103-111.
Khansari, N., Y. Shakiba and M. Mahmoudi (2009). "Chronic inflammation and oxidative stress as a major cause of age-related diseases and cancer." Recent Pat Inflamm Allergy Drug Discov **3**(1): 73-80.
Kim, H.-J., S. Y. Lee, C. Y. Kim, Y. H. Kim, W. Ju and S. C. Kim (2017). "Subcellular localization of FOXO3a as a potential biomarker of response to combined treatment with inhibitors of PI3K and autophagy in PIK3CA-mutant cancer cells." Oncotarget **8**(4): 6608-6622.
Kim, H.-N., J.-H. Lee, S.-C. Bae, H.-M. Ryoo, H.-H. Kim, H. Ha and Z. H. Lee (2011). "Histone deacetylase inhibitor MS-275 stimulates bone formation in part by enhancing Dhx36-mediated TNAP transcription." Journal of Bone and Mineral Research **26**(9): 2161-2173.
Kim, H. J., J. H. Kim, S. C. Bae, J. Y. Choi, H. J. Kim and H. M. Ryoo (2003). "The protein kinase C pathway plays a central role in the fibroblast growth factor-stimulated expression and transactivation activity of Runx2." J Biol Chem **278**(1): 319-326.
Kim, H. J., W. J. Kim and H. M. Ryoo (2020). "Post-Translational Regulations of Transcriptional Activity of RUNX2." Mol Cells **43**(2): 160-167.
Kim, H. J., W. J. Kim, H. R. Shin, H. I. Yoon, J. I. Moon, E. Lee, J. M. Lim, Y. D. Cho, M. H. Lee, H. G. Kim and H. M. Ryoo (2022). "ROS-induced PADI2 downregulation accelerates cellular senescence via the stimulation of SASP

production and NFκB activation." Cell Mol Life Sci **79**(3): 155.
Kim, H. N., L. Han, S. Iyer, R. de Cabo, H. Zhao, C. A. O'Brien, S. C. Manolagas and M. Almeida (2015). "Sirtuin1 Suppresses Osteoclastogenesis by Deacetylating FoxOs." Mol Endocrinol **29**(10): 1498-1509.
Kim, S.-J., Y. Piao, M. G. Lee, A. R. Han, K. Kim, C.-J. Hwang, J. T. Seo and S. J. Moon (2020). "Loss of Sirtuin 6 in osteoblast lineage cells activates osteoclasts, resulting in osteopenia." Bone **138**: 115497.
Kim, W.-J., J.-W. Lee, C. Quan, H.-J. Youn, H.-M. Kim and S.-C. Bae (2011). "Nicotinamide Inhibits Growth of Carcinogen Induced Mouse Bladder Tumor and Human Bladder Tumor Xenograft Through Up-Regulation of RUNX3 and p300." Journal of Urology **185**(6): 2366-2375.
Kim, W.-J., J.-W. Lee, C. Quan, H.-J. Youn, H.-M. Kim and S.-C. Bae (2011). "Nicotinamide Inhibits Growth of Carcinogen Induced Mouse Bladder Tumor and Human Bladder Tumor Xenograft Through Up-Regulation of RUNX3 and p300." The Journal of Urology **185**(6): 2366-2375.
Kim, W. J., H. L. Shin, B. S. Kim, H. J. Kim and H. M. Ryoo (2020). "RUNX2-modifying enzymes: therapeutic targets for bone diseases." Exp Mol Med.
Komori, T. (2010). "Regulation of osteoblast differentiation by Runx2." Adv Exp Med Biol **658**: 43-49.
Komori, T., H. Yagi, S. Nomura, A. Yamaguchi, K. Sasaki, K. Deguchi, Y. Shimizu, R. T. Bronson, Y. H. Gao, M. Inada, M. Sato, R. Okamoto, Y. Kitamura, S. Yoshiki and T. Kishimoto (1997). Targeted disruption of Cbfa1 results in a complete lack of bone formation owing to maturational arrest of osteoblasts. 89.
Komori, T., H. Yagi, S. Nomura, A. Yamaguchi, K. Sasaki, K. Deguchi, Y. Shimizu, R. T. Bronson, Y. H. Gao, M. Inada, M. Sato, R. Okamoto, Y. Kitamura, S. Yoshiki and T. Kishimoto (1997). "Targeted disruption of Cbfa1 results in a complete lack of bone formation owing to maturational arrest of osteoblasts." Cell **89**(5): 755-764.
Kong, Y. Y., H. Yoshida, I. Sarosi, H. L. Tan, E. Timms, C. Capparelli, S. Morony, A. J. Oliveira-dos-Santos, G. Van, A. Itie, W. Khoo, A. Wakeham, C. R. Dunstan, D. L. Lacey, T. W. Mak, W. J. Boyle and J. M. Penninger (1999). "OPGL is a key regulator of osteoclastogenesis, lymphocyte development and lymph-node organogenesis." Nature **397**(6717): 315-323.
Kornberg, R. D. (1974). "Chromatin structure: a repeating unit of histones and DNA." Science **184**(4139): 868-871.
Lee, D. H., B. S. Lim, Y. K. Lee and H. C. Yang (2006). "Effects of hydrogen

peroxide (H2O2) on alkaline phosphatase activity and matrix mineralization of odontoblast and osteoblast cell lines." Cell Biology and Toxicology **22**(1): 39-46.
Lee, H. W., J. H. Suh, A. Y. Kim, Y. S. Lee, S. Y. Park and J. B. Kim (2006). "Histone deacetylase 1-mediated histone modification regulates osteoblast differentiation." Mol Endocrinol **20**(10): 2432-2443.
Lee, K.-S., H.-J. Kim, Q.-L. Li, X.-Z. Chi, C. Ueta, T. Komori, J. M. Wozney, E.-G. Kim, J.-Y. Choi, H.-M. Ryoo and S.-C. Bae (2000). "Runx2 Is a Common Target of Transforming Growth Factor β1 and Bone Morphogenetic Protein 2, and Cooperation between Runx2 and Smad5 Induces Osteoblast-Specific Gene Expression in the Pluripotent Mesenchymal Precursor Cell Line C2C12." Molecular and Cellular Biology **20**(23): 8783-8792.
Lee, K. K. and J. L. Workman (2007). "Histone acetyltransferase complexes: one size doesn't fit all." Nature Reviews Molecular Cell Biology **8**(4): 284-295.
Lemieux, M. E., X. Yang, K. Jardine, X. He, K. X. Jacobsen, W. A. Staines, M. E. Harper and M. W. McBurney (2005). "The Sirt1 deacetylase modulates the insulin-like growth factor signaling pathway in mammals." Mechanisms of Ageing and Development **126**(10): 1097-1105.
Lepetsos, P. and A. G. Papavassiliou (2016). "ROS/oxidative stress signaling in osteoarthritis." Biochimica et Biophysica Acta (BBA) - Molecular Basis of Disease **1862**(4): 576-591.
Li, Q., Z. Gao, Y. Chen and M. X. Guan (2017). "The role of mitochondria in osteogenic, adipogenic and chondrogenic differentiation of mesenchymal stem cells." Protein Cell **8**(6): 439-445.
Li, X., B. Li, Y. Shi, C. Wang and L. Ye (2021). "Targeting reactive oxygen species in stem cells for bone therapy." Drug Discovery Today **26**(5): 1226-1244.
Lin, M. T. and M. F. Beal (2006). "Mitochondrial dysfunction and oxidative stress in neurodegenerative diseases." Nature **443**(7113): 787-795.
Lin, Z. F., H. B. Xu, J. Y. Wang, Q. Lin, Z. Ruan, F. B. Liu, W. Jin, H. H. Huang and X. Chen (2013). "SIRT5 desuccinylates and activates SOD1 to eliminate ROS." Biochem Biophys Res Commun **441**(1): 191-195.
Ling, W., K. Krager, K. K. Richardson, A. D. Warren, F. Ponte, N. Aykin-Burns, S. C. Manolagas, M. Almeida and H.-N. Kim (2021). "Mitochondrial Sirt3 contributes to the bone loss caused by aging or estrogen deficiency." JCI Insight **6**(10).
Liu, W., S. Toyosawa, T. Furuichi, N. Kanatani, C. Yoshida, Y. Liu, M. Himeno, S. Narai, A. Yamaguchi and T. Komori (2001). "Overexpression of Cbfa1 in

osteoblasts inhibits osteoblast maturation and causes osteopenia with multiple fractures." J Cell Biol **155**(1): 157-166.

Long, A. N., K. Owens, A. E. Schlappal, T. Kristian, P. S. Fishman and R. A. Schuh (2015). "Effect of nicotinamide mononucleotide on brain mitochondrial respiratory deficits in an Alzheimer's disease-relevant murine model." BMC Neurology **15**(1): 19.

Luo, Y. X., X. Tang, X. Z. An, X. M. Xie, X. F. Chen, X. Zhao, D. L. Hao, H. Z. Chen and D. P. Liu (2017). "SIRT4 accelerates Ang II-induced pathological cardiac hypertrophy by inhibiting manganese superoxide dismutase activity." Eur Heart J **38**(18): 1389-1398.

Lv, Y. J., Y. Yang, B. D. Sui, C. H. Hu, P. Zhao, L. Liao, J. Chen, L. Q. Zhang, T. T. Yang, S. F. Zhang and Y. Jin (2018). "Resveratrol counteracts bone loss via mitofilin-mediated osteogenic improvement of mesenchymal stem cells in senescence-accelerated mice." Theranostics **8**(9): 2387-2406.

Ma, C., Y. Sun, C. Pi, H. Wang, H. Sun, X. Yu, Y. Shi and X. He (2020). "Sirt3 Attenuates Oxidative Stress Damage and Rescues Cellular Senescence in Rat Bone Marrow Mesenchymal Stem Cells by Targeting Superoxide Dismutase 2." Frontiers in Cell and Developmental Biology **8**.

Ma, L., W. Maruwge, A. Strambi, P. D'Arcy, P. Pellegrini, L. Kis, A. de Milito, S. Lain and B. Brodin (2014). "SIRT1 and SIRT2 inhibition impairs pediatric soft tissue sarcoma growth." Cell Death Dis **5**: e1483.

Malik, A. N., A. Czajka and P. Cunningham (2016). "Accurate quantification of mouse mitochondrial DNA without co-amplification of nuclear mitochondrial insertion sequences." Mitochondrion **29**: 59-64.

McGee-Lawrence, M. E. and J. J. Westendorf (2011). "Histone deacetylases in skeletal development and bone mass maintenance." Gene **474**(1): 1-11.

Melnikova, I. N., B. E. Crute, S. Wang and N. A. Speck (1993). "Sequence specificity of the core-binding factor." Journal of Virology **67**(4): 2408-2411.

Meng, Y., Z. Ren, F. Xu, X. Zhou, C. Song, V. Y.-F. Wang, W. Liu, L. Lu, J. A. Thomson and G. Chen (2018). "Nicotinamide Promotes Cell Survival and Differentiation as Kinase Inhibitor in Human Pluripotent Stem Cells." Stem Cell Reports **11**(6): 1347-1356.

Mihaylova, M. M. and R. J. Shaw (2013). "Metabolic reprogramming by class I and II histone deacetylases." Trends Endocrinol Metab **24**(1): 48-57.

Miller, H. E. and A. J. R. Bishop (2021). "Correlation AnalyzeR: functional

predictions from gene co-expression correlations." BMC Bioinformatics **22**(1): 206.

Mody, N., F. Parhami, T. A. Sarafian and L. L. Demer (2001). "Oxidative stress modulates osteoblastic differentiation of vascular and bone cells." Free Radical Biology and Medicine **31**(4): 509-519.

Mohrin, M., J. Shin, Y. Liu, K. Brown, H. Luo, Y. Xi, C. M. Haynes and D. Chen (2015). "A mitochondrial UPR-mediated metabolic checkpoint regulates hematopoietic stem cell aging." Science **347**(6228): 1374-1377.

Morigi, M., L. Perico and A. Benigni (2018). "Sirtuins in Renal Health and Disease." Journal of the American Society of Nephrology **29**(7): 1799.

Mouchiroud, L., R. H. Houtkooper, N. Moullan, E. Katsyuba, D. Ryu, C. Cantó, A. Mottis, Y. S. Jo, M. Viswanathan, K. Schoonjans, L. Guarente and J. Auwerx (2013). "The NAD(+)/Sirtuin Pathway Modulates Longevity through Activation of Mitochondrial UPR and FOXO Signaling." Cell **154**(2): 430-441.

Mundlos, S., F. Otto, C. Mundlos, J. B. Mulliken, A. S. Aylsworth, S. Albright, D. Lindhout, W. G. Cole, W. Henn, J. H. M. Knoll, M. J. Owen, R. Mertelsmann, B. U. Zabel and B. R. Olsen (1997). "Mutations Involving the Transcription Factor CBFA1 Cause Cleidocranial Dysplasia." Cell **89**(5): 773-779.

Nasrin, N., X. Wu, E. Fortier, Y. Feng, O. C. Bare, S. Chen, X. Ren, Z. Wu, R. S. Streeper and L. Bordone (2010). "SIRT4 Regulates Fatty Acid Oxidation and Mitochondrial Gene Expression in Liver and Muscle Cells." Journal of Biological Chemistry **285**(42): 31995-32002.

Okado-Matsumoto, A. and I. Fridovich (2001). "Subcellular distribution of superoxide dismutases (SOD) in rat liver: Cu,Zn-SOD in mitochondria." J Biol Chem **276**(42): 38388-38393.

Olins, A. L. and D. E. Olins (1974). "Spheroid chromatin units (v bodies)." Science **183**(4122): 330-332.

Oliver, K. L., V. Lukic, N. P. Thorne, S. F. Berkovic, I. E. Scheffer and M. Bahlo (2014). "Harnessing Gene Expression Networks to Prioritize Candidate Epileptic Encephalopathy Genes." PLOS ONE **9**(7): e102079.

Olmos, Y., I. Valle, S. Borniquel, A. Tierrez, E. Soria, S. Lamas and M. Monsalve (2009). "Mutual Dependence of Foxo3a and PGC-1α in the Induction of Oxidative Stress Genes." Journal of Biological Chemistry **284**(21): 14476-14484.

Otto, F., H. Kanegane and S. Mundlos (2002). "Mutations in the RUNX2 gene in patients with cleidocranial dysplasia." Hum Mutat **19**(3): 209-216.

Otto, F., M. Lübbert and M. Stock (2003). "Upstream and downstream targets of RUNX proteins." J Cell Biochem **89**(1): 9-18.

Pan, H., D. Guan, X. Liu, J. Li, L. Wang, J. Wu, J. Zhou, W. Zhang, R. Ren, W. Zhang, Y. Li, J. Yang, Y. Hao, T. Yuan, G. Yuan, H. Wang, Z. Ju, Z. Mao, J. Li, J. Qu, F. Tang and G.-H. Liu (2016). "SIRT6 safeguards human mesenchymal stem cells from oxidative stress by coactivating NRF2." Cell Research **26**(2): 190-205.

Park, O.-J., H.-J. Kim, K.-M. Woo, J.-H. Baek and H.-M. Ryoo (2010). "FGF2-activated ERK Mitogen-activated Protein Kinase Enhances Runx2 Acetylation and Stabilization." Journal of Biological Chemistry **285**(6): 3568-3574.

Park, S.-Y. and J.-S. Kim (2020). "A short guide to histone deacetylases including recent progress on class II enzymes." Experimental & Molecular Medicine **52**(2): 204-212.

Park, S. Y., K. B. Lee, M. J. Lee, S. C. Bae and J. J. Jang (2012). "Nicotinamide inhibits the early stage of carcinogen-induced hepatocarcinogenesis in mice and suppresses human hepatocellular carcinoma cell growth." J Cell Physiol **227**(3): 899-908.

Park, T. K. N., K. Vargervik and S. Oberoi (2013). "Orthodontic and surgical management of cleidocranial dysplasia." kjod **43**(5): 248-260.

Peoples, J. N., A. Saraf, N. Ghazal, T. T. Pham and J. Q. Kwong (2019). "Mitochondrial dysfunction and oxidative stress in heart disease." Experimental & Molecular Medicine **51**(12): 1-13.

Popov, L. D. (2020). "Mitochondrial biogenesis: An update." J Cell Mol Med **24**(9): 4892-4899.

Qiao, X., Y. Nie, Y. Ma, Y. Chen, R. Cheng, W. Yin, Y. Hu, W. Xu and L. Xu (2016). "Irisin promotes osteoblast proliferation and differentiation via activating the MAP kinase signaling pathways." Scientific Reports **6**(1): 18732.

Qin, W., T. Yang, L. Ho, Z. Zhao, J. Wang, L. Chen, W. Zhao, M. Thiyagarajan, D. MacGrogan, J. T. Rodgers, P. Puigserver, J. Sadoshima, H. Deng, S. Pedrini, S. Gandy, A. A. Sauve and G. M. Pasinetti (2006). "Neuronal SIRT1 activation as a novel mechanism underlying the prevention of Alzheimer disease amyloid neuropathology by calorie restriction." J Biol Chem **281**(31): 21745-21754.

Quiros, P. M., A. Goyal, P. Jha and J. Auwerx (2017). "Analysis of mtDNA/nDNA Ratio in Mice." Current Protocols in Mouse Biology **7**(1): 47-54.

Richter, K., A. Konzack, T. Pihlajaniemi, R. Heljasvaara and T. Kietzmann (2015). "Redox-fibrosis: Impact of TGFβ1 on ROS generators, mediators and functional

consequences." Redox Biol **6**: 344-352.
Roberts, T., L. Stephen and P. Beighton (2013). "Cleidocranial dysplasia: a review of the dental, historical, and practical implications with an overview of the South African experience." Oral Surgery, Oral Medicine, Oral Pathology and Oral Radiology **115**(1): 46-55.
Rolfe, H. M. (2014). "A review of nicotinamide: treatment of skin diseases and potential side effects." Journal of Cosmetic Dermatology **13**(4): 324-328.
Russell, A. P., V. C. Foletta, R. J. Snow and G. D. Wadley (2014). "Skeletal muscle mitochondria: A major player in exercise, health and disease." Biochimica et Biophysica Acta (BBA) - General Subjects **1840**(4): 1276-1284.
Schoppa, A. M., X. Chen, J. M. Ramge, A. Vikman, V. Fischer, M. Haffner-Luntzer, J. Riegger, J. Tuckermann, K. Scharffetter-Kochanek and A. Ignatius (2022). "Osteoblast lineage Sod2 deficiency leads to an osteoporosis-like phenotype in mice." Dis Model Mech **15**(5).
Sedelnikova, O. A., I. Horikawa, D. B. Zimonjic, N. C. Popescu, W. M. Bonner and J. C. Barrett (2004). "Senescing human cells and ageing mice accumulate DNA lesions with unrepairable double-strand breaks." Nature Cell Biology **6**(2): 168-170.
Sedelnikova, O. A., C. E. Redon, J. S. Dickey, A. J. Nakamura, A. G. Georgakilas and W. M. Bonner (2010). "Role of oxidatively induced DNA lesions in human pathogenesis." Mutation Research/Reviews in Mutation Research **704**(1): 152-159.
Sena, L. A. and N. S. Chandel (2012). "Physiological roles of mitochondrial reactive oxygen species." Mol Cell **48**(2): 158-167.
Seto, E. and M. Yoshida (2014). "Erasers of histone acetylation: the histone deacetylase enzymes." Cold Spring Harb Perspect Biol **6**(4): a018713.
Shares, B. H., M. Busch, N. White, L. Shum and R. A. Eliseev (2018). "Active mitochondria support osteogenic differentiation by stimulating β-catenin acetylation." Journal of Biological Chemistry **293**(41): 16019-16027.
She, J., R. Sheng and Z.-H. Qin (2022). "Pharmacology and Potential Implications of Nicotinamide Adenine Dinucleotide Precursors." Aging and disease **12**(8): 1879-1897.
Shin, H. R., H. S. Bae, B. S. Kim, H. I. Yoon, Y. D. Cho, W. J. Kim, K. Y. Choi, Y. S. Lee, K. M. Woo, J. H. Baek and H. M. Ryoo (2018). "PIN1 is a new therapeutic target of craniosynostosis." Hum Mol Genet **27**(22): 3827-3839.

Shum, L. C., N. S. White, B. N. Mills, K. L. Bentley and R. A. Eliseev (2016). "Energy Metabolism in Mesenchymal Stem Cells During Osteogenic Differentiation." Stem Cells Dev **25**(2): 114-122.

Sidorova-Darmos, E., R. Sommer and J. H. Eubanks (2018). "The Role of SIRT3 in the Brain Under Physiological and Pathological Conditions." Front Cell Neurosci **12**: 196.

Simic, P., K. Zainabadi, E. Bell, D. B. Sykes, B. Saez, S. Lotinun, R. Baron, D. Scadden, E. Schipani and L. Guarente (2013). "SIRT1 regulates differentiation of mesenchymal stem cells by deacetylating β-catenin." EMBO Mol Med **5**(3): 430-440.

Srivastava, S. (2016). "Emerging therapeutic roles for NAD+ metabolism in mitochondrial and age-related disorders." Clinical and Translational Medicine **5**(1): 25.

Stope, M. B. (2021). "Phosphorylation of histone H2A.X as a DNA-associated biomarker (Review)." World Acad Sci J **3**(3): 31.

Sugatani, T., O. Agapova, H. H. Malluche and K. A. Hruska (2015). "SIRT6 deficiency culminates in low-turnover osteopenia." Bone **81**: 168-177.

Tai, P. W. L., H. Wu, A. J. van Wijnen, G. S. Stein, J. L. Stein and J. B. Lian (2017). "Genome-wide DNase hypersensitivity, and occupancy of RUNX2 and CTCF reveal a highly dynamic gene regulome during MC3T3 pre-osteoblast differentiation." PLOS ONE **12**(11): e0188056.

Thoma, A., T. Akter-Miah, R. L. Reade and A. P. Lightfoot (2020). "Targeting reactive oxygen species (ROS) to combat the age-related loss of muscle mass and function." Biogerontology **21**(4): 475-484.

Treiber, N., P. Maity, K. Singh, M. Kohn, A. F. Keist, F. Ferchiu, L. Sante, S. Frese, W. Bloch, F. Kreppel, S. Kochanek, A. Sindrilaru, S. Iben, J. Högel, M. Ohnmacht, L. E. Claes, A. Ignatius, J. H. Chung, M. J. Lee, Y. Kamenisch, M. Berneburg, T. Nikolaus, K. Braunstein, A.-D. Sperfeld, A. C. Ludolph, K. Briviba, M. Wlaschek and K. Scharffetter-Kochanek (2011). "Accelerated aging phenotype in mice with conditional deficiency for mitochondrial superoxide dismutase in the connective tissue." Aging Cell **10**(2): 239-254.

Tseng, A. H., L. H. Wu, S. S. Shieh and D. L. Wang (2014). "SIRT3 interactions with FOXO3 acetylation, phosphorylation and ubiquitinylation mediate endothelial cell responses to hypoxia." Biochem J **464**(1): 157-168.

Uddin, M. S., A. Al Mamun, M. T. Kabir, J. Ahmad, P. Jeandet, M. S. Sarwar, G. M.

Ashraf and L. Aleya (2020). "Neuroprotective role of polyphenols against oxidative stress-mediated neurodegeneration." Eur J Pharmacol **886**: 173412.

Wan, H. F., J. X. Li, H. T. Liao, M. H. Liao, L. Luo, L. Xu, K. F. Yuan and Y. Zeng (2018). "Nicotinamide induces liver regeneration and improves liver function by activating SIRT1." Molecular Medicine Reports.

Wang, F. and Q. Tong (2009). "SIRT2 suppresses adipocyte differentiation by deacetylating FOXO1 and enhancing FOXO1's repressive interaction with PPARgamma." Mol Biol Cell **20**(3): 801-808.

Wang, R.-H., K. Sengupta, C. Li, H.-S. Kim, L. Cao, C. Xiao, S. Kim, X. Xu, Y. Zheng, B. Chilton, R. Jia, Z.-M. Zheng, E. Appella, X. W. Wang, T. Ried and C.-X. Deng (2008). "Impaired DNA Damage Response, Genome Instability, and Tumorigenesis in SIRT1 Mutant Mice." Cancer Cell **14**(4): 312-323.

Wang, X.-X., X.-L. Wang, M.-m. Tong, L. Gan, H. Chen, S.-s. Wu, J.-X. Chen, R.-L. Li, Y. Wu, H.-y. Zhang, Y. Zhu, Y.-x. Li, J.-h. He, M. Wang and W. Jiang (2016). "SIRT6 protects cardiomyocytes against ischemia/reperfusion injury by augmenting FoxO3α-dependent antioxidant defense mechanisms." Basic Research in Cardiology **111**(2): 13.

Wang, X. Z., X. Y. Sun, C. Y. Zhang, X. Yang, W. J. Yan, L. H. Ge and S. G. Zheng (2016). "RUNX2 Mutation Impairs 1alpha,25-Dihydroxyvitamin D3 mediated Osteoclastogenesis in Dental Follicle Cells." Sci Rep **6**: 24225.

Wang, X. Z., X. Y. Sun, C. Y. Zhang, X. Yang, W. J. Yan, L. H. Ge and S. G. Zheng (2016). "RUNX2 Mutation Impairs 1α,25-Dihydroxyvitamin D3 mediated Osteoclastogenesis in Dental Follicle Cells." Scientific Reports **6**(1): 24225.

Wassmann, S., K. Wassmann and G. Nickenig (2004). "Modulation of Oxidant and Antioxidant Enzyme Expression and Function in Vascular Cells." Hypertension **44**(4): 381-386.

Wen, Y. D., V. Perissi, L. M. Staszewski, W. M. Yang, A. Krones, C. K. Glass, M. G. Rosenfeld and E. Seto (2000). "The histone deacetylase-3 complex contains nuclear receptor corepressors." Proc Natl Acad Sci U S A **97**(13): 7202-7207.

Wilson, C. (2014). "Oxidative stress and osteoporosis." Nature Reviews Endocrinology **10**(1): 3-3.

Wise, G. E., S. Frazier-Bowers and R. N. D'Souza (2002). "Cellular, Molecular, and Genetic Determinants of Tooth Eruption." Critical Reviews in Oral Biology & Medicine **13**(4): 323-335.

Wise, G. E. and G. J. King (2008). "Mechanisms of tooth eruption and

orthodontic tooth movement." Journal of dental research **87**(5): 414-434.
Wise, G. E., S. J. Lumpkin, H. Huang and Q. Zhang (2000). "Osteoprotegerin and Osteoclast Differentiation Factor in Tooth Eruption." Journal of Dental Research **79**(12): 1937-1942.
Wise, G. E., S. Yao, P. R. Odgren and F. Pan (2005). "CSF-1 regulation of osteoclastogenesis for tooth eruption." J Dent Res **84**(9): 837-841.
Wu, H., T. W. Whitfield, J. A. Gordon, J. R. Dobson, P. W. Tai, A. J. van Wijnen, J. L. Stein, G. S. Stein and J. B. Lian (2014). "Genomic occupancy of Runx2 with global expression profiling identifies a novel dimension to control of osteoblastogenesis." Genome Biol **15**(3): R52.
Yang, K., F. Cao, Y. Xue, L. Tao and Y. Zhu (2022). "Three Classes of Antioxidant Defense Systems and the Development of Postmenopausal Osteoporosis." Front Physiol **13**: 840293.
Yoda, S., N. Suda, Y. Kitahara, T. Komori and K. Ohyama (2004). "Delayed tooth eruption and suppressed osteoclast number in the eruption pathway of heterozygous Runx2/Cbfa1 knockout mice." Arch Oral Biol **49**(6): 435-442.
Zahan, O. M., O. Serban, C. Gherman and D. Fodor (2020). "The evaluation of oxidative stress in osteoarthritis." Med Pharm Rep **93**(1): 12-22.
Zainabadi, K., C. J. Liu, A. L. M. Caldwell and L. Guarente (2017). "SIRT1 is a positive regulator of in vivo bone mass and a therapeutic target for osteoporosis." PLOS ONE **12**(9): e0185236.
Zainabadi, K., C. J. Liu and L. Guarente (2017). "SIRT1 is a positive regulator of the master osteoblast transcription factor, RUNX2." PLoS One **12**(5): e0178520.
Zhang, H., D. Ryu, Y. Wu, K. Gariani, X. Wang, P. Luan, D. D'Amico, E. R. Ropelle, M. P. Lutolf, R. Aebersold, K. Schoonjans, K. J. Menzies and J. Auwerx (2016). "NAD^+ repletion improves mitochondrial and stem cell function and enhances life span in mice." Science **352**(6292): 1436-1443.
Zhang, J., H. Xiang, J. Liu, Y. Chen, R. R. He and B. Liu (2020). "Mitochondrial Sirtuin 3: New emerging biological function and therapeutic target." Theranostics **10**(18): 8315-8342.
Zheng, C.-X., B.-D. Sui, X.-Y. Qiu, C.-H. Hu and Y. Jin (2020). "Mitochondrial Regulation of Stem Cells in Bone Homeostasis." Trends in Molecular Medicine **26**(1): 89-104.
Zhou, L., F. Wang, R. Sun, X. Chen, M. Zhang, Q. Xu, Y. Wang, S. Wang, Y. Xiong, K. L. Guan, P. Yang, H. Yu and D. Ye (2016). "SIRT5 promotes IDH2

desuccinylation and G6PD deglutarylation to enhance cellular antioxidant defense." EMBO Rep **17**(6): 811-822.

국문초록

니코틴아마이드의 뼈 대사 조절 효과에 관한 연구

윤 희 인

서울대학교 대학원
치의과학과 분자유전학전공
(지도교수 류 현 모)

니코틴아마이드 (nicotinamide;NAM)는 수용성 비타민 B3의 하나로, 안전성이 높다고 알려져 여러 질병을 치료하기 위한 약물로 오랫동안 사용되어왔다. 니코틴아마이드는 제 3형 히스톤 탈아세틸화 효소로, Sirtuin (Sirt)의 반응 중에 형성된다. 여러 연구를 통해 Sirt는 골 발달과 골 항상성 유지에 중요한 역할을 한다고 알려져 있다. 또한, 니코틴아마이드 리보사이드 (nicotinamide riboside; NR)와 니코틴아마이드 모노뉴클레오타이드 (nicotinamide mononucleotide; NMN)와 같은 NAD+ 전구체들이 뼈 항상성을 조절한다는 사실이 보고된 바 있다. 그러나 니코틴아마이드가 뼈 항상성 유지에 미치는 영향과 그 기전에 대해서 아직 명확하게 밝혀지지 않았다.

조골세포의 분화 과정에서는 분화에 필요한 에너지를 공급하기 위한 미토콘드리아 호흡이 매우 중요하고 세포 호흡에 의해 자연적으로

발생하는 활성산소종을 적절한 수준으로 유지하기 위한 항산화 효소의 작용이 중요하다. 또한 뼈 항상성을 위해서는 조골세포와 파골세포 사이의 상호작용에서 두 세포 간 기능의 균형이 필수적이다. 따라서 Part 1에서는 니코틴아마이드의 조골세포 분화 및 대사에 미치는 영향을 알아보고 조골세포의 항상성 유지에 관여하는지 확인하고자 하였다. Part 2에서는 Runx2 유전자 반수체부족에 의해 발생하는 두개쇄골이형성증(Cleidocranial dysplasia; CCD)에서 나타나는 영구치 맹출 장애의 기전을 밝히고 니코틴아마이드가 조골세포와 파골세포의 조절을 통해 치아 맹출 지연 증상에 대해 회복 효과를 보일 수 있는지 관찰하였다.

Part 1에서 니코틴아마이드가 항산화 효소를 유도하여 조골세포의 분화를 증가시키고, 조골세포 분화에 필요한 에너지를 공급하는 미토콘드리아 호흡을 촉진시킴을 확인하였다. 또한, 니코틴아마이드는 미토콘드리아 Sirt3를 활성화하고, FOXO3a를 활성화하여 항산화 효소의 발현을 유도함을 확인하였다. 이러한 결과를 통해 니코틴아마이드가 미토콘드리아 대사와 항산화 효소를 촉진하여 조골세포의 분화를 증가시켰음을 알 수 있다. Part 2에서는 니코틴아마이드가 CCD표현형을 나타내는 *Runx2*$^{+/-}$ 마우스의 치아 맹출 지연 증상을 회복시킬 수 있는지를 관찰하였다. Runx2가 결핍된 조골세포에서는 파골세포 분화 유도에 중요한 인자인 colony stimulating factor 1 (CSF1)의 발현이 감소되어 있었다. 니코틴아마이드는 RUNX2를 활성화하고, RUNX2가 CSF1의 프로모터 부분에 직접 결합하여 발현을 촉진시킨다는 것을 확인하였다. 또한 니코틴아마이드는 Sirt2를 직접적으로 억제하여 RUNX2의 활성을 조절한다는 것을 밝혔다. 이와 같은 결과들을 통해, CCD 표현형 마우스에서 나타나는 치아 맹출 이상은 Runx2가 결핍된 조골세포에서 저하되어 있는 CSF1에 의한 것이며, 니코틴아마이드는 RUNX2의 활성을 촉진하여 파골세포 분화를 유도하여 이를 회복시킴을 확인하였다.

본 논문에서 우리는 니코틴아마이드가 조골세포의 분화를 직접적으로 촉진할 뿐 아니라, 조골세포에서 발현되는 파골세포 분화 유도 인자를 조절하여 파골세포의 분화를 조절할 수 있음을 밝혔다. 니코틴아

마이드는 조골세포 내에서 미토콘드리아 대사와 항산화 효소를 촉진하여 골 항상성을 유지하도록 하였기에, 산화적 스트레스와 관련되어 있는 다양한 근골격계 질환을 완화시킬 수 있는 약물로서 가능성을 보인다. 또한, CCD환자들에서 나타나는 치아 맹출 지연의 발생 기전을 규명하였으며, 약물치료법이 전무하였던 CCD 환자의 치과적 문제를 치료하기 위한 치료제로서의 가능성을 확인하였다.

Keywords : 니코틴아마이드, 조골세포, 파골세포, 항산화효소, Runx2, 두개쇄골이형성증
Student Number : 2016-22038